INSIGHTS INTO MECHANISMS OF ANTIFUNGAL ACTIVITY BY INNATE IMMUNE CELLS

By

BENJAMIN N. NELSON

Bachelor of Science in Multidisciplinary Studies
University of Oklahoma
Norman, OK
2015

Submitted to the Faculty of the
Graduate College of the
Oklahoma State University
in partial fulfillment of
the requirements for
the Degree of
DOCTOR OF PHILOSOPHY
May, 2023

INSIGHTS INTO MECHANISMS OF ANTIFUNGAL ACTIVITY BY INNATE IMMUNE CELLS

Dissertation Approved:

Dr. Karen L. Wozniak

Dissertation Adviser

Dr. Jeffrey A. Hadwiger

Dr. Erika I. Lutter

Dr. Matthew T. Cabeen

Dr. Antonius G. P. Oomens

ACKNOWLEDGEMENTS

I would first like to thank my mentor Dr. Karen Wozniak. Without her everyday push and strive for quality, I would have never made it to the finish line. She took a chance on me to bring me into her lab. Her demand for excellence pushed me to heights I never dreamed possible while her kindness allowed me the room to falter along the journey.

Next, I must thank my committee members Drs. Oomens, Hadwiger, Lutter, and Cabeen. Their expertise and support provided me a unique perspective on the project and growth as a scientist. Special thanks are also in order for Drs. Oomens and Cabeen who stepped up without hesitation to fill positions within my committee as other faculty moved on.

To Oklahoma State University, the department of Microbiology and Molecular Genetics, and friends of Stillwater: thank you for being so welcoming and giving me a place to call home these past years! During my first visit to the area, I was uncertain about the future, but everyone made me feel both accepted as a peer and wanted as an individual.

I would also like to thank Deborah Botts and the U.S. Department of Veterans Affairs. She went above and beyond to help get my degree funded and made sure I was well taken care of. I know it was not easy and I will forever be grateful for your diligence.

Foremost, I must thank my family for their support and encouragement. To Meg, my wife, who convinced me to come here and then to push through when it was difficult. We started this journey together and I look forward to where it might take us. To my wonderful mother, who since the birth of my son, Charlie, has become his primary caretaker and has taken the brunt of the responsibilities while allowing me to focus on my work. Thank you for all you do!

Name: BENJAMIN N. NELSON

Date of Degree: MAY, 2023

Title of Study: INSIGHTS INTO MECHANISMS OF ANTIFUNGAL ACTIVITY BY INNATE IMMUNE CELLS

Major Field: MICROBIOLOGY, CELL AND MOLEULAR BIOLOGY

Abstract: *Cryptococcus neoformans* is an opportunistic fungal pathogen that causes over 180,000 annual deaths in HIV/AIDS patients. Innate phagocytes such as dendritic cells (DCs) and macrophages are the first cells to interact with the pathogen, with destruction inside a mature lysosome through degradation with acid hydrolases and reactive oxygen/nitrogen species. This work investigates the mechanisms of antifungal activity by innate immune cells. Previous studies have shown that innate immune cells will either allow for intracellular growth or kill the fungus by recognizing, phagocytosing, and finally destroying the fungus within a mature lysosome using both oxidative and nonoxidative mechanisms. We hypothesize that there are certain subsets that allow for differential interactions of the fungus and that killing by nonoxidative means is made possible by many different lysosomal proteins. Results showed several lysosomal proteins affected the growth of *C. neoformans*. Proteins that killed or inhibited the fungus did so in a dose-dependent manner. Furthermore, protein concentrations needed for cryptococcal inhibition were found to be non-cytotoxic to mammalian cells. Results also showed all macrophage and dendritic cell subsets interacted with the fungus, and both living and killed morphologies were discernable within the subsets using imaging flow cytometry. Single-cell RNA-seq identified several different clusters of cells which more closely related to interactions with *C. neoformans* and its protective capacity against the pathogen rather than discrete cellular subsets. Differential gene expression analyses identified several changes in the innate immune cell as it kills the fungus, including increases of TNF-α and a switch to fatty acid metabolism by upregulation of *FABP4*. Also, increases of TNF-α correlated to cryptococcal interactions. These data show signaling networks that regulate expression of many different genes—both metabolic and immune—as certain clusters of cells mount a protective response. This protective response is facilitated by proteins that have antifungal activity and are well tolerated by mammalian cells. Future studies will examine these proteins, genes, and networks to understand the exact mechanism(s) these subsets use to kill *C. neoformans* in order to develop immunotherapeutic strategies to combat this deadly disease.

TABLE OF CONTENTS

Chapter Page

LIST OF TABLES

Table Page

LIST OF FIGURES

Figure Page

LIST OF ABBREVIATIONS

Abbreviation	Meaning
AM	alveolar macrophage
AMP	antimicrobial peptide
AmpB	amphotericin B
APC	antigen presenting cell
ART	antiretroviral therapy
BAL	bronchoalveolar lavage
BBB	blood brain barrier
BMDC	bone marrow derived dendritic cell
CD	cluster of differentiation
CFU	colony forming units
CFW	calcofluor white
C-IRIS	cryptococcal immune reconstitution inflammatory syndrome
CLSI	Clinical and Laboratory Standards Institute
CMI	cell mediated immunity
CN	*Cryptococcus neoformans*
CNS	central nervous system
DC	dendritic cell
FABP4	fatty acid binding protein 4
FACS	fluorescence-activated cell sorting
FICI	fractional inhibitory concentration index
GalXM	galactoxylomannan
GXM	glucuronoxylomannan
HNE	human neutrophil elastase
IFN	interferon
IL	interleukin
IPA	Ingenuity Pathway Analysis
MFI	mean fluorescence intensity
MHC	major histocompatibility complex
MIC	minimum inhibitory concentration
MMP25	matrix metalloproteinase
MOI	multiplicity of infection
MPO	myeloperoxidase
Mtb	*Mycobacterium tuberculosis*

Abbreviation	Meaning
NOSTRIN	nitric oxide synthase trafficking
oxLDL	oxidized low-density lipoproteins
PBS	phosphate buffered saline
RNS	reactive nitrogen species
ROS	reactive oxygen species
PAMP	pathogen-associated molecular pattern
PRR	pattern recognition receptor
scRNA-seq	single cell RNA sequencing
Th1/Th2	Type 1 or Type 2 T helper cell
TNF	tumor necrosis factor
UMAP	uniformed manifold approximation and projection
YPD	yeast extract-peptone-dextrose

CHAPTER I

REVIEW OF LITERATURE

1.1 *Cryptococcus* Species Complex: Taxonomy and Worldwide Distribution

Historically, the etiological agent of cryptococcosis was classified as a single species as *Cryptococcus neoformans* [1]. However, the species has been separated into two species, *C. neoformans* and *C. gattii*, due to differences in molecular characteristics, ecology, and epidemiology [2,3]. Now the species *C. neoformans* is further divided into three serotypes in two varieties: A (variety *grubii*), D (variety *neoformans*), and AD (which is a hybrid of A and D), while *C. gattii* has only the two serotypes B and C which have not been elevated to the variety status [2]. Molecular techniques such as PCR (polymerase chain reaction) fingerprinting, AFLP (amplified fragment length polymorphism), and MLST (multilocus sequence typing) have further subdivided these into eight major molecular types that correlate to the serotypes [4-6]. For *C. neoformans* (serotype), they are VNI (A), VNII (A), VNIII (all AD hybrids), and VNIV (D) while *C. gattii* includes VGI-VGIV which are all associated with both serotypes B and C (VNI = variety *neoformans* number one, VGI = variety *gattii* number one). More recently, in part due to the intensive genome sequencing, there have been proposals to further split *C. neoformans* into two separate species (*C. neoformans* and *C. deneoformans*) and *C. gattii* into five species (*C. gattii*, *C. bacillisporus*, *C. deuterogattii*, *C. tetragattii*, and *C. decagattii*) [7]. Geographically, *C. neoformans* has been found worldwide in all climates, while *C. gattii* is more selective and is

most prevalent in North/South America and Oceania [3]. Worldwide, most isolates come from the continents of Asia and Africa, but the countries reporting the most cases are in order: South Africa, China, and the United States. This is due to both a lack of data from many other African countries and also the sampling rate from the United States being the highest of any country [2]. This distribution of the fungus is intertwined with both the habitats is prefers and also incident rates among affected populations.

1.2 *Cryptococcus neoformans*: Epidemiology, Ecological Niche, and Life Cycle

C. neoformans var. *grubii* (serotype A) is the most common cause of cryptococcal meningitis encompassing around 80% of total infections [8]. It generally affects immunocompromised individuals and is most associated with the progression to clinical AIDS, and it is considered an AIDS-defining illness [9]. Therefore, it is understandable that most cases are concentrated in the sub-Saharan region of Africa. *C. gattii* is different in that it causes infections in immunocompetent people as well (see Pacific Northwest Outbreak). Curiously, a recent study noted that *C. gattii* infections in China are rare, and most of these cryptococcal cases were from apparently immunocompetent individuals. Researchers attributed this to possibly genetic factors among the predominate population including those that include polymorphisms to the Fc-gamma receptor 2B (*FCGR2B*) and mannose-binding lectin (MBL), both instrumental in immunity against the pathogen [10]. Both of these species inhabit ecological niches that include decaying matter within tress with *C. gattii* preferring tress that have leaves with waxier surface coatings such as the Douglas fir (also prevalent in the Pacific Northwest) and Eucalyptus trees (Australia) [11]. *C. neoformans* is also highly present in avian excreta and is associated with pigeons in urban areas [12]. In the environment, *C. neoformans* can switch between a vegetative budding yeast and sexual growth phases which are multicellular [13]. While the unicellular yeast cell is the predominant form in both the environment and the human hosts, sexual reproduction is vital to the pathogenicity of the organism. Researchers have identified at least three important

reasons for this: 1) spores from sexual development are infectious, 2) sexual development contributes to genetic variation among the species complex, and 3) the genes controlling this behavior (located in the *MAT* locus) also contribute to cryptococcal virulence [14]. Despite this dimorphic life cycle, *C. neoformans* is sometime considered monomorphic as yeast cells are the predominant morphology, especially in the context of infections, and most of what makes it a pathogen concerns the single-cell lifestyle as well.

1.3 Cryptococcal Virulence Factors

As a successful pathogen, *Cryptococcus neoformans* employs many different strategies to overcome the host immune system. The most notable of these that all virulent cryptococcal strains have are a polysaccharide capsule and the ability to produce melanin. *C. neoformans* is remarkable as it is the only fungal pathogen capable of producing this type of capsule [15]. The two main components of the capsule are glucuronoxylomannan (GXM) and galactoxylomannan (GalXM) with the later only making up about 8% of the mass [16]. GXM is composed of α-1,3-linked mannose residues with xylosyl and glucuronyl side groups while GalXM has a α-1,6-galactan backbone and xylose and mannose side groups, hence the naming conventions [17]. Recently, however, GalXM was found to also have β-D-glucuronic acid and there have been proposals to change its name to glucuronoxylomannogalactan (GXMGal) to represent its nature more accurately [18]. The exact makeup and irregularity between these side groups translate into antigenic variability and immunomodulatory differences between serotypes [19]. While the exact reason for capsular production in the environment is debatable, one theory suggests that its presence is the result of interaction with predatory amoebae [20]. It was later shown that *C. neoformans* does indeed increase traits associated with virulence when incubated with predatory amoeba [21]. In a host, these same virulence factors are the main defenses against an immune system: inhibition of phagocytosis and repressing T cell responses. The large capsule covers many of the pathogen associated molecular patterns (PAMPs) the innate immune system usually

uses to detect harmful pathogens, which proceeds to inhibit/reduce phagocytosis [22]. Therefore, the host must identify this irregular capsule by other means such as specific antibodies or through complement recognition. Additionally, the capsule has been shown to directly suppress T cell proliferation and even induce apoptosis among T cells [23-26]. The second major virulence factor that *C. neoformans* has at its disposal is the ability to produce melanin. Melanin can protect the pathogen against oxidative damage from both reactive oxygen and nitrogen species produced by host cells, usually by macrophages and dendritic cells in response to an infection [27]. Additionally, melanin has been shown to exert some protective effects by reducing the efficacy of antifungal drugs such as amphotericin B and fluconazole by decreasing their toxicities against the fungus [28]. Aside from these two main defenses against the host immune system, *C. neoformans* has a plethora of other secreted enzymes able to promote fungal survival by destroying tissues and disrupting normal immune functions [15]. These include DNase, proteases, lipases, and hydrolases (urease, superoxide dismutase). The fungus also has the ability to grow at human body temperature (37°C), and along with the aforementioned virulence factors, *C. neoformans* can be a successful pathogen [29].

1.4 Cryptococcosis and Cryptococcal Meningitis

Despite inhabiting an environmental niche, *C. neoformans* can find its way to humans to initiate disease. While cryptococcal exposure is common (one study showed that 70% of children by age 5 have anticryptococcal antibodies in their sera) [30], symptomatic disease occurs primarily among those with compromised immune systems. Current numbers state about 220,000 yearly cases of worldwide cryptococcal meningitis among those living with HIV/AIDS (the most affected population), which results in over 181,000 annual deaths [31]. The vast majority of these cases (>80%) occur in sub-Saharan Africa (where the AIDS epidemic is currently ongoing). Estimates place cryptococcosis second, only narrowly behind tuberculosis, as the most common cause of AIDS-related deaths. Despite this, cryptococcal research remains underfunded compared

to tuberculosis research (~1% of total budget) [32]. Humans come into contact with *C. neoformans* from the environment as yeast cells or desiccated spores become airborne which we then breathe into our lungs. Generally, in immunocompetent individuals, the immune system will quickly fight off the few invading cells without any clinical presentation [33]. However, in people without functional $CD4^+$ T cells, the pathogen can persist and replicate within the lung which leads to pulmonary cryptococcosis. Clinical presentation of this is usually in the form of nonspecific symptoms such as coughing, chest pains, and difficulty breathing [34]. Physical examination may reveal indication of pleural effusion, and chest x-rays or CT scans often shows both pneumonia and multiple nodules resembling those from microbial infections, excessive inflammation, cancer, or infarctions [35,36]. These symptoms are caused by the increased fungal burden that occurs within the lung from the persistence of cryptococcal cells and subsequent replication, often intracellularly. Once the fungus has established a niche within the host, it then can disseminate throughout the rest of the body via the bloodstream to various organs such as the liver, kidneys, or brain, causing extreme damage and/or organ failure [37-39]. Dissemination to the brain (cryptococcal meningitis) is the deadliest form of the disease [31]. The brain usually has protections in place in the form of the blood brain barrier (BBB) to prevent crossing of immune cells, pathogens and other unwanted substances into the central nervous system (CNS) [40]. However, *C. neoformans* has tools to circumvent this protection. Direct transcellular migration of the fungus across the BBB has been shown in the laboratory setting with urease, metalloprotease Mpr1, laccase, phospholipase B1, a serine protease, and tyrosine kinase receptor (TKR) EphA2 all being implicated as cryptococcal virulence factors that promote brain infiltration [41]. Additionally, macrophages or other phagocytes can cross the BBB, and if one traverses this barrier while harboring an intracellular yeast cell, the pathogen can circumvent this obstacle in this manner as well. This has been known in the community as the Trojan horse theory and is one of the leading concepts of how cryptococcal meningitis can develop [42-44]. After traveling to the brain inside a pulmonary phagocyte, *C. neoformans* can exit the cell either by lytic or non-

lytic means and cause infection and damage to the brain tissue [45,46]. Specifically, inflammation to the meninges (meningitis) is the most common form of damage, but other damage may also occur to the parenchyma, so the term meningoencephalitis may be more appropriate [39]. Clinically, these often present as fever, headaches, or other altered mental states. At this state of cryptococcal meningitis, the mortality rate of people living with HIV/AIDS remains unacceptably high even with modern antiretroviral therapy (ART) with rates 13-19% in high resource areas and skyrocketing to over 80% in more impoverished areas [9,31]. Treatment for this deadly combination is a major area of concern with the current armamentarium of antifungal drugs.

1.5 Antifungal Treatments against *Cryptococcus neoformans*

There are currently four major classes of antifungal drugs (polyenes, azoles, allylamines, echinocandins) on the market with many other miscellaneous ones as well (such as flucytosine). Due to fungi and humans both being eukaryotic, there is increased risk of toxicities due to the similarities of substrates between target and host (for example the fungal ergosterol is structurally similar to human cholesterol). The gold standard for treating cryptococcosis is a combination of amphotericin B and flucytosine for at least two weeks followed by eight weeks of fluconazole monotherapy [47]. Amphotericin B (AmpB) is a polyene class of antifungals that targets and binds to the fungal specific cell membrane sterol ergosterol, causing increased membrane permeability and cell leakage [48]. At certain concentrations the drug is fungicidal and prevents cell division [49]. However, at higher concentrations, AmpB can become toxic to organs (especially to the liver) which is why different preparations are being developed including a less toxic lipid formulation (Ambisome) [50]. Acquired resistance to AmpB is rare, however, natural resistance does occur as some fungal species have ergosterol that is not as susceptible to the drug [51]. Resistance to polyenes can also occur over prolonged exposure [52]. Recently, AmpB has also been shown to induce oxidative stress on the pathogen, but the extent of the damage and mechanism of action is currently being investigated [53]. Flucytosine's (or 5-fluorocytosine; 5-

FC) antifungal activity comes from its conversion into 5-fluorouracil in susceptible cells which then proceeds to inhibit both DNA and RNA synthesis [54]. Combination therapy of 5-FC with AmpB has shown a synergistic effect but can also increase host toxicities as well [55]. If used as a monotherapy, 5-FC is vulnerable to drug resistance [56]. The final part of the antifungal drug regime consists of fluconazole monotherapy. Fluconazole is a fungistatic drug that interrupts the fungal conversion of lanosterol to ergosterol which leads to an accumulation of 14-methylsterols and disrupted membrane permeability [57]. Fluconazole has better host tolerance and lower toxicity than AmpB, but there are multiple mechanisms for fungal resistance through either mutations to the substrate (*ERG11*) which blocks its catalytic activity or by increasing efflux pumps to remove the drug [51]. It is worth mentioning the route of administration of these anticryptococcal drugs. Both fluconazole and flucytosine are available as oral medication which lends itself for better compliance with timing, dosage, and frequency. This is in opposition is AmpB, which is administered by a healthcare professional intravenously [9]. Echinocandins, such as caspofungin, are not used for the treatment of cryptococcosis, as cryptococcal strains are naturally resistant to the drug, albeit paradoxically, as the target, β-1,3-glucan synthase, is essential for the growth of *C. neoformans* [58]. The last major class of antifungal drugs are the allylamines (terbinafine) which inhibit squalene epoxidase (also necessary for ergosterol synthesis) and have no effect on human cholesterol [59]. Usually used to treat dermatophytic infections and onychomycosis (nail fungus), there has been little traction for the drug to be used to treat cryptococcosis. However, some studies have shown some *in vitro* efficacy both alone and in combination with other antifungal drugs [60]. The financial considerations for drug development are steep and, as previously mentioned, funding for such discoveries is scant. Much work has been done with both elucidating combinatorial effects of current drugs and the repurposing of other compounds. However, there is a proverbial arms race between the drugs and pathogens, and investigations for new targets and pathways are necessary [61].

1.6 Host Innate Immunity Against *Cryptococcus neoformans*

The innate immune system is one of the main branches of the human immune system (the other being the adaptive system and discussed later). Against fungal infection, the main job for this branch is quick recognition and elimination of the pathogen. This is accomplished through three main effector cells in the pulmonary tissue: macrophages, dendritic cells, and neutrophils [62]. Resident to the lung and pulmonary tissues, macrophages and DC are the first to encounter the pathogen upon entry into the lungs [63]. Both macrophages and DCs have a variety of pattern recognition receptors (PRRs) on their surface and serve as surveillance cells in the lung and other tissues [62]. These PRRs include Toll-like receptors (TLRs), C-type lectin receptors (CLRs), and NOD-like receptors (NLRs) which can detect antigens such as β-glucans, capsular GXM, mannose, and internalized fungal components [64-66]. Critical among these are the CLRs Dectin-1, -2, and -3 which signal through CARD9 that itself is a central molecule in signaling pathways for fungal infections [67,68]. Upon recognition by a macrophage, there are several potential fates for *Cryptococcus*. Some studies report the anticryptococcal properties of macrophages, while others show intracellular replication of the organism [69,70]. Part of this outcome depends on the polarization status of the macrophage to either the antifungal M1 (classical) or permissive M2 (alternative). M1 macrophages kill the fungus through either oxidative (ROS/RNS) or non-oxidative means (enzymatic proteins), and this plasticity of macrophages is dependent on local cytokines [71]. Cytokines such as IFN-γ push macrophages towards M1 polarization through STAT1 dependent mechanisms, while IL-4 and IL-13 lead to M2 polarization [72,73]. In the case of fungal destruction, macrophages also have a second important job: presentation of cryptococcal antigen to activated $CD4^+$ T cells to enhance the adaptive immune system through MHC-II [74]. This, in turn, steers other local effector cells to take a more antifungal stance [75]. The next major effector innate immune cell is the dendritic cell (DC). They share similar effector functions as macrophages with their phagocytosis and killing of *C. neoformans* [76].

Additionally, DCs are tasked with being the bridge between the innate and adaptive immune systems. Once phagocytosis and fungal killing has occurred, they begin to mature and present antigen (also through MHC-II), but this time, they travel to peripheral lymph nodes to prime and activate naïve T cells leading to a Th1-type adaptive response [77,78]. Neutrophils are the most abundant white blood cell in the bloodstream and are recruited to the site of infection through complement activation [79]. However, neutrophil recruitment has been shown to have little to no effect on fungal burden, and these cells are not required for cryptococcal clearance [80]. Furthermore, some studies have shown that infiltration of neutrophils can be detrimental and increase fungal burden [81,82].

Complicating the specific interactions of *C. neoformans* with innate immune cells is the heterogeneity among immune cell populations. While the majority of immune cells are generated through hematopoiesis from the bone marrow[83], some immune cells, including tissue-resident macrophages, instead have other sources [84]. Tissue-resident macrophages are seeded before birth and stay in their respective organs through life. The origin of these is the fetal yolk sac and fetal liver before the onset of hematopoiesis [85,86]. Concerning macrophages, these include the alveolar macrophages in the lung, Kupffer cells in the liver, and microglia in the brain. These resident macrophage populations have been shown to have their own distinct interactions with *C. neoformans* [63,87-89]. With alveolar macrophages representing around 80- 90% of total leukocytes in the alveoli of healthy lungs, the pathogen has the most chance at encountering them more than any other cell type [90-92]. Due to their differences in origin compared to bone marrow-derived macrophages, cryptococcal-macrophage interactions need also be studied within the context of these tissue resident cells. Researchers have shown that these interactions are vital to the prognosis of cryptococcosis. In some instances, the fungal cell is able to avoid macrophage killing and survive and replicate intracellularly [90,93,94]. However, these studies did not account for further heterogeneity among the innate immune cells other than the origin and lineage

of the cell. Recently, researchers have begun to uncover subpopulations among the lung resident innate immune cells, which are characterized by differences in cell surface markers and transcriptomes [63,95,96]. It has been hypothesized that these differences are the result of a division of labor among the whole population, with certain cells being better suited for specific functions. In mice, it was shown that macrophages in healthy lungs can be divided into four groups (alveolar, interstitial, $Ly6c^+$, and $Ly6c^-$; both Ly6c groups contain a mixture of monocyte-like and macrophage-like cells) and DCs divided into two conventional subsets ($CD11c^+$ $CD103^+$ and $CD11c^+$ $CD11b^+$) and plasmacytoid DCs (pDCs) [96,97]. Studies of these subsets indicate that the $Ly6c^+$ monocyte-like macrophage population is anticryptococcal, while the $CD11b^+$ DCs are permissive for intracellular growth[98]. Alveolar macrophages can vary in their antifungal activity, and the interstitial macrophages can enable dissemination to the CNS [98,99]. Humans have similar subsets with one study identifying three macrophage subsets (AMs, $CD1c^-CD14^+$, $CD1c^-CD14^-$) and three DC subsets (Langerin$^+$, $CD1c^+CD14^+$, $CD1c^+CD14^-$) [95]. Studies have shown that all human pulmonary subsets except the $CD1c^-CD14^+$ and $CD1c^-CD14^-$ macrophage subsets were anticryptococcal [92].

1.7 Host Adaptive Immunity Against *Cryptococcus neoformans*

The human body is equipped with two arms of an immune system: the innate for quick and specific recognition of PAMPs and an adaptive system which takes longer to start but is antigen-specific in its targets [62]. These two arms of the immune system also work in concert with each other to increase the overall effectiveness of the defense, which is the situation in a protective response against *C. neoformans* [75]. Typically, innate antigen presenting cells (APCs) will phagocytose and kill a pathogen and present cryptococcal antigen to the adaptive system through the MHC-II system [100]. DCs are special in that they can present this antigen to naïve $CD4^+$ T cells (T helper cells) in secondary lymphoid organs for the initiation of T cell effector function, thereby bridging the gap between the innate and adaptive immune systems [101].

Depending on the cytokines produced by the APC during antigen presentation, T helper cells can differentiate into subtypes Th1 Th2 and Th17 and others [102]. Protective responses against cryptococcosis include the Th1- and Th17-type (which stimulate cell-mediated immunity), while differentiation into Th2-type can lead to detrimental host responses and exacerbation of disease [75]. DCs that produce IL-12 lead to the formation of protective Th1-type $CD4^+$ helper T cells [103]. However, if DCs express the costimulatory molecules CD86 and OX40L and produce IL-4, Th2-type T cells will be the effector cell induced [104-106]. Finally, in the absence of producing both IFN-γ and IL-4, DCs that produce IL-23 (with costimulatory molecules CD28 and ICOS) will induce the differentiation of Th17-type effector T cells, which is sometimes protective and beneficial to the host against the disease [107,108]. On the other hand, it has been reported that IL-17 was increased in the CSF of cryptococcal meningitis cases both with and without HIV [109]. $CD4^+$ T cells are the predominate producers of IL-17 and it is currently unclear of the source in patients with AIDS ($CD4^+$ T cell counts <100 cells/μl). However, IL-17 can be produced by $CD8^+$ T cell, γδ T cells, neutrophils, and natural killer (NK) cells [81,110,111]. Regardless of the source, IL-17 has been linked with STAT3 signaling in response to fungal stimulation [109,112]. These responses are distinct from the IFN-γ produced by Th1 $CD4^+$ T cells that enhances macrophage function and polarizes them into the M1 phenotype through STAT1 signaling, which makes them more capable of killing *C. neoformans* [75]. While usually within the purview of adaptive immunity, memory against cryptococcal infections has also been seen in innate immune cells. Both macrophages and DCs have been shown to have "trained immunity" against previous infection to *C. neoformans,* which is mediated by epigenetic changes to the cells during priming with IFN-γ-producing *C. neoformans* [113,114]. These changes may induce subpopulations among the cells or changes in PRR expression to impart some functional phenotype [115].

1.8 Immunotherapies

Aside from using antifungal compounds directly against fungal pathogens, immunotherapies can also be efficacious. This type of treatment enhances the host's own immune system to fight off and eliminate invading pathogens [58]. While there is no current vaccine available against cryptococcal infection, there have been studies that used cryptococcal protein antigens to initiate the adaptive immune system through cell-mediated immunity (CMI) [116]. These treatments must strike a balance between protective Th1 responses and excessive inflammation that can exacerbate the disease [117]. Necessary to this type of immunity, however, are $CD4^+$ Th1-type T cells (and corresponding cytokines such as IL-2, IL-12, TNF-α, and IFN-γ), which are absent or deficient in the immunocompromised situations where the disease normally manifests. In situations that are devoid of $CD4^+$ T cells, it has been shown that $CD8^+$ T cells, which can also produce IFN-γ, can still expand and traffic to the lung to improve overall prognosis [118]. Additionally, there is some evidence for antibody-mediated immunity through the use of cryptococcal capsular components (including GXM, GalXM, and mannoproteins) [119]. However, as noted earlier, cryptococcal capsule has an immunosuppressive effect and does not induce either a strong or long-lasting immune response. Additionally, there is no evidence that this type of immunity is possible without CMI [116]. Therefore, there have also been studies on enhancing the immune systems' ability in eliminating the fungus. Adjunctive therapy using IFN-γ along with antifungal drugs has been shown to increase the effectiveness of amphotericin B in the mouse model, both *in vitro* and *in vivo* [120,121]. Despite the extensive work in the mouse model, there are limited data available for the efficacy of adjunctive IFN-γ therapy in humans. These limited studies have shown that this type of therapy is well-tolerated in humans and can lead to positive outcomes [122-124]. The current mechanisms that underlie this therapy in first-line defenders such as lung macrophages and DCs are unknown, and further research is required before large scale immunotherapeutics can be implemented.

CHAPTER II

ANTIFUNGAL ACTIVITY OF DENDRITIC CELL LYSOSOMAL PROTEINS AGAINST *CRYPTOCOCCUS NEOFORMANS* †

† This chapter is reproduced with slight modifications from the following publication:

Nelson, B.N., Beakley, S.G., Posey, S., Conn, B., Maritz, E., Seshu, J., Wozniak, K.L. (2021). Antifungal Activity of Dendritic Cell Lysosomal Proteins against *Cryptococcus neoformans*. *Scientific Reports*, 11(13619). Reprinted with permission.

Abstract

Cryptococcal meningitis is a life-threatening disease among immune compromised individuals that is caused by the opportunistic fungal pathogen *Cryptococcus neoformans*. Previous studies have shown that the fungus is phagocytosed by dendritic cells (DCs) and trafficked to the lysosome where it is killed by both oxidative and non-oxidative mechanisms. While certain molecules from the lysosome are known to kill or inhibit the growth of *C. neoformans*, the lysosome is an organelle containing many different proteins and enzymes that are designed to degrade phagocytosed material. We hypothesized that multiple lysosomal components, including cysteine proteases and antimicrobial peptides, could inhibit the growth of *C. neoformans*. Our study identified the contents of the DC lysosome and examined the anticryptococcal properties of different proteins found within the lysosome. Results showed several DC lysosomal proteins affected the growth of *C. neoformans in vitro*. The proteins that killed or inhibited the fungus did so in a dose-dependent manner. Furthermore, the

concentration of protein needed for cryptococcal inhibition was found to be non-cytotoxic to mammalian cells. These data show that many DC lysosomal proteins have antifungal activity and have potential as immune-based therapeutics.

2.1 Introduction

Cryptococcus neoformans is an encapsulated fungal pathogen that can cause pneumonia and meningitis in immune compromised individuals [125,126]. *C. neoformans* is an environmental yeast that is associated with decayed wood and pigeon droppings, and therefore, humans and animals breathe it in frequently [106,127]. Fortunately, the pathogen is typically quickly cleared from the lungs by a Th1 type $CD4^+$ T cell response before it can cause a symptomatic infection [126]. However, in cases where a person has a compromised immune system, such as reduced $CD4^+$ T cells in patients with HIV/AIDS or in individuals taking immunosuppressive drugs to prevent organ transplant rejection, the fungus can cause an infection [128,129]. The prevalence between AIDS and cryptococcosis is so high that the CDC has named it an AIDS-defining illness, and the occurrence of cryptococcal meningitis is most prevalent in sub-Saharan Africa [130,131]. An analysis of the 2014 Joint UN Programme on HIV and AIDS showed that of the 223,100 yearly cases of cryptococcal meningitis, 73% occurred in sub-Saharan Africa (162,500 cases) with estimated yearly death totals of 181,100 and 135,900 worldwide and in sub-Saharan Africa, respectively [31]. While these numbers have been trending downwards in recent years, due to its high mortality rate there is still a case to be made for the World Health Organization (WHO) to name cryptococcal meningitis as a neglected tropical disease [32,130,132]. The most popular treatment programs are all based around three drugs: Amphotericin B, flucytosine, and fluconazole [133,134]. However, each is associated with certain barriers and limitations such as bioavailability, host toxicity, and emergence of resistant cryptococcal strains [135-137].

While an adaptive T cell response is required for normal host clearance of *C. neoformans*, initial interactions with the fungus occur with innate immune cells in the lung such as dendritic cells (DCs) which are the cells responsible for antigen presentation to naive T cells [75,138]. The lungs contain a dense network of DCs, and during a cryptococcal infection, additional monocyte-derived DCs are recruited to the site of infection [76,139-141]. Upon encountering the fungus, DCs will phagocytose the opsonized pathogen, killing the organism in the phagolysosome [142-144]. The lysosome itself contains many different molecules (including proteases and antimicrobial peptides - AMPs) each with their own distinct role in degrading many different pathogens and/or facilitating the presentation of antigens via the MHC-II pathway to the adaptive immune system [145-148]. For instance, AMPs such as cationic defensins are antifungal and the suggested mechanism of action is insertion into the fungal membrane leading to cell lysis [149-151]. Also, mice deficient in cathepsins L and S, which are cysteine proteases (these make up the majority of proteases in the lysosome), have problems with invariant chain (Ii) cleavage, which is necessary for antigen presentation [152]. Resolution of *C. neoformans* requires proper antigen presentation and activation of T cells [63,128].

It has been previously shown that DCs (both murine bone marrow-derived DCs and human PBMC-derived DCs) can kill *C. neoformans* both *in vitro* and *in vivo* by oxidative and non-oxidative mechanisms [145,153,154]. However, it is possible for the fungus to survive and replicate inside other immune cells such as macrophages [155,156]. Furthermore, the purified contents of DC lysosomes can also kill the fungus *in vitro* in a dose-dependent manner [145,154]. These studies illustrate that it is indeed the components of the lysosome that act upon the pathogen. Since the lysosome is a generalized killing organelle designed to destroy many pathogens, it contains many different substances that individually may or may not have an effect on *C. neoformans* [157]. Thus far, it has been shown that one component within the DC lysosome can inhibit the growth of this yeast: cathepsin B. This cysteine protease is able to form a hole in

the cell wall that results in osmotic lysis of *C. neoformans* [145]. In addition, use of enzymatic inhibitors of cathepsin B enhances the antifungal activity, suggesting that this protease may be acting in a non-enzymatic fashion [145]. Further studies are underway in our laboratory to determine cathepsin B's mechanism of action against *C. neoformans*.

Our previous studies showed that in an acidic buffer (pH 5.5) the entire contents of the DC lysosome as well as a specific lysosomal component could kill *C. neoformans* [145,154]. The lysosome is rich in enzymes and other antimicrobial mediators [146,158], and we hypothesized that additional lysosomal components have antifungal properties. Therefore, in the present study, the contents of the DC lysosome were investigated to identify additional anticryptococcal molecules that have activity in similar conditions to the DC lysosome (pH 5.5). First, the lysosome extract was fractionated by molecular weight and individual fractions were tested for antifungal activity. Next, mass spectrometry was performed on the DC lysosome extract fractions to identify all of the components present. A panel of lysosomal components was selected for their antimicrobial properties and screened against *C. neoformans in vitro,* and those that showed antifungal activity were further studied in dose-dependent assays. Finally, those concentrations that inhibited the growth of the fungus were assessed for cytotoxic effects against mammalian cells near physiological pH (7.5). The purpose of the current study was to identify the anticryptococcal components of the DC lysosome and to assess their potential to be used as therapeutics.

Methods

2.2.1 Strains and Media

Cryptococcus neoformans strain H99 (serotype A, mating type α) was recovered from 15% glycerol stocks stored at -80°C and were cultured for 18 h at 30°C with shaking in yeast extract-peptone-dextrose (YPD) broth (BD Difco; Franklin Lakes, NJ) and collected by

centrifugation. Organisms were washed three times with sterile phosphate-buffered saline (PBS), and viable yeast cells were quantified using trypan blue dye exclusion in a hemocytometer. Cryptococcal cells were resuspended in appropriate medium at the concentration needed for each experiment.

2.2.2 Mice

Female and male BALB/c (*H-2*^{d}) mice were purchased from the National Cancer Institute/Charles River Laboratories and were housed either at Oklahoma State University Animal Resources or at The University of Texas at San Antonio Small Animal Laboratory Vivarium. Mice were handled according to approved guidelines, authors complied with the ARRIVE guidelines, and the study and experimental design was approved by the Oklahoma State University Institutional Animal Care and Use Committee (IACUC) or the University of Texas at San Antonio IACUC.

2.2.3 Generation of Bone Marrow-derived Dendritic Cells (BMDCs)

BMDC culture was performed as previously described [145,154]. Briefly, bone marrow was flushed from the femurs and tibiae of mice using sterile HBSS. Bone marrow cells were washed, counted, and plated in complete medium (RPMI-1640 supplemented with 10% FBS, 2 mM L-glutamine, 100 U penicillin/ml, 100 μg streptomycin/ml, and 50 mM 2-mercaptoethanol) supplemented with 20 ng/ml recombinant murine GM-CSF (Peprotech, Rocky Hill, NJ) at a concentration of $2x10^5$ cells/ml in 10ml ($2x10^6$ cells/plate). Cells were incubated at 37°C, 5% CO_2 for a total of eight days. At day 3 of incubation, 10ml complete medium + GM-CSF was added to each plate. At day 6 of incubation, half of the medium was removed, and 10ml fresh complete medium + GM-CSF was added. BMDCs were harvested at day 8, and DCs were purified by negative selection using anti-F4/80 microbeads (Miltenyi Biotec, Auburn, CA) (to remove contaminating macrophages) followed by positive selection using magnetically labeled

anti-CD11c microbeads according to the manufacturer's protocol (Miltenyi Biotec). Dendritic cell purity following this procedure was >90% by flow cytometry.

2.2.4 Generation of lysosomal extract from BMDCs

DC lysosomal extracts were obtained as previously described using the lysosome isolation kit (Sigma-Aldrich, St. Louis, MO) [145,154]. Briefly, DCs were lysed using 1X extraction buffer (Sigma-Aldrich) followed by homogenization with a PowerGen 700 homogenizer (Fisher Scientific, Pittsburgh, PA) using the 7x110mm homogenizer tip passed through the cells 15-20 times to disrupt 75-80% of the cells. The homogenized cells were then centrifuged at 1000 x *g* for 10 minutes to remove intact cells and cellular debris. The first supernatant was removed and centrifuged at 20,000 x *g* for 20 minutes to pellet lysosomes. Lysosome purity was verified by flow cytometry for lysosomal marker LAMP1 (BD Biosciences, San Jose, CA), which showed >90% pure lysosomes from this procedure. The pellet containing lysosomes was resuspended and sonicated for 20 seconds at 40% power on a Model 300 VT Ultrasonic Homogenizer (BioLogics, Inc., Manassas, VA), resulting in lysosome extract (600 mg/ml).

2.2.5 Fractionation and SDS-PAGE of lysosomal extract

Twelve molecular weight protein fractions of crude lysosomal extract were separated using the were separated from crude lysosomal extract GELFREE 8100 System (Expedeon, San Diego, CA). The system uses HEPES running buffer and Tris Acetate sample buffer (Expedeon), and the system was run according to manufacturer's instructions as previously described [159]. Briefly, lysosomal extract was mixed with sample buffer and loaded into the 8% Tris-Acetate cartridge (Expedeon). Following loading of the sample, the instrument was paused for sample collection at predefined intervals. This process was repeated until all 12 fractions were collected. After the collection of fractions, standard SDS-PAGE was performed. For this, a 12.5% Precast

Gel (Bio-Rad, Hercules, CA) was loaded with a Precision Protein Plus ladder (Bio-Rad) and each of the 12 samples. Gels were run for 55 minutes at 200V in Tris/glycine/SDS running buffer (Bio-Rad). Protein bands in the gel were stained using BioSafe Coomassie Stain (Bio-Rad), and a Gel Doc XR+ system (Bio-Rad) was used for visualization.

2.2.6 Anticryptococcal assays with lysosomal fractions

Anticryptococcal assays were performed as previously described [145,154]. Briefly, *C. neoformans* was resuspended in phosphate buffer (10 mM potassium phosphate monobasic supplemented with 2% RPMI-1640, pH 5.5) at concentration of 1 x 10^5 cells/ml and added to triplicate wells of a 96-well plate in a 50 µl volume. Lysosomal fractions were added to individual triplicate well sets at 50 µl volume for a final concentration of 50 µg/ml. Negative control wells included 50 µl *C. neoformans* with 50 µl of phosphate buffer to equal the volume of experimental wells. Positive control wells contained 50 µl *C. neoformans* and 50 µl DC lysosomal extract (at 50 ug/ml). Plates were incubated for 24 h at 37°C, 5% CO_2. Following incubation, cryptococcal cells in the plates were diluted in PBS and plated onto yeast extract-peptone-dextrose plates supplemented with 1 mg/ml chloramphenicol (YPD agar). The plates were incubated at 30°C for 2 days, and then CFUs were enumerated. Killing was defined as significantly reduced CFUs compared to the inoculum, and inhibition was defined as significantly reduced CFUs compared to *Cryptococcus* grown alone in phosphate buffer. Each assay was conducted in three independent experiments (n=3), with each condition performed in duplicate.

2.2.7 Identification of lysosomal proteins by HPLC-ESI-MS/MS

Peptide identifications were performed at the Institutional Mass Spectrometry Laboratory at The University of Texas Health Science Center at San Antonio as previously described [159]. Briefly, individual fractions were digested overnight at 37°C with trypsin (Promega, sequencing grade, Madison, WI) in 40 mM NH_4CO_3/10% ACN. The tryptic peptides were extracted with 0.1% TFA

followed by 0.1% TFA/50% ACN. The extracts were dried by vacuum centrifugation and resuspended in 0.5% TFA. Digests were analyzed by capillary HPLC-ESI-MS/MS using a Thermo Fisher LTQ linear ion trap mass spectrometer fitted with a New Objective PicoView 550 nanospray interface. On-line HPLC separation of the digests was accomplished with an Eksigent NanoLC micro HPLC: column, PicoFrit (New Objective; 75 μm id) packed to 10 cm with C18 adsorbent (Vydac; 218MS 5 μm, 300 Å); mobile phase A, 0.5% acetic acid/0.005% TFA; mobile phase B, 90% ACN/0.5% acetic acid/0.005% TFA; gradient 2 to 42% B in 30 min; flow rate, 0.4 μl/min. MS conditions were: ESI voltage, 2.9 kV; isolation window for MS/MS, 3; relative collision energy, 35%; scan strategy, survey scan followed by acquisition of data-dependent CID spectra of the seven most intense ions in the survey scan above a set threshold. Methionine oxidation and cysteine carbamidomethylation were considered as variable modifications for all searches. Scaffold 4.0 (Proteome Software, Portland, OR, USA) was used to conduct an X! Tandem subset search of the Mascot data followed by cross-correlation of the results of both searches. The Scaffold confidence levels for acceptance of peptide assignments and protein identifications were 95 and 99%, respectively. (Supplementary Table S2.1).

2.2.8 Anticryptococcal assays using DC lysosomal proteins

Anticryptococcal assays were performed as described above. Proteins were chosen based on previously-described antimicrobial activity, cysteine protease activity (similar to cathepsin B) [145] or calcium interference, which affects calcineurin, a known virulence factor for *C. neoformans* [160]. All proteins were derived from commercial sources and were >95% pure. Each protein was prepared at a concentration determined by either published studies or from our previous studies with lysosomal proteins [145,161-164]. Lysosomal proteins tested included calmodulin (1 mM) (Enzo Life Sciences, Farmingdale, NY), calnexin (50 μg/ml) (Novus Biologicals, Centennial, CO), coronin 1a (CORO1A) (25 μg/ml) (LSBio, Seattle, WA), cystatin B (5 μg/ml) (R&D Systems), human neutrophil elastase (HNE) (50 μg/ml) (LSBio), matrix

metalloproteinase-25 (MMP25) (50 μg/ml) (OriGene, Rockville, MD), myeloperoxidase (MPO) (18 μg/ml) (Novus Biologicals), recombinant nitric oxide synthase traffic inducer (NOSTRIN) (2 μg/ml) (Novus Biologicals), S100A6 (25 μg/ml) (Novus Biologicals), and striatin (100 μg/ml) (Novus Biologicals). Lysosomal proteins were diluted to a 2X concentration in 0.1mM phosphate buffer, pH 5.5 (phosphate buffer) and added to wells (50 μl) with $1x10^5$ cells/ml *C. neoformans* strain H99 yeast cells diluted in phosphate buffer (50 μl) to equal 100 μl in each well, and plates were incubated at 37°C, 5% CO_2 for 24h. After incubation, contents of wells were diluted and plated on YPD agar to quantify CFUs. Each protein was tested in three independent experiments (n=3), with each condition performed in triplicate. Additional anticryptococcal assays were performed to test dose-dependent activity of the DC lysosomal proteins. For these, proteins used were diluted from working concentrations to 1:10 and 1:100 with phosphate buffer for 10% and 1% concentrations, respectively, and the anticryptococcal assay was conducted as described above. Each antifungal assay was conducted in three independent experiments (n=3), with each condition performed in triplicate. Percent inhibition was defined as 100% (positive inhibition control) minus the experimental condition CFUs divided by the negative inhibition CFUs x 100%. Negative percent inhibition is the result of higher CFUs in the experimental compared to negative inhibition control.

2.2.9 Minimum inhibitory concentration (MIC) assays of anticryptococcal DC lysosomal proteins

Fungal growth inhibition of anticryptococcal DC lysosomal proteins were performed according to Clinical Laboratory Standards Institute (CLSI) guidelines M27: Reference Method for Broth Dilution Antifungal Susceptibility Testing of Yeasts, 4th edition [165-168]. Proteins were evaluated in 2-fold dilutions in concentrations ranging from 50 μg/ml to 0.0488 μg/ml (for HNE and MMP25), 25 μg/ml to 0.0224 μg/ml (for coronin), 18 μg/ml to 0.0176 μg/ml (for MPO), and 2 μg/ml to 0.0020 μg/ml (for NOSTRIN). Dilutions occurred in either phosphate

buffer (10 mM potassium phosphate monobasic supplemented with 2% RPMI-1640, pH 5.5) or RPMI-MOPS (RPMI-1640 supplemented with 34.5 g/L MOPS, pH 7.0) in a 96-well microtiter plate. MICs assay were conducted with a non-visible concentration ($0.5x10^3$ cells/ml) of *C. neoformans* strain H99 yeast cells. Plates were incubated for 48h at 35°C and optical densities of 490nm were taken on a Synergy HTX multi-mode plate reader (BioTek). MIC was defined as the lowest concentration of protein with no visible fungal growth. Each MIC assay was conducted in two independent experiments (n=2), with each condition performed in at least duplicate.

2.2.10 Checkerboard assay using AmpB in combination with lysosomal proteins against C. neoformans

Anticryptococcal activity of AmpB in combination with anticryptococcal lysosomal proteins was measured *in vitro* using a checkerboard method as previously described [169]. Assays were conducted in either phosphate buffer (pH 5.5) or RPMI-MOPS (pH 7.0) (both described above) in 100 µl total. A 96-well plate was used with rows A-G and columns 1-9 used to create the checkerboard titrations between AmpB and a lysosomal protein. Controls used were protein only (row H), AmpB only (column 10), cryptococcal growth control (column 11), and media control (column 12). Concentrations were evaluated in 2-fold dilutions ranging from 4 µg/ml to 0.062 µg/ml (for AmpB), 25 µg/ml to 0.098 µg/ml (for coronin), 50 µg/ml to 0.195 µg/ml (for HNE and MMP25), 72 µg/ml to 0.281 µg/ml (for MPO), and 2 µg/ml to 0.0078 µg/ml (for NOSTRIN). *C. neoformans* strain H99 ($0.5x10^3$ cells/ml) was used to evaluate efficacy of combinations. Plates were incubated for 48h at 35°C and optical densities of 490nm were taken on a Synergy HTX multi-mode plate reader (BioTek). Combinatory results were analyzed using the Fractional Inhibitory Concentration Index (FICI, a non-parametric model based on the Loewe additivity theory) whereas FICI ≤ 0.5 is synergistic, FICI 0.5-4 is indifference, and FICI ≥ 4 is antagonistic. FICIs were defined as the summation of individual FICs ($FICI = FIC_{Amp\ B} + FIC_{Protein}$) with FICs being defined as the MIC in combination divided by the MIC alone (FIC =

$MIC_{Combination}/MIC_{Alone}$). Off-scale MICs were considered to be the highest or lowest concentration tested in the assay. Each checkerboard assay was conducted in two independent experiments (n=2) for each lysosomal protein and for each buffer.

2.2.11 Time-kill assay

Rate of cryptococcal killing by lysosomal protein was measured using a time-kill assay as previously described [170]. *C. neoformans* strain H99 was tested at a concentration of $1x10^5$ cells/ml with lysosomal proteins at 2X their respective MICs (coronin: 25 μg/ml, HNE: 3.125 μg/ml, MPO: 18 μg/ml, MMP25: 0.78 μg/ml, NOSTRIN: 0.25 μg/ml) in 1000 μl of phosphate buffer (pH 5.5). Solutions were incubated for 48h at 35°C with 50 μl aliquots being taken at hours 0-8, 12, 24, 36, and 48 post inoculation. Aliquots were diluted and plated on YPD agar for 48h at 30°C to enumerate CFUs. Each time-kill assay was conducted in two independent experiments (n=2) for each protein along with fungus only growth control. Percent inhibition was calculated as described above with any negative inhibition values displayed as 0% inhibition.

2.2.12 Cytotoxicity assay

The macrophage cell line J774A.1 (TIB-67; ATCC, Manassas, VA) was used for cytotoxicity assays of the present study. J774A.1 cells were grown in cell culture medium (DMEM supplemented with 10% heat-inactivated fetal bovine serum (FBS), 10% NCTC-109, 1% non-essential amino acids, 100 U penicillin/ml, and 100 μg streptomycin/ml) in CytoOne T75 tissue culture flasks (USA Scientific, Ocala, FL) at 37°C, 5% CO_2. J774A.1 cells were passaged according to manufacturer's directions. For detection of cytotoxicity of DC lysosomal proteins, the Vybrant Cytotoxicity Assay Kit (Molecular Probes, Eugene, OR) was used according to manufacturer's instruction at near physiological pH (7.5). Briefly, J774A.1 cells were added to a 96-well plate in triplicate at a concentration of 10×10^5 cells/ml in 25 μl. Lysosomal proteins were prepared similarly to the anticryptococcal assay except cell culture media was used for

dilutions instead of phosphate buffer. Each protein was used at 25 µl per well. Controls included no-cell, untreated cells, and fully lysed cells. All wells were prepared in triplicate. Plates were incubated for 24 h at 37°C, 5% CO_2. After incubation, 50 µl of reaction mixture was added to all wells. Fluorescent readings were taken on a Synergy HTX multi-mode plate reader (BioTek, Winooski, VT) with filters for 530/25 (excitation) and 590/20 (emission). Each cytotoxicity assay was conducted in three independent experiments (n=3), with each condition performed in triplicate.

2.2.13 Statistical analysis

Unpaired two-tailed t-tests were used to compare CFUs using GraphPad Prism version 5.00 for Windows (GraphPad Software, San Diego, CA). Significant differences were defined as $p < 0.05$ and $\alpha = 0.05$ unless noted otherwise.

2.3 Results

2.3.1 C. neoformans growth is inhibited by DC-derived lysosomal fractions

Previous studies have shown that *C. neoformans* growth can be inhibited by DCs [76,153] as well as by DC-derived lysosomal extract [154]. Our previous studies showed that cathepsin B, which is found in the DC lysosome, can also significantly inhibit the growth of the fungus [145]. In order to identify other proteins within the lysosome that can inhibit the growth of *C. neoformans*, DC-derived lysosomal extract was first fractionated by molecular weight, and fractions were verified by SDS-PAGE (Figure 2.1A). Protein concentration was measured in each fraction, and those containing at least 50 µg/ml protein (the protein concentration that was antifungal for DC lysosomal extract [154]) - fractions 1, 7, 8, and 10 - were used in anticryptococcal assays. *C. neoformans* strain H99 was incubated at 1 x 10^5 cells/ml with either individual fractions in phosphate buffer (pH 5.5), total extract in phosphate buffer, or in

phosphate buffer alone for 24 h at 37°C, 5% CO_2. All fractions that were tested (fractions 1, 7, 8, and 10) showed significant killing ($p < 0.0001$) of the cryptococcal growth when compared to the *C. neoformans* inoculum (Figure 2.1B). These data show that multiple fractions of DC lysosomal extract have anticryptococcal activity, and therefore, there are multiple compounds within the lysosomal extract that can kill *C. neoformans* or inhibit cryptococcal growth. In order to further identify individual proteins within the lysosomal extract with anticryptococcal activity, the fractions were analyzed by mass spectrometry to identify the contents of each fraction. Analysis revealed over 3000 different proteins present within the lysosomal fractions (Supplementary Table S2.1).

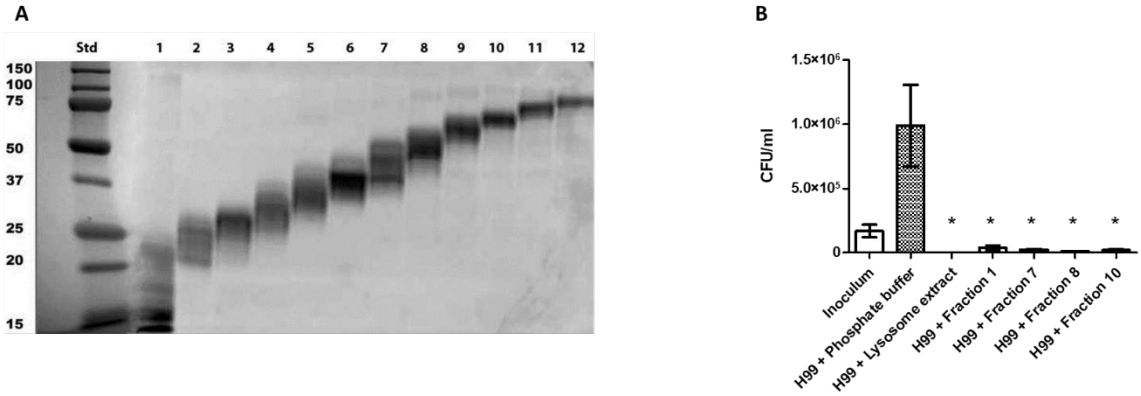

Figure 2.1. Fractions of DC Lysosomal Extract Have Anticryptococcal Activity. (A) Crude DC-derived lysosomal extracts were separated by molecular weight using a GELFrEE™ 8100 system into 12 different fractions and further resolved by standard SDS-PAGE. Proteins in the 12.5% gels were stained using BioSafe Coomassie Stain and visualized using a Gel Doc XR+ system. (B) *C. neoformans* serotype A strain H99 yeast cells (1 x 10^5 cells/ml) were incubated in phosphate buffer (pH 5.5) with whole lysosomal extract or fractions of lysosomal extract for 24 h at 37°C, 5% CO_2, following which CFUs in the wells were determined. Data shown are means ± standard errors of the means (SEM) of the results of three independent experiments (n=3), with each condition performed in duplicate. Two-tailed t-tests comparing H99 inoculum to each treatment were performed with asterisks (*) indicating significantly lower CFUs of treatment compared to the H99 inoculum (fraction 8: $p = 0.0001$, all others: $p < 0.0001$).

2.3.2 DC Lysosomal Proteins Have Anticryptococcal Activity

In order to determine the anticryptococcal potential of DC lysosomal proteins, ten different lysosomal proteins were tested for anticryptococcal activity. From the >3000 proteins identified by mass spectrometry, ten test proteins were selected based on potential antimicrobial activity, such as those that are known antimicrobial peptides or cysteine proteases [160,171-173]. Concentrations of individual proteins used in our anticryptococcal assay were based upon either prior published concentrations [161-164] or were based on our previous studies with cathepsin B [145,161-164], where concentrations of 50 and 10 μg/ml were used. Specific protein concentrations used in this study are provided in the methods section. *C. neoformans* strain H99 was incubated at 1 x 10^5 cells/ml in a 50 μl volume separately with each protein in sterile 0.1 mM phosphate buffer, pH 5.5 (phosphate buffer) or in phosphate buffer alone for 24 h at 37°C, 5% CO_2, followed by diluting then plating on YPD agar to quantify CFUs. Percent cryptococcal inhibition was defined as CFUs of the experimental condition (*C. neoformans* incubated with test protein) divided by the CFUs of the control condition (*C. neoformans* incubated with phosphate buffer alone). We observed that incubation of *C. neoformans* with five of the lysosomal proteins (Coronin, HNE, MMP25, MPO, NOSTRIN) led to a significant ($p < 0.0001$) reduction of CFUs when compared to the *C. neoformans* grown in phosphate buffer alone which is shown as a high percent inhibition (Figure 2.2A), while the remaining five proteins either did not inhibit fungal growth with low percent inhibition (cystatin B, striatin) or significantly enhanced fungal growth (calmodulin, $p < 0.0001$; calnexin, $p < 0.0001$; S100A6, $p = 0.0034$), as shown by negative percent inhibition (Figure 2.2B).

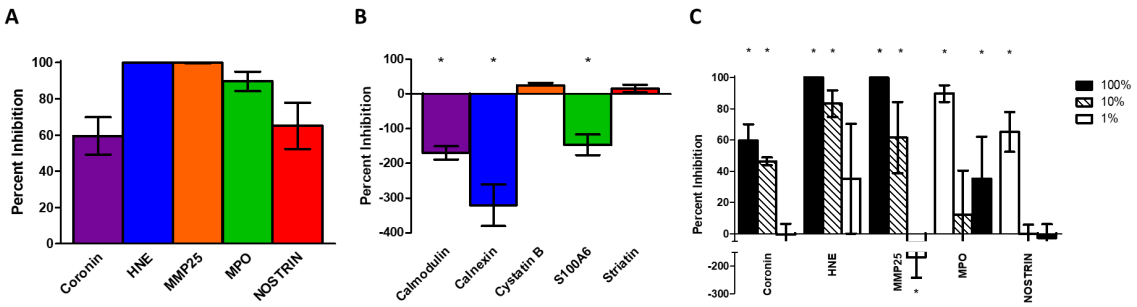

Figure 2.2. Cryptococcal Inhibition by Lysosomal Proteins. *C. neoformans* strain H99 yeast cells were grown in YPD broth for 18h in a 30°C shaking incubator, then washed and adjusted to a concentration of 1 x 10^5 cells/ml. Fungi were incubated in phosphate buffer alone (pH 5.5) or in phosphate buffer with each protein for 24h at 37°C, 5% CO_2, and percent inhibition defined as 100% - (protein CFUs/control CFUs) x 100%. Data shown are means ± standard error of the means (SEM) of the percent inhibition of three independent experiments (n=3), with each condition performed in triplicate. (A) Lysosomal proteins that showed significant cryptococcal inhibition (*) compared to H99 in phosphate buffer alone as indicated by two-tailed t-tests ($p < 0.0001$ for all). (B) Lysosomal proteins that showed no cryptococcal inhibition or significantly enhanced growth (*) by two-tailed t-tests when compared to H99 in phosphate buffer alone ($p = 0.0034$ for S100A6, $p < 0.0001$ for calmodulin and calnexin). (C) Reduced concentrations of select lysosomal proteins with white bars, striped bars, and black bars indicating protein concentration at 100%, 10%, and 1%, respectively. Two-tailed t-test comparing fungal growth with protein against growth in phosphate buffer alone confirmed significant inhibition (*) at 10% for coronin ($p < 0.0001$), HNE ($p < 0.0001$), and MMP25 ($p = 0.0008$). MPO showed significant inhibition at 1% (p = 0.0213) but not 10% while NOSTRIN was not able to reduce growth at any of the lower concentrations. At 1% original concentration, MMP25 significantly (p =0.0010) increased cryptococcal growth.

2.3.3 Cryptococcal Inhibition Is Dose-Dependent

To further elucidate the effective anticryptococcal concentration of each lysosomal protein, similar assays with reduced protein concentration were conducted on the five proteins that showed cryptococcal inhibition. Each of the five proteins were diluted to 10% and 1% of original concentration and incubated under the same conditions. Of those tested (coronin, HNE,

MMP25, MPO, and NOSTRIN), only coronin ($p < 0.0001$), HNE ($p < 0.0001$), and MMP25 ($p = 0.0008$) significantly inhibited cryptococcal growth at the 10% protein concentration, but did not inhibit growth at the 1% concentration (Figure 2.2C). Surprisingly, MMP25 significantly enhanced fungal growth ($p = 0.0010$) at 1% of the original concentration when compared to growth in phosphate buffer alone. While MPO was not able to reduce the growth of H99 at 10% concentration, when tested at 1%, it did have the capacity to significantly inhibit ($p = 0.0213$) the growth of the fungus. NOSTRIN was not effective at either of the reduced concentrations.

2.3.4 Minimum Inhibitory Concentration (MIC) of Anticryptococcal Lysosomal Proteins

Next, in order to verify that the concentrations used for the previous experiments were similar to the minimum inhibitory concentrations (MIC), the five anticryptococcal lysosomal proteins were evaluated for MICs against *C. neoformans* strain H99 yeast cells. Highest concentrations of proteins started at the same maximum value as previous assays and ranged from 50 μg/ml to 0.0488 μg/ml (for HNE and MMP25), 25 μg/ml to 0.0224 μg/ml (for coronin), 18 μg/ml to 0.0176 μg/ml (for MPO), and 2 μg/ml to 0.0020 μg/ml (for NOSTRIN). Proteins were assessed in phosphate buffer (pH 5.5) as in our antifungal assays above as well as a more physiological relevant condition in RPMI-MOPS (pH 7.0), which is the media typically used in fungal MIC assays. Assays were completed over 48h at 35°C as per Clinical and Laboratory Standards Institute (CLSI) [165-168]. Results for these assays are summarized in Table 2.1. When testing in lysosomal-like conditions (pH 5.5) HNE, MMP25, and NOSTRIN retained similar anticryptococcal efficacy. In addition, these three compounds also retained some ability to inhibit yeast growth at pH 7.0. MPO was unable to inhibit cryptococcal growth at the highest tested concentration of 18 μg/ml under both conditions and did not replicate its previous effectiveness (Figure 2A). MIC values for coronin were not able to be determined in these assays.

Due to the nephrotoxicity associated with high doses of Amphotericin B (AmpB), examining methods to increase efficacy and lower dosage has become an area of intense research [9,51,174]. One method is the use of a combination of compounds that, by themselves, display anticryptococcal properties, such as current guidelines that advise treating cryptococcal meningitis using combination therapy with AmpB and flucytosine [47]. Therefore, we tested our anticryptococcal lysosomal proteins in combination with AmpB against the fully virulent *C. neoformans* strain H99 using a checkerboard method and categorized data based on the fractional inhibitory concentration indices (FICI) [169]. While still retaining their previously stated anticryptococcal capacity, none of the lysosomal proteins showed any synergistic effects when used in combination with AmpB (Supplemental Table S2.2). Each protein/AmpB combination scored between 1.0 and 1.8 placing them comfortably within the indifference category (0.5-4.0) and provided neither antagonistic nor synergistic results.

Table 2.1. Minimum inhibitory concentrations (MIC) of anticryptococcal lysosomal proteins in phosphate buffer (pH 5.5) or RPMI-MOPS (pH 7.0).

	Minimum Inhibitory Concentration (μg/ml)	
	Phosphate Buffer (pH 5.5)	**RPMI-MOPS (7.0)**
Coronin	Undetermined[1]	Undetermined[1]
HNE	3.125	50
MPO	>18[2]	>18[2]
MMP25	0.78	6.25
NOSTRIN	0.25	2

[1]ODs of the protein were higher than yeast growth. [2]Growth present in the highest tested concentration.

2.3.5 Time-Kill Kinetics of Lysosomal Proteins against C. neoformans

MIC assays are useful starting points for understanding antimicrobial properties of unknown compounds, since they have been standardized by various laboratories and agencies. The time-kill assay studies the kinetic rates of inhibition over a period of time rather than examining only the end result. While they give great quantitative results and the ability to explore fungicidal rates,

their methods are not as widely uniform and they can become time consuming the more time points and concentration one examines [175]. For this, we used a modified version of the method proposed in a paper by Klepser *et. al* which has since been cited over 200 times since its publication [170]. Cryptococcal cells were incubated with 2X MIC values (listed in Table 2.1 or 2X highest concentration tested if none could be determined) in an acidic phosphate buffer (pH 5.5) for 48h. As conditions change within the test chamber, properties of the proteins may also be altered, therefore, pH was monitored throughout the study, but we did not observe any changes in pH over the course of the study. We measured the percent inhibition of cryptococcal growth over time using the five anticryptococcal lysosomal proteins (Figure 2.3). Three of the five (NOSTRIN, HNE, and MPO) displayed sustained inhibition starting from as early as three hours post inoculation. Meanwhile, at the 3h time point, coronin and MMP25 exhibited intermediate and no inhibition, respectively. However, by 24 hours, the latter two proteins showed inhibition and caught up to the other three by 48 hours.

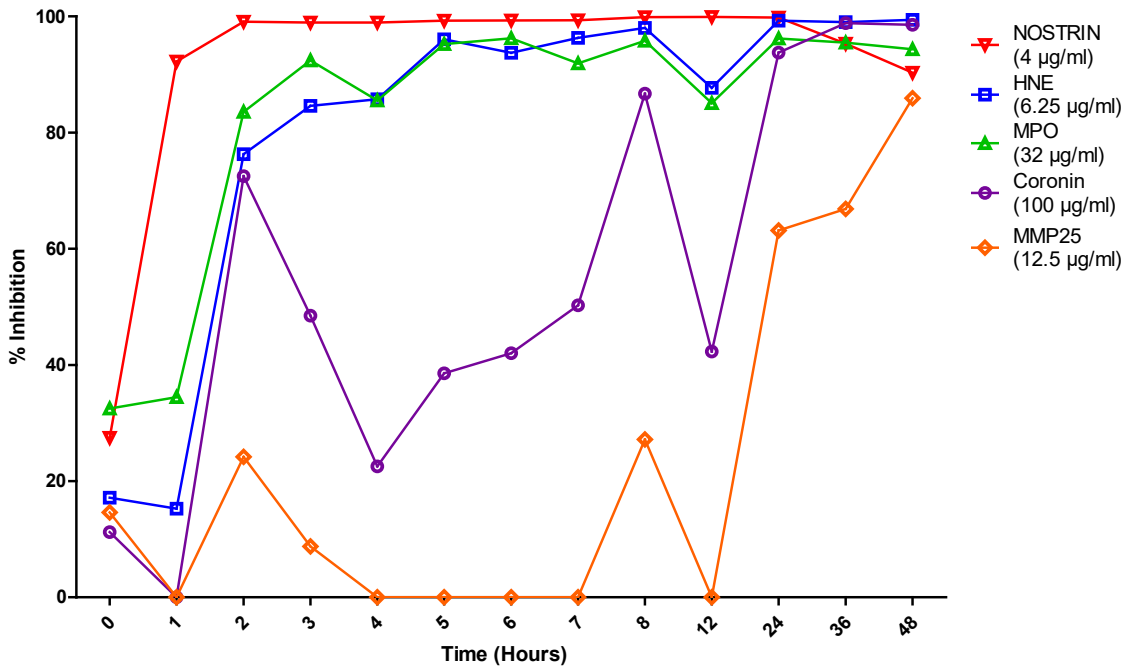

Figure 2.3. Time-kill Plots Demonstrating Cryptococcal Inhibition by Lysosomal Proteins. *C. neoformans* strain H99 yeast cells were grown in YPD broth for 18h in a 30°C shaking incubator, then washed and adjusted to a concentration of 1 x 10^5 cells/ml. Fungi were incubated in phosphate buffer alone (pH 5.5) or in phosphate buffer with each protein at 2X MIC for 48h at 35°C. Aliquots were taken and plated for CFUs for each hour 0-8, and at 12, 24, 36, and 48 hours. Percent inhibition is defined as 100% - (protein CFUs/control CFUs) x 100%. Data shown are means of two independent experiments (n=2). Lysosomal proteins NOSTRIN, HNE, and MPO showed sustained cryptococcal inhibition by 3 hours post inoculation while coronin displayed intermediate inhibition and MMP25 exhibited no cryptococcal inhibition at the same time point. By 24 hours all proteins presented with cryptococcal inhibition through 48 hours.

2.3.6 Cytotoxicity of DC Lysosomal Proteins

To test the relative cytotoxicity of these anticryptococcal lysosomal proteins on mammalian cells, a murine macrophage cell line (J774A.1) was used in conjunction with the Vybrant Cytotoxicity Assay Kit (G6PD assay) (Molecular Probes, Eugene, OR). Mammalian cells were incubated with the highest concentration of anticryptococcal protein (stated in methods section) in cell culture media or in cell culture media alone for 24 h at 37°C, 5% CO_2, then cytotoxicity assay was performed at near physiological pH (7.5). After fluorescence was normalized to control wells (J774A.1 macrophages in cell culture media alone), percent cytotoxicity was defined as fluorescence of experimental wells (macrophages and proteins) divided by positive control wells (macrophages and cell-lysis buffer). A compound is defined as "cytotoxic" if there is a reduction of more than 30% of viable cells when compared to control wells [176]. All proteins showed low cytotoxicity (<20%) at the highest concentration tested for cryptococcal inhibition assays (Figure 2.4).

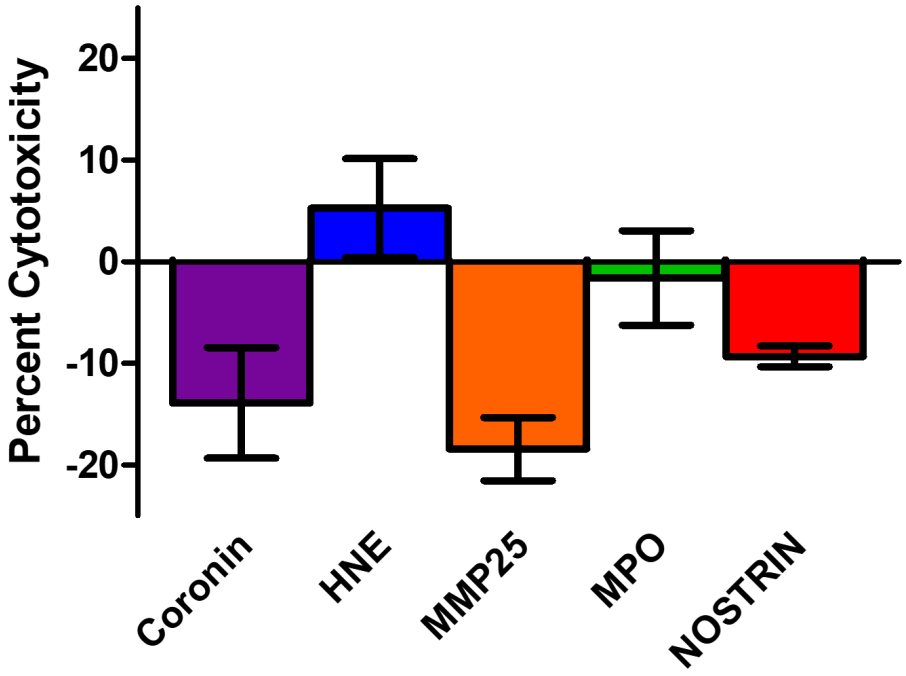

Figure 2.4. Cytotoxicity of Lysosomal Proteins. J774A.1 macrophages (5 x 10^5 cells/ml) were incubated in cell culture media alone or cell culture media with each antifungal protein at 100% concentration for 24 h at 37°C, 5% CO_2, and percent cytotoxicity was calculated as per manufacturer's instructions (pH 7.5). Data shown are means ± standard error of the means (SEM) of the cumulative results of three independent experiments (n=3), with each condition performed in triplicate. All proteins tested had low cytotoxicity (<20%).

2.4 Discussion

The primary function of the DC lysosome is to break down many different biomolecules including pathogens that may cause harm to a host in order to generate peptide fragments for antigen presentation [157,177]. This rapid degradation by the lysosome favors presentation through the MHC-II pathway rather than cross presentation via MHC-I [178]. Studies have shown that it can kill a wide variety of pathogens regardless of whether they are fungal, bacterial, or viral [179-183]. Previous studies have shown that *C. neoformans* traffics to the lysosomal compartment of DCs and is killed by its components [153,154]. It was also shown that contents of

the DC lysosomal extract have activity against the fungus *in vitro* [145,154]. Furthermore, the DC lysosomal component cathepsin B can inhibit or kill the pathogen [145]. Due to the problems associated with current anticryptococcal drug therapies, finding new sources of treatment has become a major area of research.

To combat these ever-changing problems, most current research focuses on either discovering novel antifungal drugs or repurposing older drugs [61,184-186]. Our research focuses on identifying DC lysosomal components that are anticryptococcal and determining how these can be used to develop immune-based therapies to combat cryptococcosis. In accordance with our previous study on DC lysosomal proteins and their anticryptococcal effects, our current study has shown there are multiple DC lysosomal compounds that can inhibit and/or kill *C. neoformans* in an acidic buffer (pH 5.5) in a dose dependent manner. Three (HNE, MMP25, MPO) of the five compounds that showed anticryptococcal activity are known proteases that have been shown to have antimicrobial activity [187-189]. The other two are both associated with antimicrobial activity by other means: coronin is an actin binding protein that is involved with phagocytosis in leukocytes [190] and NOSTRIN modulates the release of the oxidative stressor nitric oxide [191]. Several of these proteins still displayed inhibition at reduced concentrations which shows dose-dependent activity. Contrary to these results, however, reduced concentrations of MMP25 showed significant increase in fungal growth and may be a cause for concern if used as a therapeutic.

In order to verify that the concentrations used in these studies were in the range of minimum inhibitory concentration (MIC) concentrations, we tested the five antifungal proteins (Fig 2) (coronin, HNE, MPO, MMP25, and NOSTRIN) in MIC assays in accordance with CLSI guidelines [165-168]. Three proteins (HNE, MMP25, and NOSTRIN) showed promising results, as not only did they recapitulate their effects in low pH, but also displayed some anticryptococcal activity at the higher pH, albeit at a lower efficiency. This was expected as pH changes can affect the activity of many lysosomal proteins, notably cathepsins [192]. Despite the lower activity,

these results point to a future of promising therapeutics for systemic cryptococcosis, since some of these proteins can also be antifungal at neutral pH. Two proteins had different MIC results compared to our original lysosomal assays. However, differences in methodology between standard MIC assays (conducted in non-CO_2 conditions and at 35°C, as is standard MIC procedures in the field) and our antifungal assays (conducted at 37°C, 5% CO_2), may have contributed to these discrepancies.

Currently, there are only a few classes of antifungal compounds, all of which can become toxic to the host at high concentrations [9,174]. Despite being the drug of choice when treating cryptococcal meningitis, AmpB does have these same concerns, especially targeting the kidneys, causing nephrotoxicity. We sought ways to reduce standard treatment concentrations by investigating synergistic activity that may exist between it and our anticryptococcal lysosomal proteins. However, none of the compounds showed any synergy when combined with AmpB at any of concentrations tested. These results are not too surprising owing to the fact that the H99 strain, while fully virulent, is still susceptible to AmpB at low doses and other compounds may not show synergistic effects. These results may differ and show synergistic effects when testing against a cryptococcal strain that is resistant to AmpB. Furthermore, synergistic combinations tend to target both pathogenic processes and cell growth to completely inhibit a fungal infection [193]. More pre-clinical research in this area is needed as these studies were conducted *in vitro*. We also wanted to further understand the kinetics of these anticryptococcal lysosomal proteins, so a time-kill assay was conducted to evaluate growth over 48 hours, the same as a standard MIC assay. Three (HNE, MPO, NOSTRIN) of the five proteins showed sustained inhibition quickly, within 3h post-inoculation. However, by the time point of our typical lysosomal assays (24h), the remaining lysosomal proteins all showed inhibition of cryptococcal growth, which was sustained through the 48h experiment.

Despite previous reports of antimicrobial activity against bacterial pathogens [194-197] and/or interference with virulence pathways (such as the calcium-binding pathway [160,198]), several proteins tested in this study (calmodulin, calnexin, cystatin B, S100A6, and striatin) showed either no cryptococcal inhibition or enhanced fungal growth. We hypothesized that this enhanced growth may be attributed to secretion of nutrients or trace metals that may enhance cryptococcal growth and we are currently analyzing the contents of media in these conditions. Additional studies are also underway in our laboratory to examine the mechanism(s) by which these components enhance cryptococcal growth. Cystatin B is a cysteine protease that inhibits cathepsin B by tightly binding to it [199]. While cystatin B did not show any efficacy in our studies, previous work has shown that when cathepsin B and other inhibitors (calpain and CA-074) are used in conjunction with cathepsin B, they lead to increased inhibition *C. neoformans* growth when compared to cathepsin B treatment alone [145]. Striatin proteins have a diverse range of functions in both filamentous fungi and mammals including the signaling of motor functions and cell division [200-202]. This family and the closely related pyristriatins that have select antimicrobial activity against Gram positive bacteria and some filamentous fungi as well as yeasts [195]. When tested against our yeast, *C. neoformans*, striatin showed no change in the cryptococcal growth. The S100 series of proteins are known antimicrobial peptides and are also known as alarmins, and these proteins have a range of antimicrobial activity [203,204]. S100A8 and S100A9 form a heterodimer named calprotectin, which has anticryptococcal activity by the depletion of zinc from the fungus [205-207]. However, the related protein S100A6, which has similar zinc-binding potential, significantly enhanced the cryptococcal growth [208]. The final two proteins tested, calmodulin and calnexin, also significantly enhanced cryptococcal growth. Calmodulin is a calcium binding protein that activates calcineurin and is implicated in increased pathogen defense [160,209]. The membrane associated protein calnexin is also a signaling protein that functions as a chaperone but has been also associated with increased adaptive immunity [210]. DCs that express higher than normal levels of calnexin were able to induce T cell function

greater than unmodified DCs [211]. It is currently unknown why these proteins had either limited or opposite effects than previously stated literature would suggest or by what means they increased cryptococcal growth.

To our knowledge, the cytotoxicity of DC lysosomal proteins has not been tested in mammalian cells. Our findings indicated that of the proteins tested, none were cytotoxic at the concentrations needed for anticryptococcal activity. This shows promise that these compounds may be used further in the treatment for cryptococcosis. However, the physiological relevance and bioavailability of these compounds in a live model remains to be seen. Our laboratory is currently in the process of testing these lysosomal components in a murine model of cryptococcosis. Furthermore, the complex interactions of these proteins with other proteins residing within the lysosome has not been investigated. None of these proteins are usually present alone or act upon pathogens individually, and we recognize that there are many more proteins and protein combinations that may add to the complexity of these interactions. To help us understand these problems, we are actively working on elucidating the mechanism(s) of action for these anticryptococcal proteins, studying interaction of multiple lysosomal proteins, and identifying the mechanism(s) of enhanced cryptococcal growth in our lab.

The present study has investigated the anticryptococcal activity of specific proteins of the DC lysosome. Five different fractions showed similar anticryptococcal activity to the entire extract. Mass spectrometry revealed many different compounds present within this extract that could potentially inhibit cryptococcal growth. Our results show that not only are there several that indeed inhibit cryptococcal growth, but these are also not cytotoxic to mammalian cells at these concentrations. From these findings, novel immune-based anticryptococcal treatments may be developed from immune-based proteins that could ease the burden brought on by this deadly disease.

2.5 Supplemental Materials

Table S2.1. Contents of dendritic cell lysosomal fractions. Mass spectrometry was conducted on each of the twelve dendritic cell (DC) lysosomal fractions (see methods for description). Each identified protein is listed along with the gene name, and the number of hits for each protein in each fraction is listed under the corresponding fraction.

https://static-content.springer.com/esm/art%3A10.1038%2Fs41598-021-92991-6/MediaObjects/41598_2021_92991_MOESM2_ESM.xlsx

Table S2.2. Fractional inhibitory concentration indices (FICI) of amphotericin B in combination with lysosomal proteins against *C. neoformans*.

Combination / Media (pH)	Amphotericin B in combination with				
	Coronin	**HNE**	**MPO**	**MMP25**	**NOSTRIN**
Phosphate Buffer (5.5)	Indifference (1.28 ± 0.00)	Indifference (1.78 ± 0.50)	Indifference (1.03 ± 0.25)	Indifference (1.18 ± 0.04)	Indifference (1.01 ± 0.04)
RPMI-MOPS (7.0)	Indifference (1.07 ± 0.07)	Indifference (1.25 ± 0.03)	Indifference (1.50 ± 0.50)	Indifference (1.13 ± 0.15)	Indifference (1.01 ± 0.20)

Numbers in parenthesis are values for FICI ± SEM for two independent experiments.

CHAPTER III

PROTECTIVE INTERACTION OF HUMAN PHAGOCYTIC APC SUBSETS WITH *CRYPTOCOCCUS NEOFORMANS* INDUCES GENES ASSOCIATED WITH METABOLISM AND ANTIGEN PRESENTATION †

† This chapter is reproduced with slight modifications from the following publication:

Nelson, B.N., Daugherty, C.S., Sharp, R.R., Booth, J.L., Patel, V.I., Metcalf, J.P., Jones, K.L., Wozniak, K.L. (2022). Protective Interaction of Human Phagocytic APC Subsets with *Cryptococcus neoformans* Induces Genes Associated with Metabolism and Antigen Presentation. *Frontiers in Immunology*, 10(1054477). Reprinted with permission.

Abstract

Cryptococcal meningitis is the most common cause of meningitis among HIV/AIDS patients in sub-Saharan Africa, and worldwide causes over 223,000 cases leading to more than 181,000 annual deaths. Usually, the fungus gets inhaled into the lungs where the initial interactions occur with pulmonary phagocytes such as dendritic cells and macrophages. Following phagocytosis, the pathogen can be killed or can replicate intracellularly. Previous studies in mice showed that different subsets of these innate immune cells can either be antifungal or permissive for intracellular fungal growth. Our studies tested phagocytic antigen-presenting cell (APC) subsets from the human lung against *C. neoformans*. Human bronchoalveolar lavage was processed for phagocytic APCs and incubated with *C. neoformans* for two hours to analyze the initial interactions and fate of the fungus, living or killed. Results showed all subsets (3 macrophage and

3 dendritic cell subsets) interacted with the fungus, and both living and killed morphologies were discernable within the subsets using imaging flow cytometry. Single-cell RNA-seq identified several different clusters of cells which more closely related to interactions with *C. neoformans* and its protective capacity against the pathogen rather than discrete cellular subsets. Differential gene expression analyses identified several changes in the innate immune cell's transcriptome as it kills the fungus including increases of TNF-α (*TNF*) and the switch to using fatty acid metabolism by upregulation of the gene *FABP4*. Also, increases of TNF-α correlated to cryptococcal interactions and uptake. Together, these analyses implicated signaling networks that regulate expression of many different genes – both metabolic and immune - as certain clusters of cells mount a protective response and kill the pathogen. Future studies will examine these genes and networks to understand the exact mechanism(s) these phagocytic APC subsets use to kill *C. neoformans* in order to develop immunotherapeutic strategies to combat this deadly disease.

3.1 Introduction

Cryptococcus neoformans is an opportunistic fungal pathogen that causes pneumonia and fatal meningitis in immunocompromised individuals [125,126]. This fungus has an environmental niche that includes decayed wood and pigeon droppings. Humans frequently encounter either their yeast cells or desiccated spores which are then inhaled into the lungs [106,127]. The polysaccharide capsule surrounding the fungus allows it to ward off many first line innate immune defenses of the lung, but cell-mediated immunity (CMI), provided by Th1-type $CD4^+$ T cells, is usually sufficient for clearance of the pathogen before any symptoms arise [126,141,212]. However, in situations where the person has a suppressed immune system, such as during immunosuppressive therapy for organ transplants or HIV/AIDS, *C. neoformans* can survive and begin to replicate within the lung. Once established, pulmonary cryptococcosis presents clinically as pneumonia [128,129]. If left untreated, *C. neoformans* can traffic to the brain, presumably inside macrophages, causing highly fatal cryptococcal meningitis [213,214]. Cases of

cryptococcal meningitis are highly associated with AIDS, which has led the CDC to name it as an AIDS-defining illness [130,131]. Evidence for this was demonstrated in an analysis of the 2014 Joint UN Programme on HIV and AIDS which estimated 223,100 yearly cases of these co-infections with a vast majority (73%) occurring within sub-Saharan Africa [31]. These cases are also frequently lethal with mortality rates exceeding 80% worldwide. These numbers are unacceptably high, and reduction of the disease burden among affected individuals is paramount.

After inhalation, *C. neoformans* interacts with pulmonary innate immune cells including macrophages and dendritic cells (DCs) [138,215]. Effective immune responses will result in either phagocytosis and destruction of the fungal cell or sequestration and development of a cryptococcal granuloma [216]. However, in immunocompromised individuals, killing does not always happen post-phagocytosis, and instead the pathogen will survive and begin to replicate within host macrophages [156,214]. From this point, it can travel throughout the rest of the body intracellularly via the bloodstream all while effectively evading the immune system [217]. Normally, the blood brain barrier (BBB) will prevent pathogens or other unwanted substances from entering the central nervous system (CNS), however, *C. neoformans* has developed ways of crossing this obstacle either by direct transcellular migration of the fungus across the BBB or intracellularly within a trafficking immune cell [41-44]. After traveling to the brain inside a pulmonary phagocyte, *C. neoformans* can exit the cell either by lytic or non-lytic means and cause infection and damage to the brain tissue [45,46].

Cryptococcal interactions with innate immune cells have been studied extensively in the context of cell origin, lineage, and host condition. The first-line defenders in the pulmonary cavity to recognize *C. neoformans* are tissue resident macrophages and DCs [63]. In both mice and humans, these innate phagocytes can kill the pathogen through both oxidative and non-oxidative means [154,155,218,219]. And while both immune cell types are antigen-presenting cells (APCs), DCs are the primary antigen-presenting cells to present *Cryptococcus* antigens to

naive T cells to initiate the CMI that is necessary in eradicating the disease [75]. Following infection, neutrophils, another innate phagocyte, can infiltrate into the pulmonary tissue. Although *C. neoformans* can be phagocytosed by neutrophils, depletion of these cells in murine models leads to increased clearance of *C. neoformans*, suggesting that neutrophils may be detrimental [80,81,220]. For cryptococcal clearance, the adaptive immune system relies on a Th1 and Th17 profile while Th2 cytokines correlate with fungal dissemination [128]. Previous studies have shown that IFN-γ, IL-12, IL-17A, and IL-23 are beneficial for host survival and IL-13 and IL-33 lead to exacerbation of disease [111,221-223]. Despite this, there is also evidence that depending on the activation phenotype, macrophages can either destroy the pathogen or harbor it intracellularly allowing for persistence of the fungus. Major factors of this include the polarization of the macrophage to the antifungal M1 (by cytokines IFN-γ and IL-12) or more permissive M2 phenotype (by cytokines IL-4, IL-5, and IL-13) [214,224,225]. However, polarization of the macrophage does not occur in the naïve macrophages in the early preliminary stages of cryptococcosis, and there may be other factors including cell origin and subsets that can account for the differences in disease progression.

Current methods of treating cryptococcosis and cryptococcal meningitis include a variety of antifungal drugs including fluconazole, flucytosine, and amphotericin B [58,133,134]. The gold standard for treatment of this disease includes a combination therapy of amphotericin B with flucytosine [47]. However, due to high cost, lack of availability, and oversight for the compliance of the treatment regime in the most needed areas, fluconazole monotherapy is the usual treatment method [226]. Complicating these problems, many of these antifungal drugs target ergosterol, the fungal analogue of cholesterol, and is often associated with toxicity to host cells at recommended doses [9]. The combination of drug-mediated host cell toxicity, lack of antifungal drug development, and emerging resistance to current therapies, make it clear that there is need for additional treatment methods [227,228]. Fortunately, there has been recent work on improving

the immune response to combat *C. neoformans* through the use of immunotherapeutics. These treatments include a variety of ways to enhance the body's intrinsic immune systems to better recognize and eliminate the fungus. Options include the use of cryptococcal proteins as antigens to initiate protection through CMI [229,230]. All of these treatments must strike a balance between the protective Th1 responses and excessive inflammation that could worsen disease outcomes [117]. In a mouse model of cryptococcal infection, adjunctive IFN-γ increases the antifungal effects of amphotericin B both *in vivo* and *in vitro* [120,121]. Despite the extensive work in this model, there is limited data directly applicable to human disease. However, these limited studies have shown that levels of IFN-γ are associated with protection in patients and that immunotherapies with adjunctive IFN-γ are well tolerated in humans and can lead to positive outcomes [122-124]. The exact mechanisms whereby this therapy optimizes immune responses, specifically in first-line defenders such as lung macrophages and DCs is unknown.

Recently, subsets of macrophages and DCs of both human and mouse lungs have been characterized [63], and their lineages have been defined in recent years [91,231]. In the pulmonary airways and tissues of humans, macrophages have been historically divided into alveolar macrophages (AMs), which are in the alveolar cavity, and interstitial macrophages (IMs), which exist in the interstitium [232]. In addition to differences in surface marker expression, there are differences of inflammatory capacity and phagocytic index between the subsets [233]. DCs are similarly subdivided based on their surface markers, expression of pattern recognition receptors, and their ability to stimulate T cell proliferation [234]. Due to these differences of lineages between tissue resident cells and circulating cells, it is important to isolate and investigate specifically the cell subset(s) *C. neoformans* comes into contact within the lungs [235-238] and the fate of the cryptococcal cells following uptake. Previous work has shown that there are indeed differences in the fate of this fungus (and other pathogens) depending on which subset it encounters. *Mycobacterium tuberculosis* (Mtb), another pulmonary pathogen which has

a similar disease progression as *C. neoformans*, has differential interactions with macrophage subsets [239,240]. Specifically, murine IMs kill Mtb with a glycolytic metabolic profile while AMs allow for increased bacterial replication and are transcriptionally committed to fatty acid oxidation [241,242]. Additionally, our lab has shown differences in murine macrophage and DC subset responses to *C. neoformans*. Ly6c$^-$ monocyte-like macrophages significantly inhibited the growth of *C. neoformans* while the CD11b$^+$ conventional DCs significantly enhanced fungal growth [98]. Between these two subsets, there were over 2,500 significantly differentially regulated genes, but the most prominent was differential regulation of MHC-I genes, with these being significantly upregulated in the antifungal Ly6c$^-$ monocyte-like macrophage subset and significantly down-regulated in the permissive CD11b$^+$ DC subset. In addition, metabolic genes – specifically those in the cytochrome P450 family (such as *CYP1B1*) were significantly up-regulated in the cells permissive for cryptococcal growth – the CD11b$^+$ DCs. While these studies have been performed using the mouse models, it is important to investigate primary cells of human origin. Recently, six human pulmonary macrophage and DC subsets were consistently observed and profiled, including alveolar macrophages, CD14$^-$ macrophages, CD14$^+$ macrophages, CD207$^+$ DCs, CD14$^-$ DCs, and CD14$^+$ DCs [95]. These subsets differed in their ability to internalize a variety of bacterial species. All the subsets were more effective at internalizing the Gram-positives *S. aureus* and *B. anthracis* when compared to the Gram-negative *E. coli*. Furthermore, the human AMs and CD14$^+$ DC and CD14$^+$ macrophage subsets were more efficient at uptake than the other subsets. While these findings are significant, there are currently no studies that investigate cryptococcosis with human pulmonary phagocytes.

In this study, we investigated the initial interactions of *C. neoformans* with resident human pulmonary innate phagocytic APCs and determined how each subset responds to coincubation with cryptococcal cells *ex vivo*. Due to the differential interactions found in previously published studies, we hypothesized that the human subsets would have similar

differential phenotypic patterns of killing versus permissive growth of the fungus as was found in the murine model [98]. Human bronchial alveolar lavage (BAL) samples were enriched for phagocytic APCs and incubated with *C. neoformans* to determine uptake, killing ability, and transcriptional response. With these studies, we aimed to uncover the differential activity of human pulmonary macrophage and DC subsets and understand the genes and signaling pathways involved in these responses.

3.2 Methods

3.2.1 Reagents and Media

Unless stated otherwise, chemical reagents of the highest quality were obtained from Sigma-Aldrich (St. Louis, MO) and tissue culture media of the Gibco brand and plasticware were both purchased from Thermo Fisher Scientific (Waltham, MA). R10 media is defined as RPMI 1640 supplemented with 10% heat-inactivated fetal bovine serum (FBS), 2 mM L-glutamine, 50 mM 2-mercaptoenthanol, 100 U penicillin/ml, and 100 μg streptomycin/ml, filter-sterilized through a 0.22μm filter. For the use of the Dead Cell Removal Kit (Miltenyi Biotech Inc., Bergisch Gladbach, Germany), 1X Binding Buffer was prepared by diluting 20X Binding Buffer Stock solution with double-distilled water. The FACS buffer used in this study was phosphate-buffered saline (PBS) + 2% FBS, filter-sterilized through a 0.22μm filter.

3.2.2 Culture of Cryptococcus neoformans

Cryptococcus neoformans strains H99 (serotype A, mating type α) and mCherry producing strain JLCN920 (serotype A, KN99 mating type α), a kind gift of Dr. Jennifer Lodge (Duke University, Durham, NC), were recovered from 15% glycerol stocks stored at -80°C and were cultured for 18h at 30°C with shaking in yeast extract-peptone-dextrose (YPD) broth (BD Difco; Franklin Lakes, NJ) and collected by centrifugation. Organisms were washed three times with sterile PBS, and viable yeast cells were quantified using trypan blue dye exclusion in a

hemocytometer. Cryptococcal cells were resuspended in appropriate medium at the concentration needed for each experiment.

3.2.3 Human bronchoalveolar lavage sample processing

Isolation and preservation of lavaged lung cells was performed as previously described [95,243]. Briefly, whole human donor lungs were obtained through LifeShare of Oklahoma (Oklahoma City, OK, USA; http://www.lifeshareoklahoma.org) and the International Institute for the Advancement of Medicine (IIAM, Edison, NJ, USA; http://www.iiam.org). Lungs were deemed nontransplantable for reasons such as histocompatibility mismatches, lung size, uncertain drug usage, or prior incarceration. Our criteria for lung acceptance included: 18–70 years of age, no history of smoking tobacco or nonsmoking a minimum of 2 years, no history of lung disease, noncardiac death, a PaO2/FiO2 ratio > 200, and normal to minimal atelectasis based on chest x-ray results, with no evidence of intercurrent infection. The donor demographics for the lungs used in this study can be found in Table S3.1. Lungs were harvested and transported as per transplant protocols. Upon arrival at the Metcalf laboratory at OUHSC, Wisconsin solution and residual blood was washed from the vasculature using sterile physiological saline (0.9% w/v). Saline was pumped at low pressure (~20 cm water) into the main bronchus to produce visible swelling of lobes. The resultant BAL collections were pooled, and cells were concentrated by centrifugation at 300 x *g* for 10 minutes, resuspended to 1×10^7 cells/ml in freeze medium (40% RPMI 1640, 50% FBS, and 10% DMSO) [244], frozen in 2 ml aliquots at a rate of ~1°C/min at -80°C, and stored in liquid nitrogen vapor at -190°C. For experiments, aliquots were thawed quickly at 37°C in a Precision™ GP-10 water bath (Thermo Fisher Scientific) and allowed to settle in R10 media for 10 minutes at room temperature (RT) followed by centrifugation at 1000 x *g* for 5 minutes. Dead cells were removed from collected cells with the Dead Cell Removal Kit (Miltenyi Biotech Inc.) as per manufacturer's protocol with the following changes: 5X recommend amount of Dead Cell Removal Microbeads (500 µl per 10^7 cells) were used in order to properly label excessive

dead cells and separation occurred within LS columns (Miltenyi Biotech Inc.). Viable cells were quantified using trypan blue exclusion dye in a hemacytometer.

3.2.4 Active cryptococcosis detection

Presence of active cryptococcal infection was determined using the Cryptococcal Antigen Lateral Flow Assay (CrAg® LFA; IMMY, Inc., Norman, OK) as per manufacturer's instructions.

3.2.5 Cryptococcal uptake by standard flow cytometry

Processed human BAL cells were incubated with fluorescent mCherry expressing *C. neoformans* strain JLCN920 at a 1:1 ratio (1×10^6 cells each) with 1 μg/ml anti-GXM mAb F12D2 (kind gift of Dr. Tom Kozel, University of Nevada Reno, Reno, NV) at 37°C, 5% CO_2 for 2h in 100 μl of R10 media. Following incubation, samples were resuspended in 100 μl of FACS buffer and stained with the CD45 leukocyte marker, a lineage cocktail (CD3, CD19, CD20, and CD56), a viability dye, calcofluor white (CFW), and subset markers (specific markers and fluorophores used are shown in Table S3.2) for 30 minutes at 4°C. Samples were washed three times and then fixed with 2% formaldehyde and subsequently analyzed on a Novocyte 3000 flow cytometer (Agilent Technologies, Inc., Santa Clara, CA) with data analyzed using NovoExpress software (Agilent Technologies, Inc.). Gating scheme for detection of populations and associations was based on previously published research [95] and are shown in Figure S3.2. Gates were determined using controls including live/dead stain, unstained cells, single color, and isotype control samples. To calculate percent uptake, the total number of cells that were double-positive (positive for subset markers and positive for mCherry) were divided by the total number of that subset, then multiplied by 100. Percent was then plotted for each individual patient.

3.2.6 Cryptococcal morphology by imaging flow cytometry

Processed human BAL cells were enriched for phagocytic populations by negative selection of CD3, CD19, CD20, and CD56 microbeads and magnetic separation (Miltenyi Biotech Inc.) as per manufacturer's instructions. Phagocytic populations were then incubated with mCherry expressing *C. neoformans* strain JLCN920 at a 1:1 ratio (1×10^6 cells each) with 1 μg/ml anti-GXM mAb F12D2 at 37°C, 5% CO_2 for 2h in 100 μl of R10 media. Following incubation, samples were separated into half (one for each of the two different staining schemes needed for analysis), resuspended in 100 μl of FACS buffer and stained with leukocyte and subset markers (specific markers and fluorophores used are shown in Table S3.2) for 30 minutes at 4°C. Samples were washed three times and then fixed with 1% paraformaldehyde and subsequently analyzed on an Amnis® ImageStream®X Mk II Imaging Flow Cytometer (Luminex Corporation, Austin, TX) with data analyzed using IDEAS® 6.2 software (Luminex Corporation). Gating scheme for detection of populations and internalization is shown in Figure S3.3. Gates were determined using single color controls with UltraComp eBeads™ Compensation Beads (Thermo Fisher Scientific). Quantification of fungal killing results was conducted by examining up to 100 morphologies of internalized cryptococcal cells for each subset. Previous research has indicated that budding and single round cryptococcal cells are viable and condensed cells and debris are nonviable cells [145]. Examples are shown in Figure 3.2A.

3.2.7 Cryptococcal uptake for single-cell RNA sequencing

Processed human BAL cells were enriched for phagocytic populations as previously stated above and incubated with *C. neoformans* strain H99 at a 1:1 ratio (1×10^6 cells each) with 1 μg/ml anti-GXM mAb F12D2 at 37°C, 5% CO_2 for 2h in 100 μl of R10 media. Controls were phagocytic populations from the same human samples in media alone incubated under the same conditions. Samples were then washed once and then resuspended with PBS + 2% BSA. Libraries were made of pairs of controls and co-incubated sets using the 10X Chromium Controller and the Chromium Next Gem Single Cell 3' GEM, Library, and Gel Bead Kit v3.1 (10X Genomics Inc.,

Pleasanton, CA) and sequenced on a Novaseq series sequencer (Illumina Inc., San Diego, CA) as per manufacturer's protocols.

3.2.8 Identification of clusters of macrophages and DCs

Single-cell analysis and cluster identification was performed on 1,654 – 16,903 captured cells per sample using the 10X Chromium single cell system (10X Genomics Inc.) at the University of Oklahoma Health Sciences Campus Genomics Core Facility and sequenced each sample to a read depth of 95-164K reads/cell, yielding 85-92% sequence saturation. Read mapping and expression quantification were performed using a combination of the 10X Cell Ranger pipeline (10X Genomics Inc.) and custom Seurat analytic scripts [245]. Briefly, single-cell reads were mapped to the human genome (GRCH38) and assigned to genes using the standard Cell Ranger pipeline. Normalized gene expression was then used to produce a UMAP plot that provided cell clusters based on similarity of gene expression. Once cells were assigned to a cluster, custom Seurat scripts were used to statistically derive the gene expression differences within and between cell clusters using *t*-tests in Seurat. Trajectory analysis was then conducted using Monocle [246]. To be statistically similar across the study, the Monocle trajectories were used to guide specific trajectory specific *t*-tests within Seurat. From these, pathway analyses were performed using Ingenuity Pathway Analysis (IPA, QIAGEN, Hilden, Germany) on the differential transcriptional profiles seen in the cell clusters and trajectory groups.

3.2.9 TNF-α intracellular imaging flow cytometry

Processed human BAL cells were enriched for phagocytic populations as previously stated and incubated with *C. neoformans* strain JLCN920 at a 1:1 ratio (1×10^6 cells each) with 1 μg/ml anti-GXM mAb F12D2 at 37°C, 5% CO_2 for 2h in 100 μl of R10 media. BD GolgiStop™ and BD GolgiPlug™ (BD Biosciences, Franklin Lakes, NJ) were used, as per manufacturer's protocol, to prevent cytokine secretion. Following incubation, samples were separated into half

(one for each of the two different staining schemes), resuspended in 100 µl of FACS buffer and stained with either TNF-α panel #1 or #2 (Table S3.2). Extracellular staining was performed as previously stated for 30 minutes at 4°C. Following extracellular staining, cells were fixed with 2% formaldehyde for 10 minutes at room temperature and permeabilized with Intracellular Staining Perm Wash Buffer (BioLegend®, San Diego, CA) for 10 minutes at room temperature. Cells were stained with intracellular markers (IL-1β, CCL3, CXCL8 and TNF-α), washed, and fixed with 1% paraformaldehyde. Samples were analyzed on an Amnis® ImageStream®X Mk II Imaging Flow Cytometer (Luminex Corporation) with data analyzed using IDEAS® 6.2 software (Luminex Corporation). Gating scheme for detection of populations and internalization are shown in Figure S3.6. Gates were determined using single color controls with UltraComp eBeads™ Compensation Beads (Thermo Fisher Scientific).

3.2.10 Statistical analysis

All statistical analyses were conducted using GraphPad Prism version 5.00 for Windows (GraphPad Software, San Diego, CA) unless noted otherwise. Significant differences were defined as $p < 0.05$ and $\alpha = 0.05$ unless noted otherwise. The student's unpaired two-tailed *t*-test was performed to calculate level of significance among MFI means of CXCL8, CCL3, IL-1β, and TNF-α between phagocytic APCs which contained *C. neoformans* versus cells without the fungus. One-way ANOVA with Tukey's Multiple Comparison Test was performed to compare medians of human phagocytic APC subsets, their uptake of *C. neoformans*, and percent cryptococcal killing of each subset. Linear regression was performed to calculate the line of best fit in correlations of JLCN920 fluorescence intensities to antibody intensities for markers CXCL8, CCL3, IL-1β, and TNF-α. scRNA-seq analysis, cluster identification, and trajectory analysis was performed with a combination of Cell Ranger pipeline, Seurat, Monocle, and custom R scripts.

3.3 Results

3.3.1 Phagocytic APC subsets were identified in human bronchoalveolar samples and interact with C. neoformans

We sought to understand the differences in cryptococcal killing by macrophage and DC subsets [98,215,217,224,247], and, therefore, chose to follow up on a study that identified subsets of phagocytic APCs within the human lung [95]. To avoid biases and remove the possibility of pre-activation that come with an active cryptococcal infection, we used a commercially available detection kit (CrAg® LFA) to identify *Cryptococcus*-positive samples. None of the samples used in this study tested positive for infection, so we could, therefore, assume the fungal cells were not activated (representative image of results in Figure S3.1 and results in Table S3.3). We next removed dead cells from the human BAL samples before incubating live cells with a fluorescent mCherry expressing *C. neoformans* strain JLCN920. Following a 2-hour incubation to allow for cryptococcal interaction and possible uptake, the phagocytic APCs were stained with fluorescent markers and analyzed by flow cytometry (gating scheme shown in Figure S3.2). Figure 3.1A shows the percent total of each of the previously identified subsets, and, in accordance with previous findings, the first three groups (AM, $CD14^{+}CD1c^{-}$, $CD14^{-}CD1c^{-}$) are macrophages while the last three groups ($CD207^{+}$, $CD14^{+}CD1c^{+}$, $CD14^{-}CD1c^{+}$) are DCs [95]. Alveolar macrophages (AMs) comprised over 85% of the total population, but despite being very low in total numbers, the other five subsets were identified within the samples (Figure 3.1B), with the occasional subset being undetectable (recorded as 0%). Next, we identified the percent that each of the detected subsets phagocytosed the fluorescent *C. neoformans*. Using calcofluor white (CFW) post-incubation, we were able to detect which fungi were external or on the surface of the phagocytic APCs and exclude those from the findings through the gating scheme. Results indicate that all six subsets interacted and phagocytosed the fungus to some degree (Figure 3.1C). However, two

macrophage subsets ($CD14^+CD1c^-$ and $CD14^+CD1c^-$) had significantly lower uptake when compared to one of the dendritic cell subsets ($CD14^-CD1c^+$).

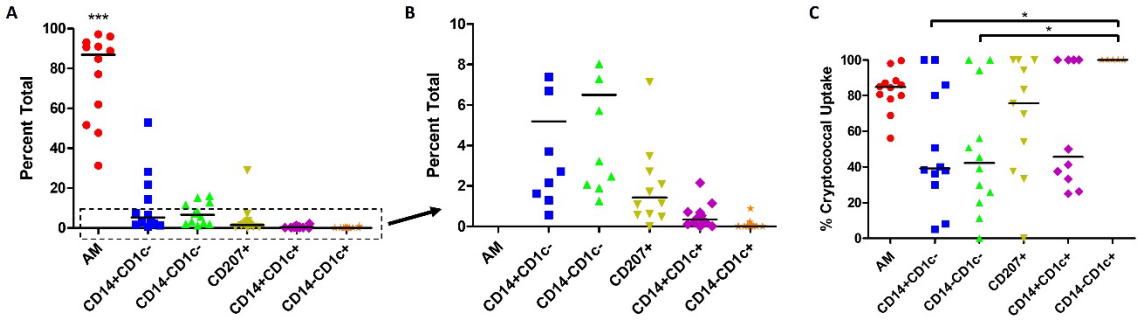

Figure 3.1. Percent Population of Each Subset Identified and Interact with *C. neoformans*. Processed human BAL cells were incubated with fluorescent mCherry expressing *C. neoformans* strain JLCN920 for 2h and then stained with fluorescent antibodies for flow cytometric analysis. (A) Representation of each phagocytic APC subset shown as a percentage of total population indicated by surface markers. (B) Inset from panel **(A)** showing relative abundance of remaining low number subsets. (C) Percentage of uptake by each phagocytic APC subset of *C. neoformans* indicated as positive for mCherry. Data points shown are individual samples with black bars as median of the results of 12 samples (n=12), with each sample performed in duplicate. One-way ANOVA with Tukey's Multiple Comparison Test was performed to compare each column against all others. *** indicates significantly different means of AM subset to all others ($p < 0.0001$) and * represents significantly different means of indicated macrophage subset to DC subset $CD14^-CD1c^+$ ($p < 0.05$).

3.3.2 Subsets of phagocytic APCs show differential killing of C. neoformans

Previous studies have shown that dead or dying *C. neoformans* take on a deformed morphology (c-shaped or condensed) rather than their usual round or budding appearance while alive [145]. Using morphology as a proxy for cryptococcal fitness, we examined several of these internalized fungal cells within each subset of phagocytic APCs. Prior to use, the human BAL cells were enriched for phagocytic APCs by removal of lineage-positive cells (CD3, CD19, CD20, CD56). Then cells were incubated with the mCherry-producing cryptococcal strain and incubated for 2 hours. Using imaging flow cytometry (gating scheme shown in Figure S3.3), we

were able to discern the different morphologies of internalized cryptococcal cells while also identifying the phagocytic subset. Fungal fitness was scored according to their morphologies and examples of the system used in this study are shown in Figure3.2A. By convention, cryptococcal cells which appeared either as round or budding are deemed alive while those that take on a more deformed shape are considered dead/dying [145]. Cells that were positive for the fungal marker (fluorescent in the mCherry channel) but showed no discernable fungal shape but rather a diffusive staining were also determined to be dead. All the captured images (up to 100) for each of the subsets were quantified and graphed according to cryptococcal fate (Figure 3.2B). Results show that one of the macrophage subsets (AMs) and all the DC subsets were able to kill the fungus with high percentages of antifungal activity (>70%). However, macrophage subsets $CD14^{+}CD1c^{-}$ and $CD14^{-}CD1c^{-}$ were unable to kill internalized *C. neoformans* (0% dead/dying morphologies).

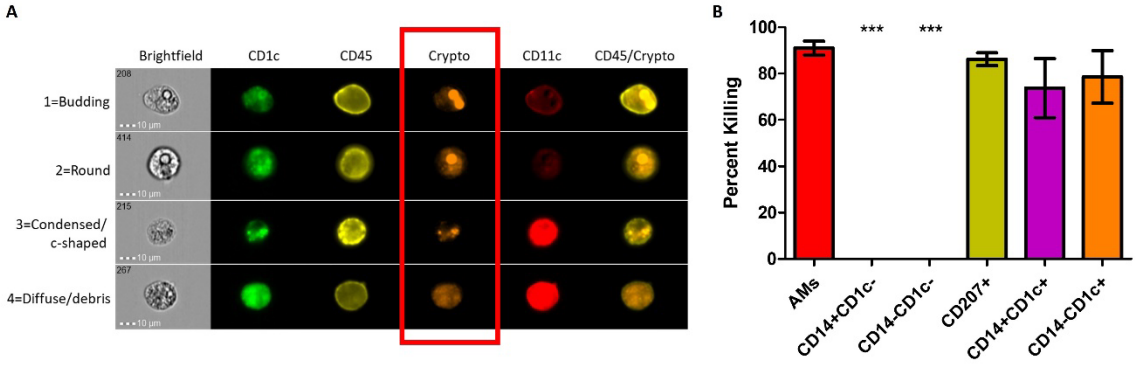

Figure 3.2. Subsets of Phagocytic APCs Show Differential Killing of *C. neoformans*. Processed human BAL cells were enriched for phagocytic APCs and incubated with fluorescent mCherry expressing *C. neoformans* strain JLCN920 for 2h and then stained with fluorescent antibodies for imaging flow cytometric analysis. (A) Representative images of internalized *C. neoformans* to determine fate of the fungus. Budding and round fungal cells were considered as living while condensed and debris were deemed at dead cells (red box). (B) Percent killing of *C. neoformans* by phagocytic APC subsets. Up to 100 images of internalized cryptococcal cells by each subset were analyzed according to panel (A). Four of the six subsets showed substantial killing (>70%) of internalized fungal cells. Macrophage subsets $CD14^{+}CD1c^{-}$ and $CD14^{-}CD1c^{-}$ allowed live fungal cells to persist internally in all analyzed images. Data shown are

means ± standard errors of the means (SEM) of the results of 2 independent experiments using 12 independent BAL samples (n=12). One-way ANOVA with Tukey's Multiple Comparison Test was performed to compare each column against all others. *** indicates significantly different means from killing subsets ($p < 0.0001$).

3.3.3 ScRNA-seq identified different clusters of phagocytic APCs

To understand the gene expression in the phagocytic APC subsets that displayed different cryptococcal killing phenotype during the early stages of cryptococcal interaction, RNA-seq was performed to investigate their transcriptome. Once the samples are thawed, the life span of cells is extremely limited (~4 hours) and physical separation of the cells into discrete groups is not possible. Therefore, single-cell RNA sequencing (scRNA-seq) was performed for the level of resolution needed to identify differential clusters prior to this time [248,249]. Human BAL samples were enriched for phagocytic APCs by removal of lineage-positive cells (CD3, CD19, CD20, CD56), and then incubated with *C. neoformans* for two hours to allow for initial interaction or uptake. Control cells from each human sample were incubated under the same conditions without the pathogen. Analysis revealed 9 individual clusters among 18,958 total cells for the control cohort (naïve) and 18 clusters among 22,344 total cells for cells incubated with *C. neoformans* (infected) (Figure 3.3A-B). We initially investigated the distribution of macrophages among the given clusters by use of the macrophage gene *APOC1* [250]. Projections of this gene onto the cluster map space revealed no pattern of clustering in either the naïve or infected cohorts (Figure 3.3C-D). Previously, identification of each phagocytic APC subset was accomplished using surface markers, and the transcriptional profile for naïve cells of each subset was determined [95]. Using a single gene from the previous transcriptional profile to identify each subset, we identified cells from each subset in our samples; however, distribution of each subset also did not follow computational clustering, so we were unable to cluster the cells according to subset for either naïve or infected cohorts (Figure S3.4A-L).

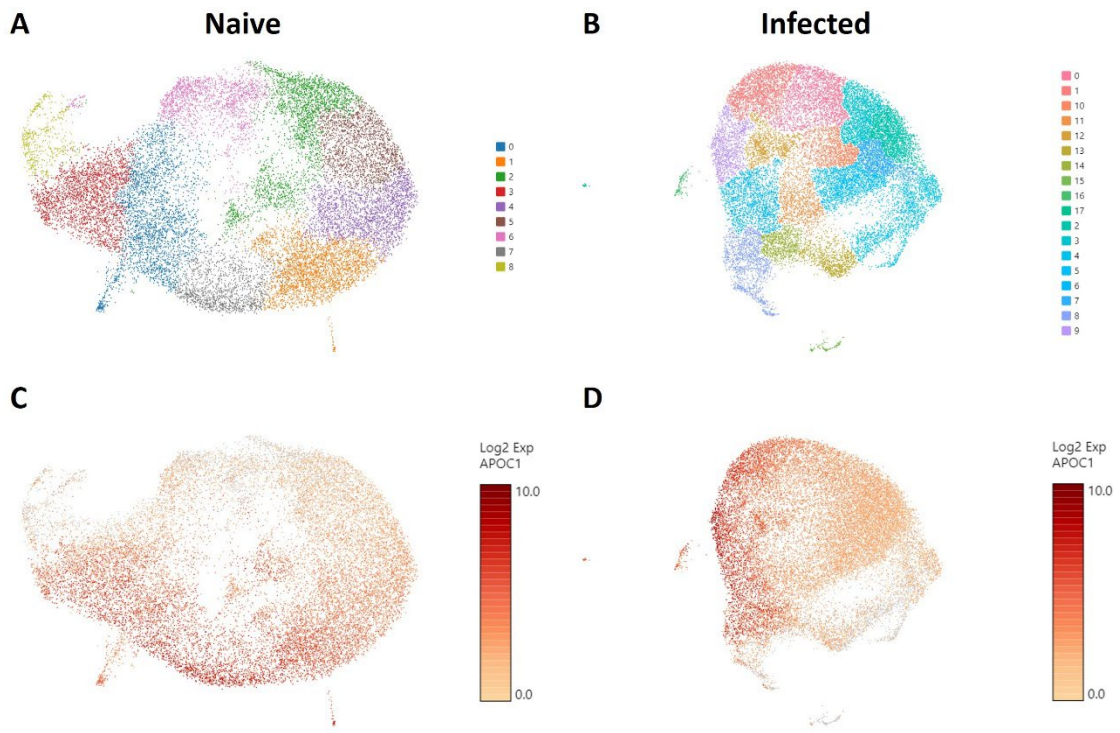

Figure 3.3. Phagocytic APCs Incubated with and without *C. neoformans* Show Distinct Clustering of Cells which Are Not Correlated with Macrophage Identity. Processed human BAL cells were enriched for phagocytic APCs and incubated with or without *C. neoformans* strain H99 for 2h and then processed for scRNA-seq. scRNA-seq analysis identified 9 and 18 discrete clusters among the naïve (A) and infected (B) cohorts, respectively. Cells were also examined for the expression and distribution of APOC1 (macrophage gene) for both naïve (C) and infected (D) cohorts. The distribution of macrophages did not follow the clustering scheme for either of the cohorts. Data shown are transcriptional regulation of shown genes for 18,958 (naïve) and 22,344 (infected) total cells for three individual experiments for each cohort (n=3).

3.3.4 Trajectory analysis splits clusters into distinct groups with different phenotypes

Since we were unable to isolate individual subsets, we sought to instead focus our efforts on the phenotypic outcomes and cellular processes rather than the inherent subset and their molecular differences. Since there are double the number of clusters in the infected cohort when compared to the naïve using the same standard for cluster discrimination and similar cell numbers, *C. neoformans* may have influenced the number of discrete clusters by causing a

transcriptional change in some of the immune cells. With this evidence of a change in gene expression, a trajectory analysis was necessary to understand the full picture of the discrete clusters and how they compared to one another. Shown in Figure 3.4 are the trajectory analyses conducted by R package Monocle on the 18 clusters identified in the infected cohort. Using cluster #0 as the starting point, there is a stark divergence between cells on the left and right side of the plot (Figure 3.4). Clusters 1 → 9 → 12 → 6 follow along one transcriptional evolution (left) while clusters 3 → 2 → 7 → 5 follow another progression (right). This departure between the paths is driven mainly by mitochondrial genes (including *MTRNR2L12* [$p \approx 0$], *MT-ND6* [$p \approx 0$], *MT-ATP8* [$p = 4.67 \times 10^{-237}$], *MT-CO3* [$p \approx 0$], *MT-CYB* [$p \approx 0$]) on the right and lipid metabolism genes (such as *FABP4* [$p \approx 0$]) coupled with immune recognition genes (such as *MARCO* [$p = 2.90 \times 10^{-185}$] and *CXCL16* [$p \approx 0$]) and antigen processing genes (*HLA-A* [$p = 5.58 \times 10^{-290}$], *-B* [$p \approx 0$], *-C* [$p \approx 0$], *HLA-DRA* [$p = 1.72 \times 10^{-188}$]) on the left (Figure 3.5A). A complete list of differentially expressed genes can be found in Table S3.4. The canonical pathways and predicted upstream regulators were analyzed by Ingenuity Pathway Analysis (IPA, QIAGEN) and the most significantly affected are shown in Figure 3.5B-C. The most altered pathways were EIF2 signaling and oxidative phosphorylation, which indicates the cells are altering their protein products and metabolism (Figure 3.5B). Pathways such as phagosome maturation and antigen presentation are affected by differences in MHC class I (*HLA-A*, *-B*, *-C*) and class II (*HLA-DR*) molecules along with the scavenger receptors *MARCO* and *CXCL16*. Most of the highest predicted upstream regulators involve mTOR (including torin-1, LARP1, and RICTOR) which can coordinate mitochondrial energy production (Figure 3.5C) [251]. Taken together, these patterns indicate a cryptococcal killing phenotype for the left-side clusters.

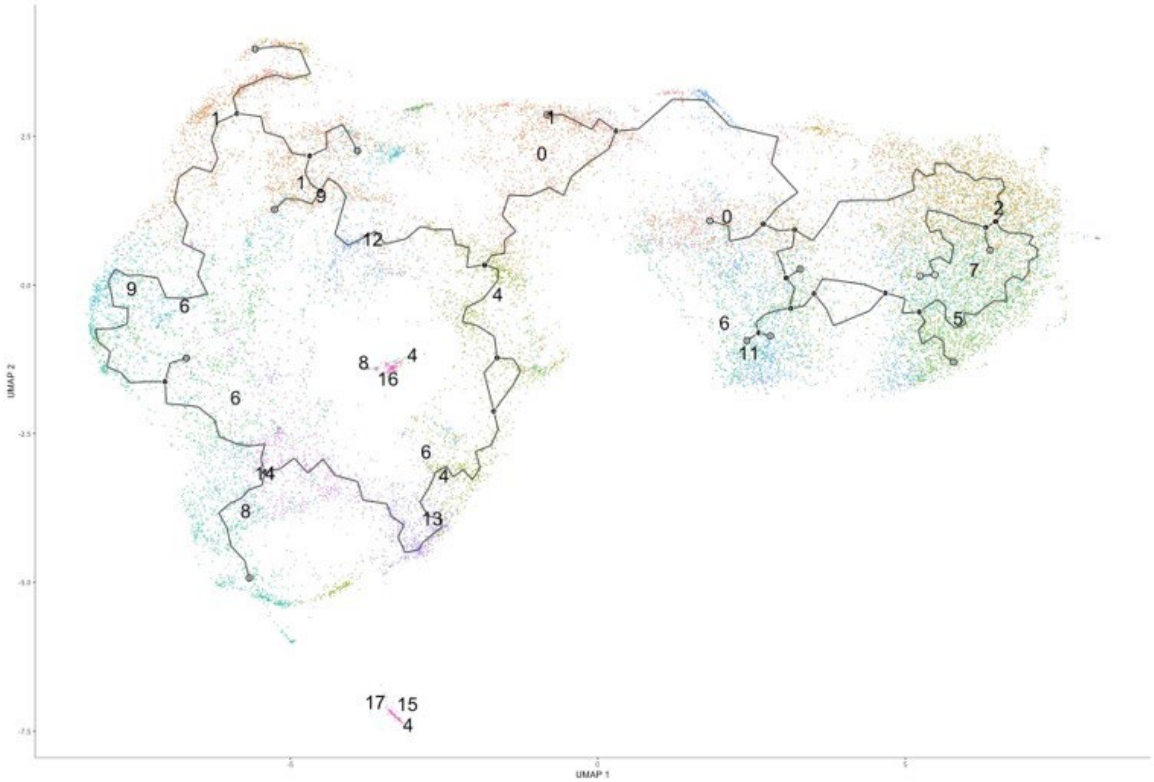

Figure 3.4. Trajectory Analysis Shows Divergent of Clusters into Two Main Groups. Processed human BAL cells were enriched for phagocytic APCs and incubated with *C. neoformans* strain H99 for 2h and processed for scRNA-seq. Uniform manifold approximation and projection (UMAP) plot was created from the 18 clusters of the infected cohort. From the initial cluster of #0, there is an immediate split of the clusters which follow clusters #1/9/6/12 towards to the left and clusters #2/7/5/3 to the right. Data shown are the 18 Seurat clusters for 22,344 total cells from the infected cohort for three individual experiments for each cohort (n=3).

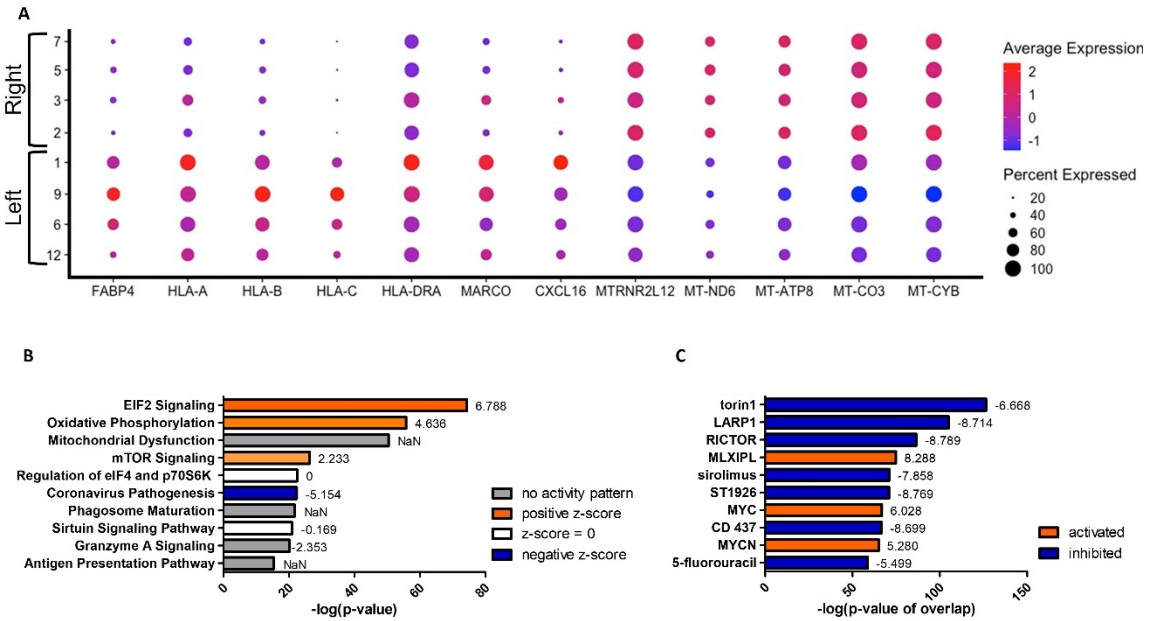

Figure 3.5. Upregulation of Antifungal Genes in Left Side Clusters #1/9/6/12. Processed human BAL cells were enriched for phagocytic APCs and incubated with *C. neoformans* strain H99 for 2h and processed for scRNA-seq. Genes differentially expressed in clusters #1/9/6/12 when compared to clusters #2/7/5/3 were analyzed by IPA. (A) Differential expression of select genes in clusters #1/9/6/12 (left) and #2/7/5/3 (right). Top 10 significantly regulated canonical pathways (B) and predicted upstream regulators (C) as ordered by *p*-value or *p*-value of overlap. To the right of each bar is the statistical z-score for each pathway or upstream regulator with positive and negative being increased and decreased, respectively (NaN = not a number, no activity pattern). Data shown are combined analysis of cells from three individual experiments (n=3).

Secondary to the initial split in the trajectory plot, on the left side there are indications of a further evolution of transcriptomes from clusters #1/9/12 (top) to #8/14 (bottom) (Figure 3.6). The most differentially expressed genes in this trajectory are *CCL3* and *CXCL8*, both genes downstream of TNF-α and indicative of a protective response against *C. neoformans* (Figure 3.6A) [252,253]. These genes are upregulated in the lower clusters. A complete list of differentially expressed genes can be found in Table S3.5. Among the upper clusters, there were an increase in expression of genes that directly recognize cryptococcal cells such as the scavenger receptors *MARCO* ($p \approx 0$) and *CXCL16* ($p \approx 0$), stress sensor PPARγ ($p = 9.93 \times 10^{-82}$), the

lysosomal indicators *LAMP1* ($p = 3.62 \times 10^{-168}$) and *LAMP2* ($p = 6.43 \times 10^{-179}$), genes that contribute to the antifungal activity of lysosomes (*CTSB* [$p = 2.64 \times 10^{-187}$] or cathepsin B; *PSAP* [$p \approx 0$], the precursor to saposins A-D), and the antigen presentation MHC-II gene *HLA-DRB5* ($p \approx 0$). All these were accompanied with an increase of gene expression indicating fatty acid metabolism (*FABP4* [$p = 1.09 \times 10^{-281}$]). As we move into the lower clusters, there is a switch from genes that deal directly with *C. neoformans* to genes involved in cytokine responses with increases in expression of the previously mentioned genes TNF-α (*TNF*) ($p = 5.30 \times 10^{-75}$), *CCL3* ($p = 1.40 \times 10^{-241}$), *CXCL8* ($p \approx 0$) along with transcriptional factors *JUN* ($p = 3.84 \times 10^{-312}$) and *FOS* ($p = 3.84 \times 10^{-159}$). Again, these differentially regulated genes were analyzed by IPA and the top changes to canonical pathways and predicted upstream regulators are shown in Figure 3.6B-C. Similar to the left versus right analysis, the most differentially regulated pathway are general pathways that control many cellular functions including mitochondrial functions, glucocorticoid receptor signaling, and oxidative phosphorylation. However, pathways that control immune responses are also present in the form of the sirtuin signaling and CLEAR (coordinated lysosomal expression and regulation) signaling pathways (Figure 3.6B) [254,255]. Among the predicted upstream regulators, LPS and dexamethasone are the most significant and are linked to the expression of *FABP4* (Figure 3.6C). This is congruent to the actual expression of *FABP4* which is relatively high in the top clusters and tapers off in bottom clusters.

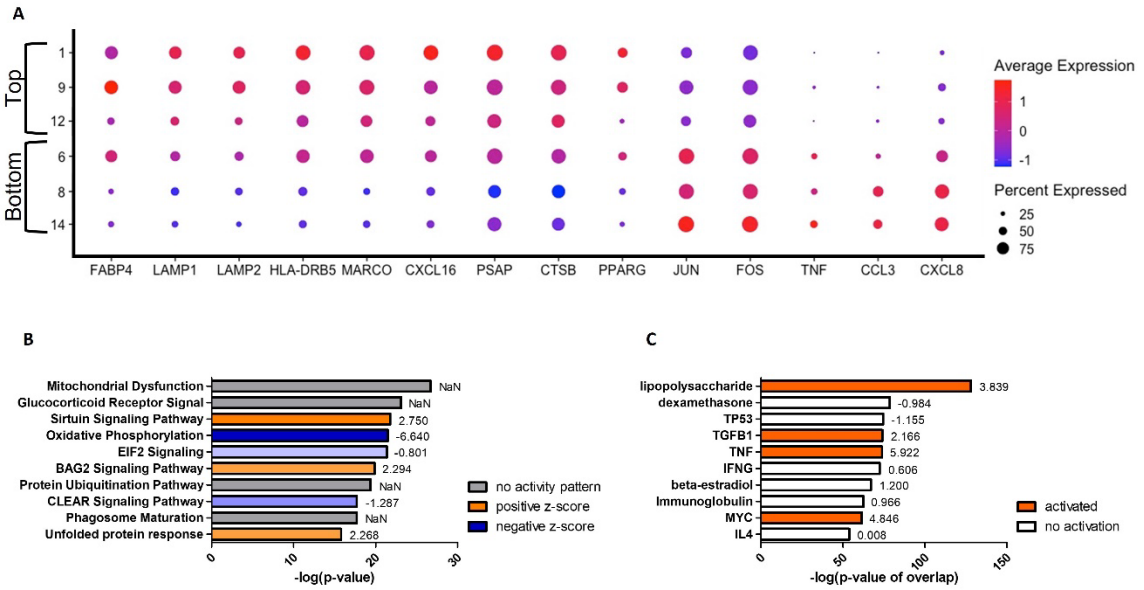

Figure 3.6. Transcriptome Evolution to Active State in Clusters #8/14. Processed human BAL cells were enriched for phagocytic APCs and incubated with *C. neoformans* strain H99 for 2h and processed for scRNA-seq. Genes differentially expressed in clusters #8/14 when compared to clusters #1/9/12 were analyzed by IPA. (A) Differential expression of select genes in clusters #6/8/14 (bottom) and #1/9/12 (top). Top 10 significantly regulated canonical pathways (B) and predicted upstream regulators (C) as ordered by *p*-value or *p*-value of overlap. To the right of each bar is the statistical z-score for each pathway or upstream regulator with positive and negative being increased and decreased, respectively (NaN = not a number, no activity pattern). Data shown are combined cells from three individual experiments (n=3).

3.3.5 Increases in TNF-α correlate with changes of cellular stress response and metabolism in early clusters

With TNF-α known to provide a protective response against *C. neoformans* [252,256] and coupled with our data on the increases of TNF-α gene expression in particular clusters, we focused our attention to the transcriptional effects that interaction with the fungus has on our phagocytic APCs. Examining the scRNA-seq data and the distribution of TNF-α gene expression in the infected cohort, we found that the cells up-regulating TNF-α (*TNF*) are in the lower left portion of the population (Figure 3.7A). This trend continues in genes downstream of TNF-α

signaling as well, including *IL-1β*, *CXCL8*, and *CCL3* (Figure 3.7B-D), which each contribute to protection against *Cryptococcus* through feedback loops [257-259]. TNF-α also manipulates macrophage activation and although this study focused on early time points and events that occur prior to macrophage activation (and in the absence of T cells or T cell-associated cytokines), activation to either the protective M1 or permissive M2 phenotypes as well as Th1/Th2-type cytokine production may also affect cryptococcal fate [72,260]. Within the clusters of the infected cohort, we found no transcriptional indication of macrophage activation to either M1 or a Th1-type phenotype (*IFN-γ*, *NOS2*, *IL-12A, IL-12B*) or M2 or a Th2-type phenotype (*IL-4*, *IL-10*, *IL-13*, *ARG1*) (Figure S3.5A-H). This information allows us to investigate the phenotypic differences caused by a cryptococcal infection as inherent differences of cellular processes among the cells of the samples as opposed to a generalized transcriptional skewing and activation of the inflammatory network.

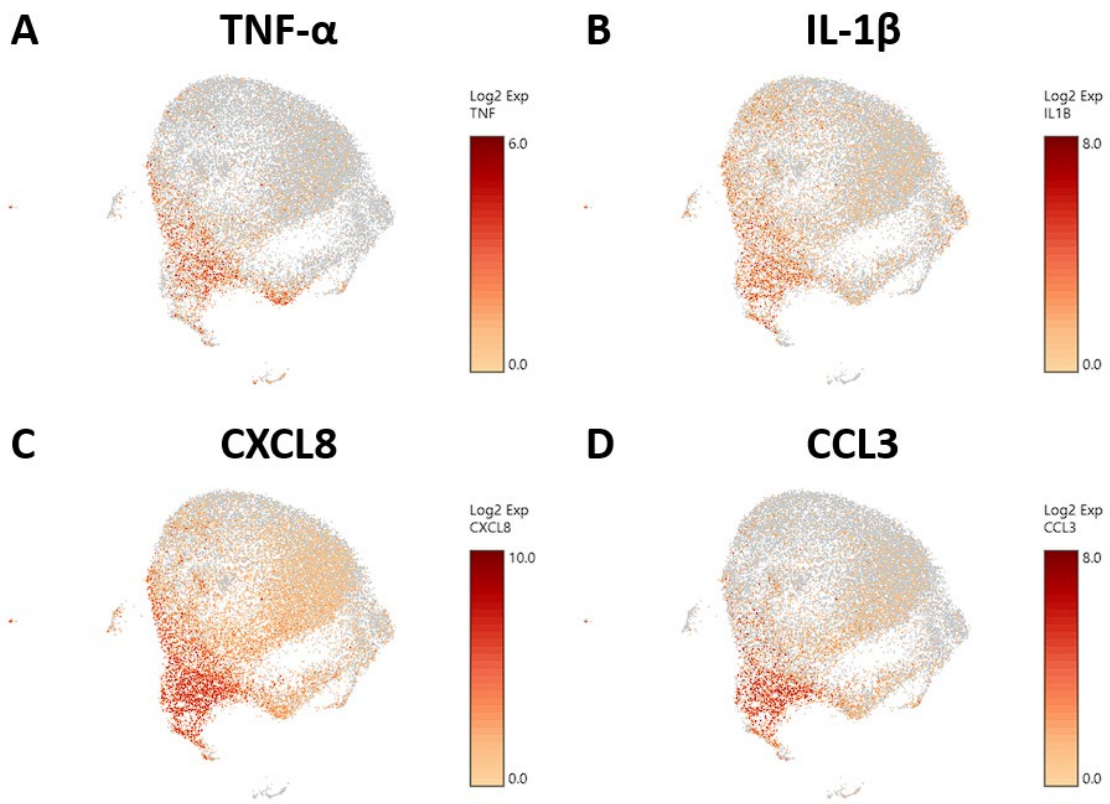

Figure 3.7. Phagocytic APCs Incubated with *C. neoformans* Are Differential in TNF-α and Genes Downstream of TNF-α. Processed human BAL cells were enriched for phagocytic APCs and incubated with *C. neoformans* strain H99 for 2h and then processed for scRNA-seq. scRNA-seq analysis identified differential regulation of TNF-α (*TNF*) (A), *IL-1β* (B), *CXCL8* (C), and *CCL3* (D) that occur primarily in cells in the bottom left portion of the plot. Data shown for are transcriptional regulation of shown genes for 22,344 total cells for three individual experiments (n=3).

To understand what occurs when TNF-α is upregulated, we investigated clusters #1 and #9, which are among the early left side group and have differential TNF-α activation ($p = 1.84 \times 10^{-11}$). Compared to cluster #9, cells in cluster #1 display an increase in genes encoding for scavenger receptors (*MARCO* [p = 0.001] and *CXCL16* [$p = 2.67 \times 10^{-95}$]), cryptococcal killing machinery (*CTSB* [$p = 2.23 \times 10^{-10}$] and *PSAP* [$p = 2.00 \times 10^{-130}$]), and the MHC-II chaperone *CD74* ($p = 6.39 \times 10^{-100}$) (Figure 3.8A). As TNF-α becomes upregulated in cluster #9, the cells do not induce the aforementioned genes, but instead switch to more signaling pathway genes that include the stress sensor *GADD45α* ($p = 1.60 \times 10^{-11}$) and the transcription factors *JUN* ($p = 5.32 \times 10^{-53}$) and *FOS* ($p = 2.41 \times 10^{-20}$). This is evident in the most highly upregulated genes being ribosomal genes (like *RPS12* [$p = 7.50 \times 10^{-305}$]) and is accompanied by a utilization of fatty acid metabolism through *FABP4* ($p = 1.46 \times 10^{-28}$). Finally, superoxide dismutase genes (*SOD1* [$p = 1.61 \times 10^{-27}$] and *SOD2* [$p = 2.71 \times 10^{-19}$]) are also increased along with TNF-α (Figure 3.8A). A complete list of differentially expressed genes can be found in Table S3.6. Examining the most regulated canonical pathways and upstream regulators, many of the affected gene sets belong to cellular wide functions including EIF2 signaling, oxidative phosphorylation, and glucocorticoid receptor signaling as well as master regulators like torin-1, LARP1, RICTOR, and MYC (Figure 3.8B-C). These results show that the cells are significantly changing their proteome and metabolism to adapt to a change in stress.

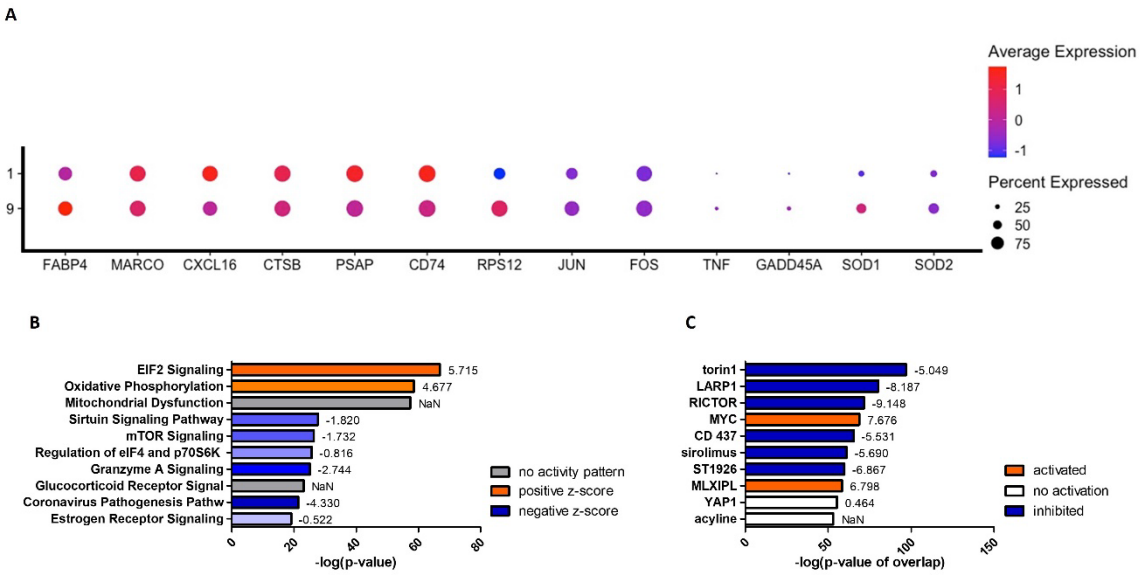

Figure 3.8. Differentially Expressed Genes in Cluster #9 Led to Changes in Cellular Stress Response and Metabolism. Processed human BAL cells were enriched for phagocytic APCs and incubated with *C. neoformans* strain H99 for 2h and processed for scRNA-seq. Genes differentially expressed in cluster #9 when compared to cluster #1 were analyzed by IPA. (A) Differential expression of select genes in clusters #9 and #1. Top 10 significantly regulated canonical pathways (B) and predicted upstream regulators (C) as ordered by *p*-value or *p*-value of overlap. To the right of each bar is the statistical z-score for each pathway or upstream regulator with positive and negative being increased and decreased, respectively (NaN = not a number, no activity pattern). Data shown are combined cells from three individual experiments (n=3).

3.3.6 Differential staining of TNF-α markers indicates cryptococcal interaction

To investigate these transcriptional differences that are accompanied with changes in TNF-α expression in the phagocytic APCs and how they relate with intracellular cryptococcal morphology, human BAL cells were again incubated with mCherry expressing *C. neoformans* strain JLCN920 followed by an examination of the intracellular cryptococcal morphology as it correlates with protein production of TNF-α (and downstream markers IL-1β, CXCL8, and CCL3) on an imaging flow cytometer (gating scheme shown in Figure S3.6). Cryptococcal

morphology was again used and scored as described above to indicate the fate of the pathogen (Figure S3.7). We found that there were no significant differences of the fluorescent intensities for TNF-α or any associated downstream markers between living and killed intracellular cryptococcal cells (Figure S3.8A-D). However, a linear regression analysis showed a strong positive correlation between all intracellular cryptococcal cells (both living and killed) and these markers (Figure S3.8E-H). This led us to examine the differences of these markers in immune cells that have either interacted (high mCherry intensity) or not interacted (low mCherry intensity) with *C. neoformans*. Using the cutoff provided by the negative cryptococcal staining control, we found significant differences of staining intensities between phagocytic APCs that have interacted with the fungus versus those that have not in three (*p*-values = TNF-α: 0.0053, IL-1β: 0.0017, CCL3: 0.0170) of the four markers, with the fourth (CXCL8, *p*-value = 0.1242) trending in the same direction (Figure 3.9A-D). These data show that TNF-α, CCL3, IL-1β, and CXCL8 protein levels are correlated with cryptococcal interaction. In addition, the expression of these genes (by scRNA-seq) was correlated to expression of other genes involved in antifungal activity (Figures 3.5-3.8).

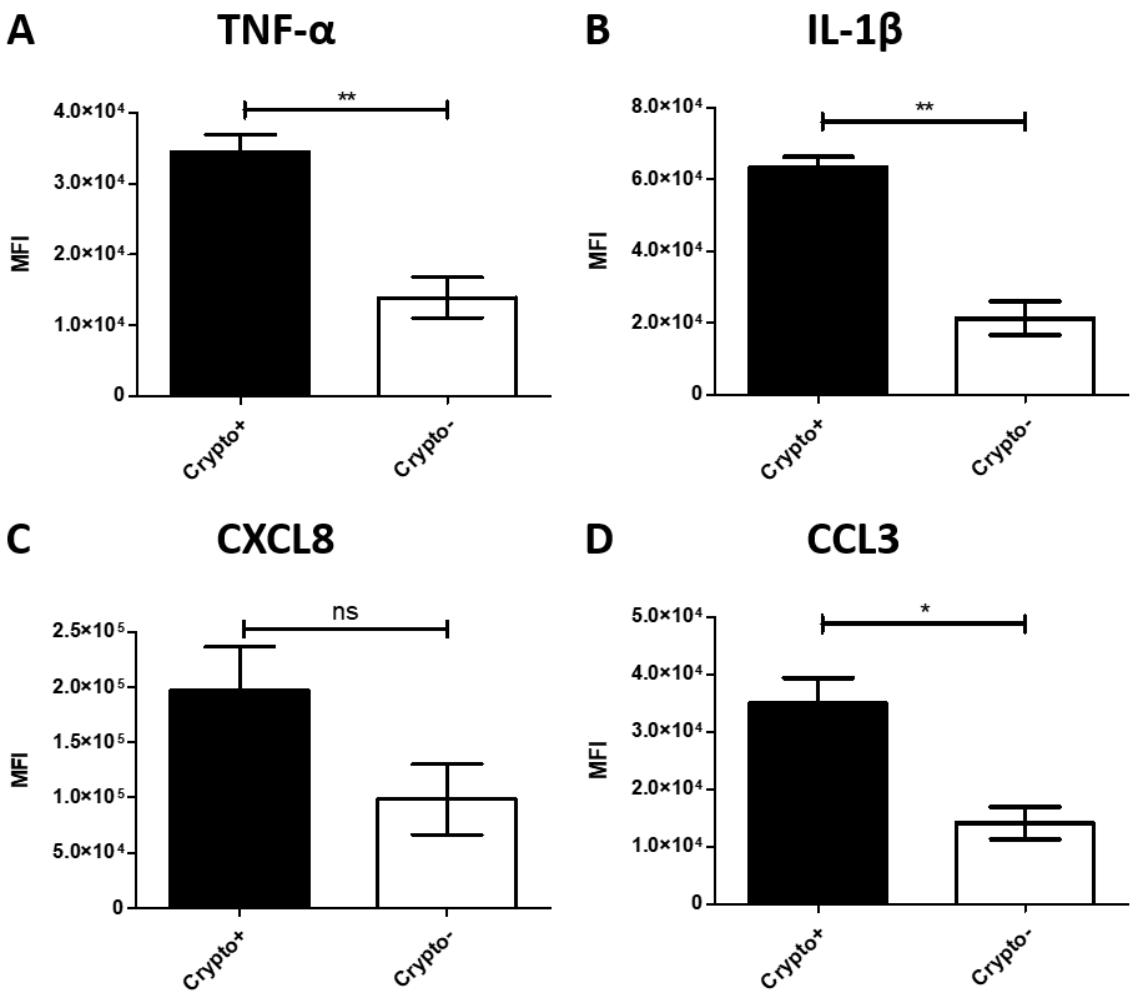

Figure 3.9. Phagocytic APCs Incubated with *C. neoformans* Show Differential TNF-α and Downstream Protein Expression Following Fungal Interaction. Processed human BAL cells were enriched for phagocytic APCs and incubated with mCherry expressing *C. neoformans* strain JLCN920 for 2h and then processed for imaging flow cytometric analysis. Analysis shows that increased presence of protein expression of TNF-α (A), IL-1β (B), and CCL3 (D) occur when interaction with cryptococcal cells was verified compared to non-interacting cells. CXCL8 (C) shows a similar but non-significant trend, as well. Data shown are mean fluorescent intensities (MFI) of individual viable $CD45^+$ phagocytic APCs from three individual experiments (n=3). Two-tailed *t*-tests were performed to compare pairs of columns. * and ** indicates significantly different means of $p < 0.05$ and $p < 0.0001$, respectively.

3.4 Discussion

With the increasing limitations of current therapies combating cryptococcosis and cryptococcal meningitis, the goal of this study was to explore the initial interaction with *C. neoformans* and lung innate immune cells in order to potentially identify other avenues for intervention. The mounting evidence of the heterogeneity of these immune cells led us to investigate subsets of macrophages and dendritic cells (DCs) that provide most of the early protection from this disease. Our first objective was to identify these subsets within the human lung. We used bronchoalveolar lavage (BAL) fluid from human lungs and examined the contents for the presence of each subset using flow cytometry. Not only did we locate each of the subsets as previously reported [95], but also identified their interaction with *C. neoformans*. Our data show that each of the six subsets (three macrophage and three DC) were able to interact with the fungus in different capacities. Our results were similar to those in previous studies where there was relatively low uptake of certain bacterial pathogens by different subsets at low MOIs [95]. These findings were also similar to the high association of cryptococcal cells with pulmonary phagocyte subsets in the mouse model [98].

In investigating the killing capacities of these subsets, we examined their intracellular morphologies and correlated that to cryptococcal fate, as previously done in both *in vitro* human and mouse models [145]. In our studies, we found that two macrophage subsets were completely unable to kill *C. neoformans*. Thus, phagocytosis by different macrophage/DC subsets can result in different specific fates for the fungus. In a mouse model, there were more subtle differences in interaction with *C. neoformans* by the phagocytic subsets, with the most significant killing ability exhibited in the $Ly6c^-$ monocyte-like macrophages, and the most significant intracellular growth in the $CD11b^+$ DCs [98]. In our data, we found that AMs and the DC subsets had antifungal activity, but the $CD14^+$ and $CD14^-$ macrophages did not have antifungal activity. *Mycobacterium tuberculosis* (Mtb) is another pathogen with a similar disease presentation as *C. neoformans* in their ability to evade the host immune system intracellularly by promoting a Th2 response [261].

Unlike this study, against Mtb, alveolar macrophages were permissive for bacterial replication and allowed rampant growth [261], whereas interstitial macrophages had antibacterial activity [241].

In identifying differential killing capacities between the subsets of phagocytic APCs, the question that now arises is the inherent molecular differences and transcriptomes between the groups. Due to these cells' short lifespan outside the human body, we were unable to separate the subsets into discrete populations and conduct a series of focused experiments on individual subsets. Therefore, we performed single-cell RNA sequencing (scRNA-seq) on the entire population to obtain the resolution needed that is required in comparing cells or groups of cells to one another. Using subset-specific genes identified previously [95], we found that subsets did not correlate with computational clustering, and we were unable to identify these discrete subsets in our samples. Despite being heterogeneous, these phagocytic APCs are still closely related to one another, and cellular processes and interactions with pathogens such as *C. neoformans* can have a more pronounced effect on their different interactions with pathogenic microbes.

To understand these effects that fungal interaction may have on the population, we performed a trajectory analysis do discover how the clusters are related to one another. Differences in mitochondrial functions and lipid metabolism coupled with immune recognition create the first divergence of the cell populations. Two main transcriptomic groups occurred, the first displaying anticryptococcal characteristics with increases of scavenger receptors to detect fungal products, phagosome maturation which kills the pathogen, and finally antigen presentation to continue the effort against the infection. These groups also displayed a higher-level gene expression relating to fatty acid metabolism (*FABP4*) than those in the second transcriptomic group. This differs from protective immune responses from Mtb, a pathogen with a similar disease manifestation, in that for Mtb, macrophages use glycolytic processes in an effort to kill the bacteria while permissive alveolar macrophages allow growth while using fatty acids and iron

[242]. However, our results do concur with the data from the cryptococcal mouse model where we observed similar gene expression associated with antifungal responses (genes involved in antigen presentation) vs permissive responses (mitochondrial genes) [98].

The trajectory analysis also informs us of a secondary path the anticryptococcal cells are taking: one that follows an increase in TNF-α transcription from top to bottom. Despite a single incubation period, individual immune cells do not interact with each fungal cell at the same time for the same amount of time but rather at different time throughout a dynamic process. The trajectory analysis can inform us of these dynamics and order the direction by way of pseudotimes [262]. Under that prism, we can see a progression of anticryptococcal activity ranging from "naïve" in the top clusters going through killing in the middle clusters and finally ending up at cessation. As first line defenders, macrophages and DCs must recognize, phagocytose, and kill the pathogen until proper adaptive immunity can emerge to control the pathogen. In the upper (early) clusters we see an increase in scavenger receptors. This is in line with other work showing that the scavenger receptor MARCO organizes and enhances antifungal activity during early cryptococcal infections [263]. Additionally, the upper clusters demonstrate increases in both lysosomal indicators, cryptococcal killing molecules, and antigen presentation pathways. Inferring, that lower (later) clusters represent more mature pathogen-host cell interactions, these processes give way to more cytokine signaling events along with increased production of TNF-α and some of its downstream products which, again, potentiates cryptococcal defenses [252].

The next step in investigating interactions between pulmonary phagocytic APCs and *C. neoformans* is to understand the extreme early time points where the host cell first reacts to the invading pathogen. Using TNF-α as the indicator for this initial recognition, we examined the differences between early clusters #1 and #9 which have differential TNF-α expression. Before the induction of this cytokine, the immune cell has most of the molecules necessary for the

detection and destruction of the fungus. As TNF-α becomes upregulated, there is a large changing of the cell's proteome as evidenced by the need to first change its protein production and increase its ribosomes. This is also accompanied by increases in fatty acid metabolism through FABP4 which then acts as a link between this metabolism and inflammation [264]. Through the scavenger receptors MARCO and CXCL16, intracellular lipid concentration is increased (possibly creating foam cells) which triggers FABP4 [265,266]. This then activates inflammation through both the IKK-NF-κβ and JNK-AP-1 pathways [267,268]. Among the inflammatory cytokines produced from these pathways include CCL3, CXCL8, IL-12, and IL-23 which each contribute to the control of a cryptococcal infection through recruitment of other immune cells or enhancing a Th1 or Th17 adaptive immune response [75].

Combining all these data, a proposed model of the initial interaction between *C. neoformans* and antifungal subsets of phagocytic APCs is displayed in Figure 3.10. In our model, the cells with the highest propensity for cryptococcal killing are those that have a higher innate usage of fatty acid metabolism ($FABP4^{Hi}$). Interactions begin with recognition of the pathogen, which may happen through scavenger receptors MARCO and CXCL16 which bind to oxidized low-density lipoprotein (oxLDL) [265]. The source of these lipids is unclear, one possible supply is from lung surfactant that is highly abundant and necessary for proper pulmonary function [93]. However, in our studies this is unlikely as these studies are *ex vivo* and do not contain any external lung surfactant, though residual phagocytosed surfactant could serve as a source. Another possible source could be from the pathogen itself while it produces extracellular vesicles (EVs) [269], which are in turn oxidized by reactive oxygen species (ROS) released by the host cell in a process known as lipid peroxidation (LPO) [270]. Whatever the source, these lipid products are taken up by the cell to increase its intracellular lipid concentration further activating FABP4. FABP4 can then initiate inflammation through either the JNK-AP-1 or IKK-NF-κβ pathways [264]. Additionally, FABP4 can directly regulate mitochondrial function [271].

Meanwhile during these early events, phagocytosis occurs with subsequent endosomal processing bringing the pathogen into a phagolysosomal compartment to begin destruction of the fungus. In this process, lysosome markers LAMP1/2 are increased along with other mediators such as ROS and cathepsin B (*CTSB*) as it combats *C. neoformans* [145,272]. Additionally, the cell will deploy saposins (from the precursor protein prosaposin [*PSAP*]) to degrade sphingolipids used by the fungus to facilitate intracellular growth [273,274]. Destroying the pathogen results in peptide fragments which can be used in antigen presentation through either the MHC-I or MHC-II pathways [74,275]. These actions put considerable stress on the host cell. This is sensed by GADD45α which activates NF-κβ through p38. Along with PPARγ, GADD45α can also increase the expression of FABP4 [276,277]. Finally, the NF-κβ pathway will increase the expression of TNF-α and its downstream mediators such as CCL3 and CXCL8 while the AP-1 pathway will upregulate the Th1 and Th17 mediators IL-12 and IL-23 [278-280]. There are additional feedback and cross loops in this model which include JUN/FOS which feedback into FABP4 and TNF-α cross-feeding into AP-1 [268,281].

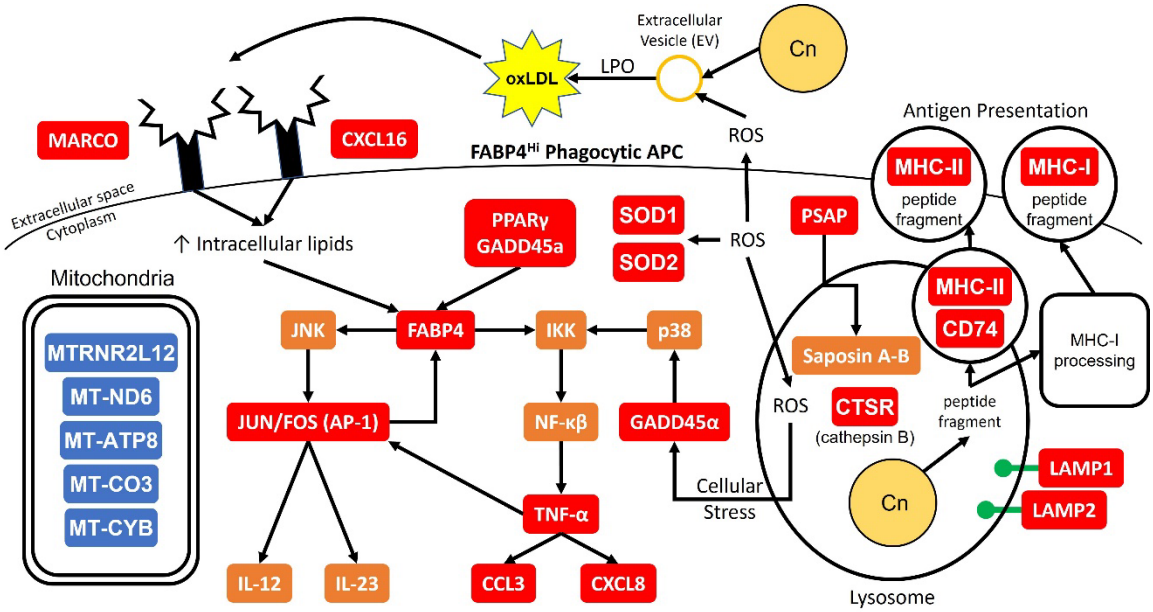

Figure 3.10. Model for Early Cryptococcal Interactions with Phagocytic APCs. Interactions of *C. neoformans* (Cn) with human pulmonary phagocytic APCs with high expression of FABP4 leads to downstream activation of genes including NF-κβ and AP-1 and phagosome maturation, and down-

regulation of many mitochondrial genes. Red and blue boxes indicate identified up- and down-regulated genes, respectively. Orange boxes indicate predicted activation.

Being one of the first studies conducted on human phagocytic APCs and their initial interactions with *C. neoformans* with single-cell resolution, we hope to provide some potential avenues for combating this pathogen. We were unable to determine the exact reason for differences in cryptococcal killing, however, our transcriptional data show that fatty acid metabolism is closely related to anticryptococcal activities by providing signals that confer a protective phenotype. Furthermore, specific proteins targets have been identified and their place in a model of cryptococcal infection must be thoroughly inspected. Identifying these protein targets and their abundance within the cells at different stages of interactions is important as the association between transcript level and protein amounts may not always strictly correlate, and may not carry a biological meaning [282]. Ongoing studies in our lab are examining this relationship closely to determine the causal effects these networks have on one another. We are conducting studies to validate the gene expression data from the single-cell RNA-seq, examining metabolic differences in antifungal cells vs permissive cells, and silencing upregulated genes in order to determine their role(s) in antifungal activity. The ultimate question is whether the expression of these genes and corresponding proteins confers a differential phenotype on the outcome of intracellular cryptococcal cells. In addition, we are interested in the networks that are activated and mechanisms used in successful antifungal host cells. The present study lays the foundation for future work to examine these areas and discover new treatments for pulmonary cryptococcosis.

3.5 Supplemental Materials

Table S3.1. Lung cell donor demographics and cell yield. Demographics for patient samples used in this study.

Donor #	Age	[a] Race	Gender	[b] Peak PaO2/FiO2	[b] Final PaO2/FiO2	Chest X-Ray Results	Cell Yield
1	29	AA	Male	438	438	Normal except for scattered areas of nodularity within right lung suggestive of bronchiolitis.	5.62×10^9
3	57	AA	Male	540	383	Normal except for stable left basilar infiltrate with layering pleural effusion and stable right mild basilar infiltrate.	4.61×10^9
4	35	AA	Male	363	262	Normal except for stable right pleural effusion and volume loss in right lung base.	6.02×10^9
5	52	C	Female	244	139	Normal except for persistent pneumomediastinum, and persistent soft tissue gas in the neck and left chest wall.	3.36×10^9
6	34	C	Male	329	321	Normal except for mild bilateral parahilar and basilar infiltrates.	7.30×10^9
7	48	C	Male	344	243	Normal except for increasing retro cardiac density, blunting in the region of the left costophrenic angle, and exclusion of the right costophrenic angle.	7.01×10^9
8	28	C	Female	283	338	Normal except for bibasilar pulmonary opacities. Possible small pleural effusion.	1.60×10^9
9	54	AA	Male	410	410	Normal except for left lower lobe atelectasis, with right basilar opacity suggesting atelectasis	1.24×10^9
10	43	C	Female	404	328	Normal except for bibasilar airspace infiltrates.	1.80×10^9
11	48	C	Female	427	416	Normal except for a few hazy low lung opacities, indicative of layering effusions, atelectasis, and/or airspace disease.	1.92×10^9
12	31	C	Female	434	211	Normal appearance. Lungs are expanded and clear. No pneumothorax or pleural effusion.	8.84×10^9
13	53	C	Female	390	390	Normal except for left basilar opacities and small left pleural effusion suspected.	4.93×10^9

[a] AA, C = African American, Caucasian
[b] PaO2/FiO2 = partial pressure arterial oxygen / fraction of inspired oxygen.

Table S3.2. Antibodies and viability dyes used for flow cytometry. List of all antibodies and conjugated fluorophores used in each flow cytometry panel.

Marker	Purpose	Fluorophore	Clone	Company	Assay used in:				
					Standard flow panel	Imaging flow panel #1	Imaging flow panel #2	TNF-α panel #1	TNF-α panel #2
Fixable Aqua	Viability	Fixable Aqua	N/A	ThermoFisher	+	-	-	-	-
Fixable Near IR	Viability	Fixable Near IR	N/A	ThermoFisher	-	-	-	+	+
CD45	Leukocyte	BV605	2D1	BioLegend	+	-	-	-	-
CD45	Leukocyte	PE	2D1	Invitrogen	-	+	-	-	-
CD45	Leukocyte	PerCP efluor 710	HI30	Invitrogen	-	-	+	+	+
Lineage cocktail (CD3, CD19, CD20, CD56)	Lymphocyte lineage	APC	UCHT1, HIB19, 2H7, 5.1H11	BioLegend	+	-	-	-	-
Calcofluor white	External fungi	Calcofluor white	N/A	ThermoFisher	+	-	-	-	-
CD207	Subset	PE	10E2	BioLegend	+	-	-	-	-
CD11c	Subset	PerCP efluor 710	3.9	Invitrogen	+	+	-	-	-
CD1c (BDCA-1)	Subset	PE-Vio 770	AD5-8E7	Miltenyi	+	-	-	-	-
CD14	Subset	APC efluor 780	61D3	Invitrogen	+	-	-	-	-
HLA-DR	Subset	BV650	G46-6	BD Biosciences	+	-	-	-	-
CD123	Subset	BV785	6H6	BioLegend	+	-	-	-	-
CD14	Subset	AF405	RPA-M1	Novus	-	+	+	-	-
CD1c	Subset	FITC	L161	Invitrogen	-	+	+	-	-
CD207	Subset	PE	10E2	BioLegend	-	-	+	-	-
CXCL8/IL-8	TNF-α marker	FITC	NAP II	Invitrogen	-	-	-	+	-
CCL3/MIP-1α	TNF-α marker	PE	CR3M	Invitrogen	-	-	-	+	-
IL-1β	TNF-α marker	FITC	CRM56	Invitrogen	-	-	-	-	+
TNF-α	TNF-α marker	PE	Mab11	Invitrogen	-	-	-	-	+

Table S3.3. Active cryptococcal detection results. Patient sample results for CrAg® LFA.

Sample Number	CrAg® LFA Results
1	Negative (-)
2	Negative (-)
3	Negative (-)
4	Negative (-)
5	Negative (-)
6	Negative (-)
7	Negative (-)
8	Negative (-)
9	Negative (-)
10	Negative (-)
11	Negative (-)
12	Negative (-)

Table S3.4. Complete list of genes differentially regulated between left and right clusters.

https://ndownloader.figstatic.com/files/38224728

Table S3.5. Complete list of genes differentially regulated between top and bottom left-side clusters.

https://ndownloader.figstatic.com/files/38224731

Table S3.6. Complete list of genes differentially regulated between clusters #1 and #9.

https://ndownloader.figstatic.com/files/38224734

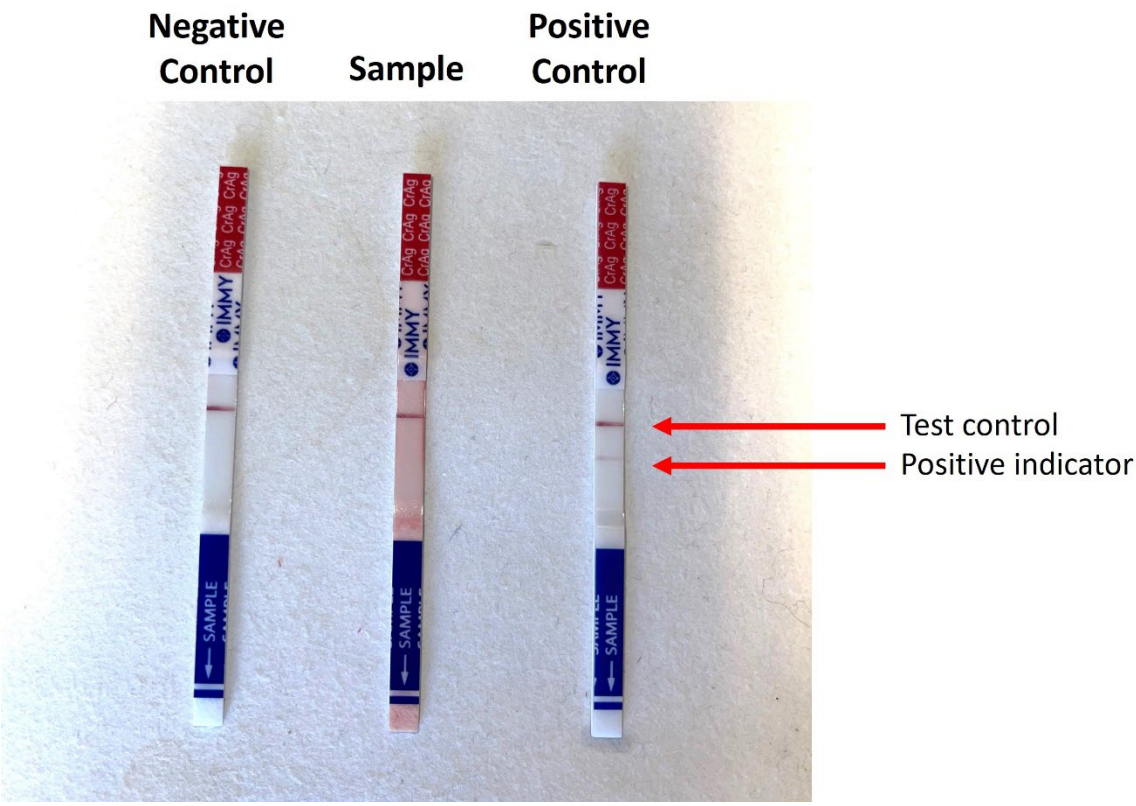

Figure S3.1. Representative Image of CrAg® LFA Results. Prior to processing, human BAL samples were tested for active cryptococcal infection by the commercially available CrAg® LFA kit. From left to right are shown representative images of a negative control, sample test result (#1), and a positive control. One line indicates a negative result while two lines indicate a positive result. Two replicate tests were performed on 12 samples (n=12).

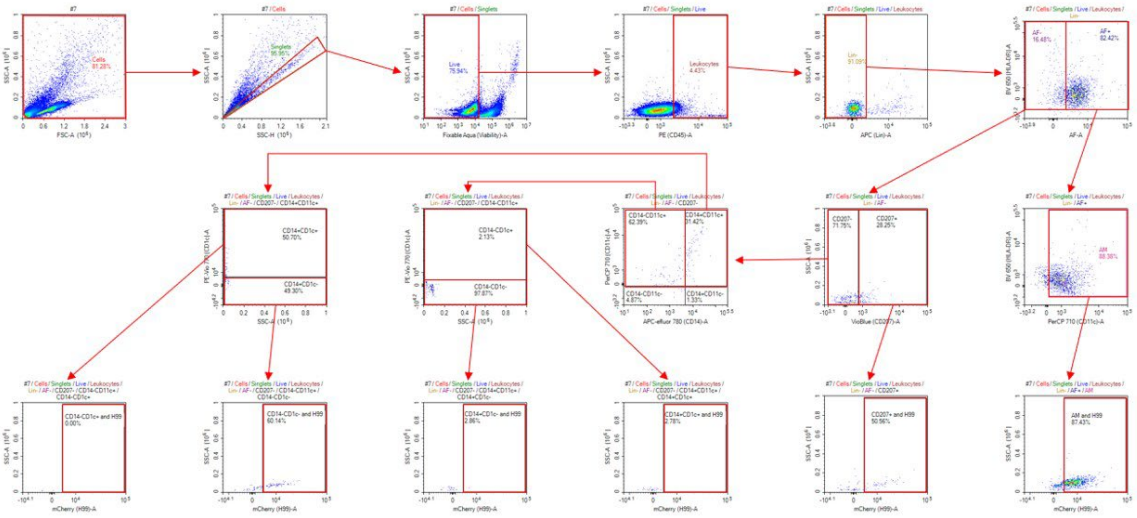

Figure S3.2. Representative Gating Scheme for Identification of Phagocytic APC Subsets during Flow Cytometry. The gating strategy used for identification of the 6 phagocytic APC subsets is shown. Red boxes indicate gates and red arrows point towards new plots from previous gates. Combination of positive and negative gating was used to identify subsets. Bottom six plots display total population for each of the six subsets with their respective uptake of mCherry expressing *C. neoformans*. Controls included unstained and single-color samples for color compensation as well as isotype control for false-positive identification.

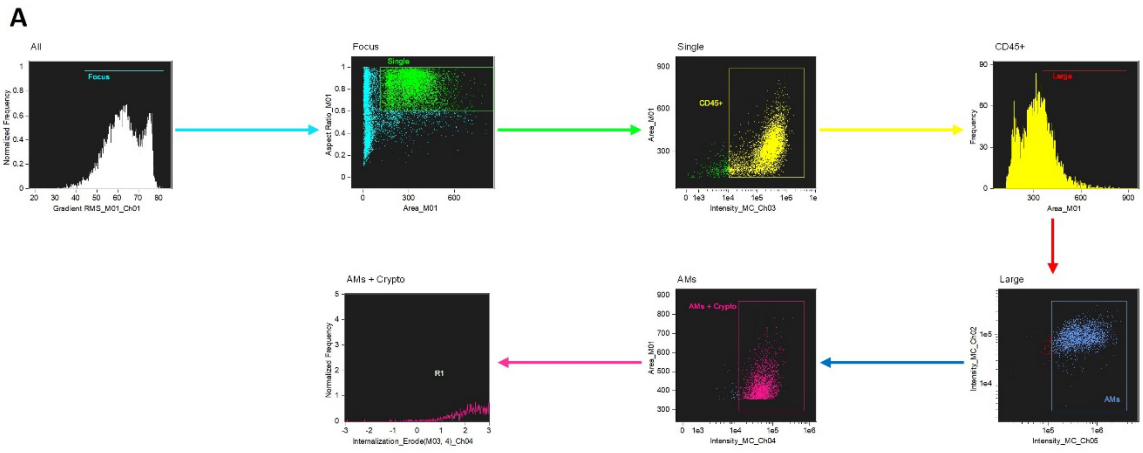

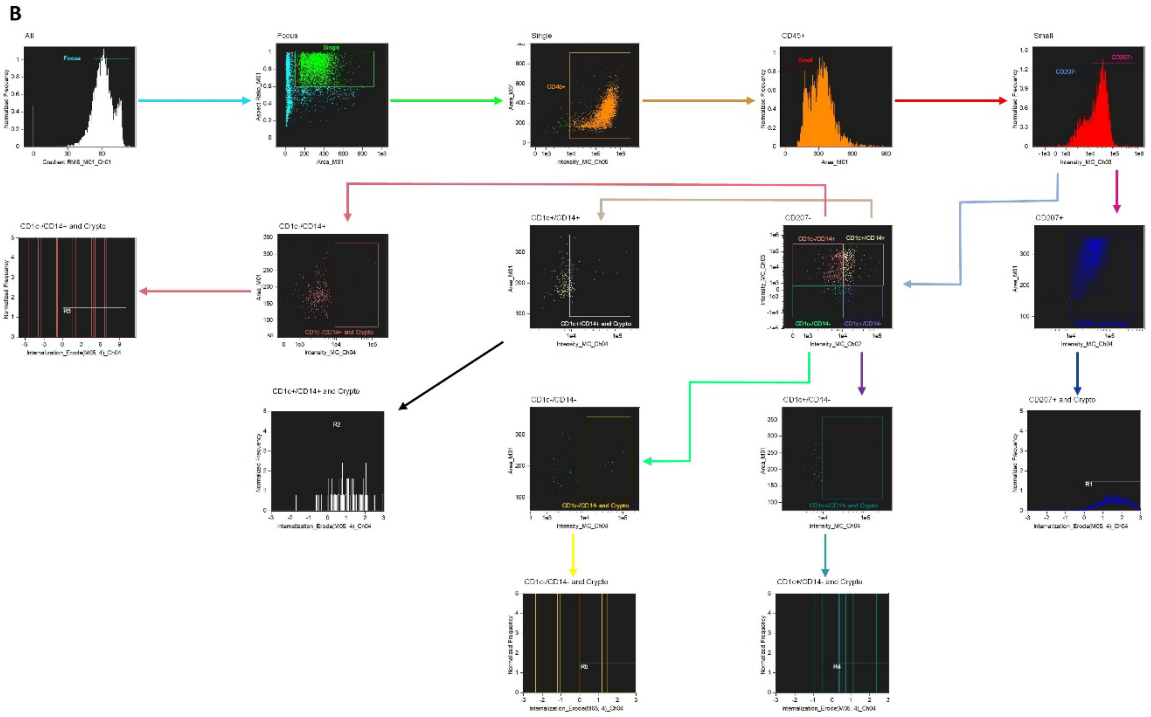

Figure S3.3. Representative Gating Scheme for Identification of Phagocytic APC Subsets during Imaging Flow Cytometry. The gating strategy used for identification of the 6 phagocytic APC subsets during imaging flow cytometry is shown. Colored boxes indicate gates and arrows point towards new plots from previous gates. (A) Scheme used with imaging flow panel #1 for the identification of alveolar macrophages. (B) Scheme used with imaging flow panel #2 for the identification of all other subsets. Combination of positive and negative gating was used to identify subsets along with internalization mask for internalized cryptococcal cells. Controls included single-color samples for color compensation.

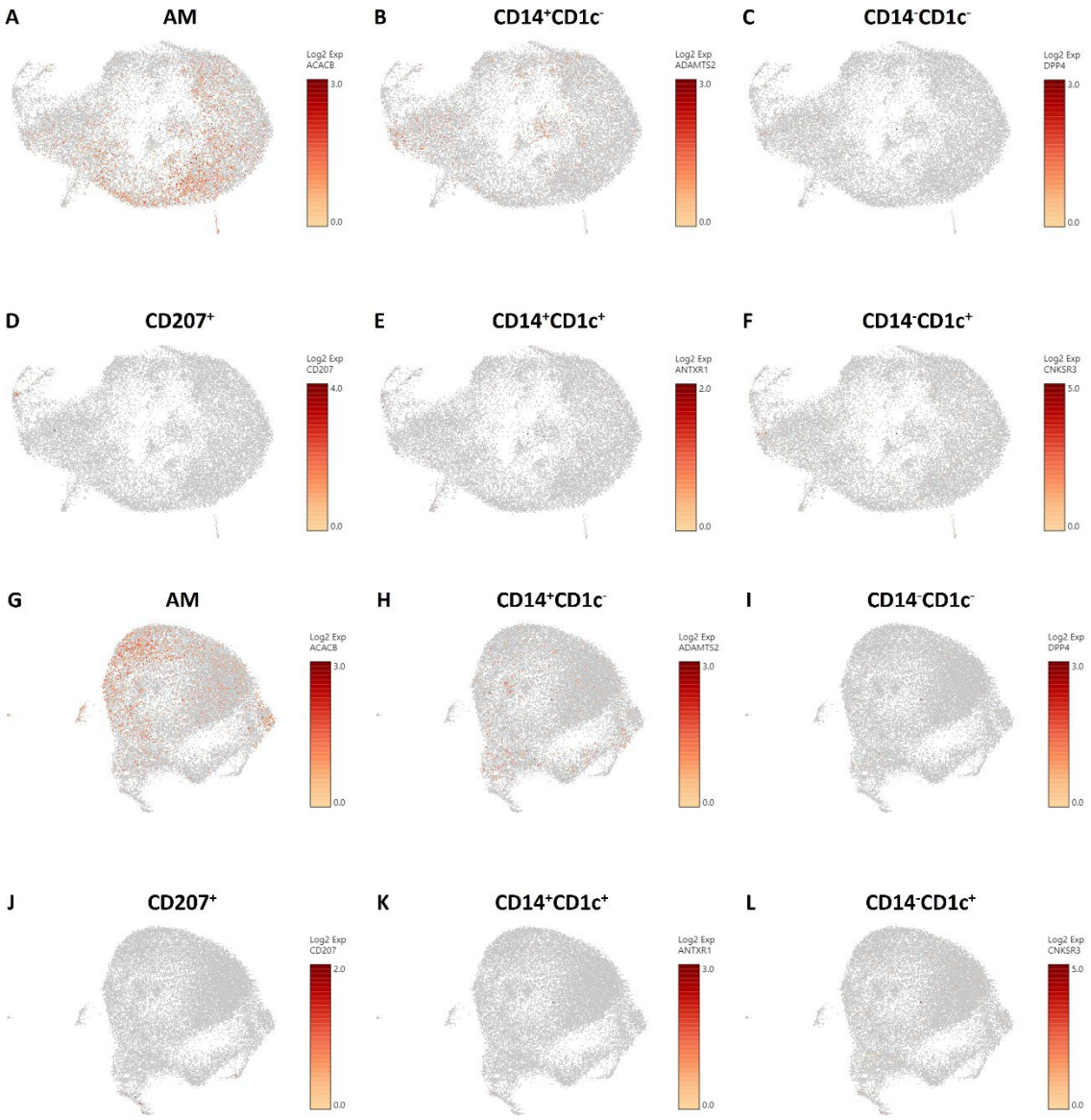

Figure S3.4. Identification of Phagocytic APC Subsets by Subset Specific Upregulated Genes.

Processed human BAL cells were enriched for phagocytic APCs and incubated with (G-L) or without (A-F) *C. neoformans* strain H99 for 2h and then processed for scRNA-seq. Phagocytic APC subsets were identified using upregulated genes *ACACB* (A/G), *ADAMTS2* (B/H), *DPP4* (C/I), *CD207* (D/J), *ANTXR1* (E/K), and *CNKSR3* (F/L) for AMs, $CD14^{+}CD1c^{-}$ macs, $CD14^{-}CD1c^{-}$ macs, $CD207^{+}$ DCs, $CD14^{+}CD1c^{+}$ DCs, and $CD14^{-}CD1c^{+}$ DCs, respectively. Data shown are transcriptional regulation of shown genes for 18,958 (naïve) and 22,344 (infected) total cells for three individual experiments for each cohort (n=3).

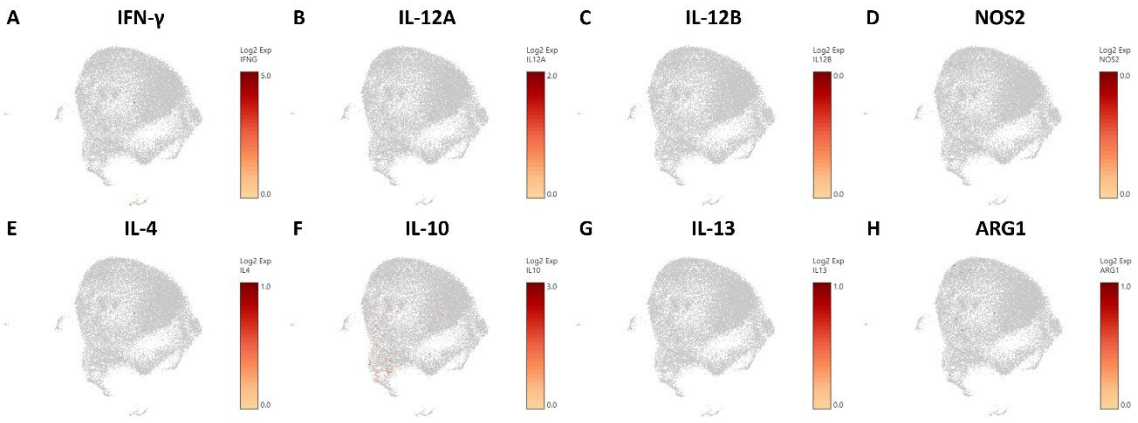

Figure S3.5. No Differential Macrophage Activation or Th1/Th2 Bias among the Cells. Processed human BAL cells were enriched for phagocytic APCs and incubated with *C. neoformans* strain H99 for 2h and then processed for scRNA-seq. Immune cells from the infected cohort were examined for markers for macrophage M1 or Th1-type cytokine genes (*IFN-γ*, *IL-12A*, *IL-12B*, *NOS2*) (A-D) and M2 or Th2-type cytokine genes (*IL-4*, *IL-10*, *IL-13*, *ARG1*) (E-H) activation. The cells experienced little to no upregulation for any of the genes. Data shown are transcriptional regulation of shown genes for 22,344 total cells for three individual experiments (n=3).

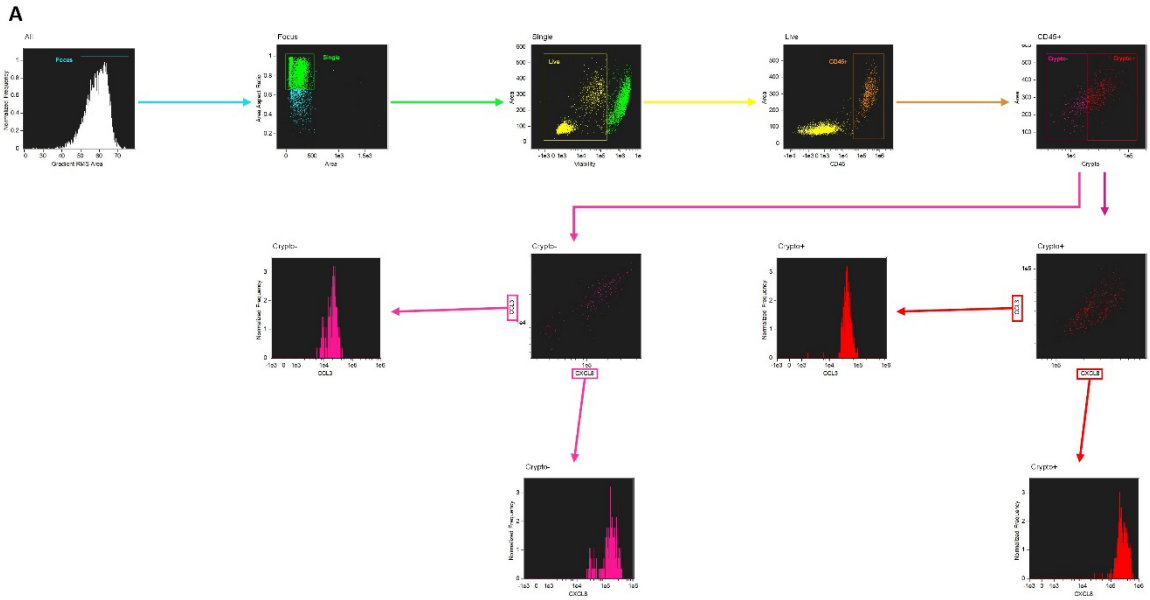

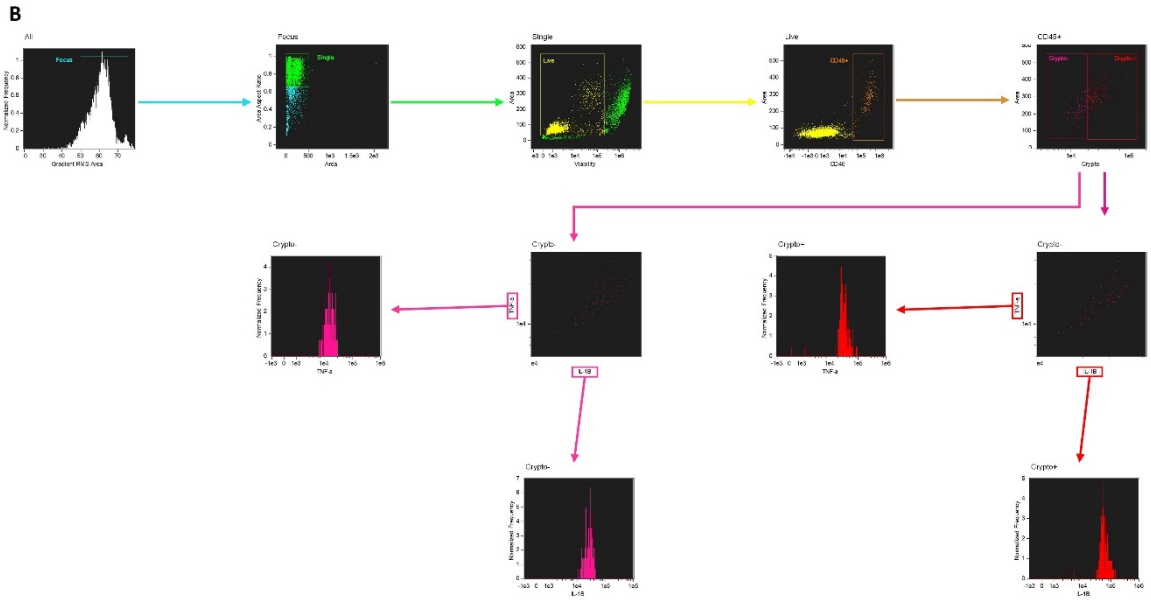

Figure S3.6. Representative Gating Scheme for Correlation of TNF-α Markers and Cryptococcal Morphology. The gating strategy used for identification of cryptococcal morphology as they correlate to TNF-α markers during imaging flow cytometry is shown. Colored boxes indicate gates and arrows point towards new plots from previous gates. (A) Scheme used with TNF-α panel #1 for correlation with markers CXCL8 and CCL3. (B) Scheme used with TNF-α panel #2 for correlation with markers TNF-α and IL-1β. Combination of positive and negative gating was used to identify individual markers and cryptococcal interaction. Controls included single-color samples for color compensation.

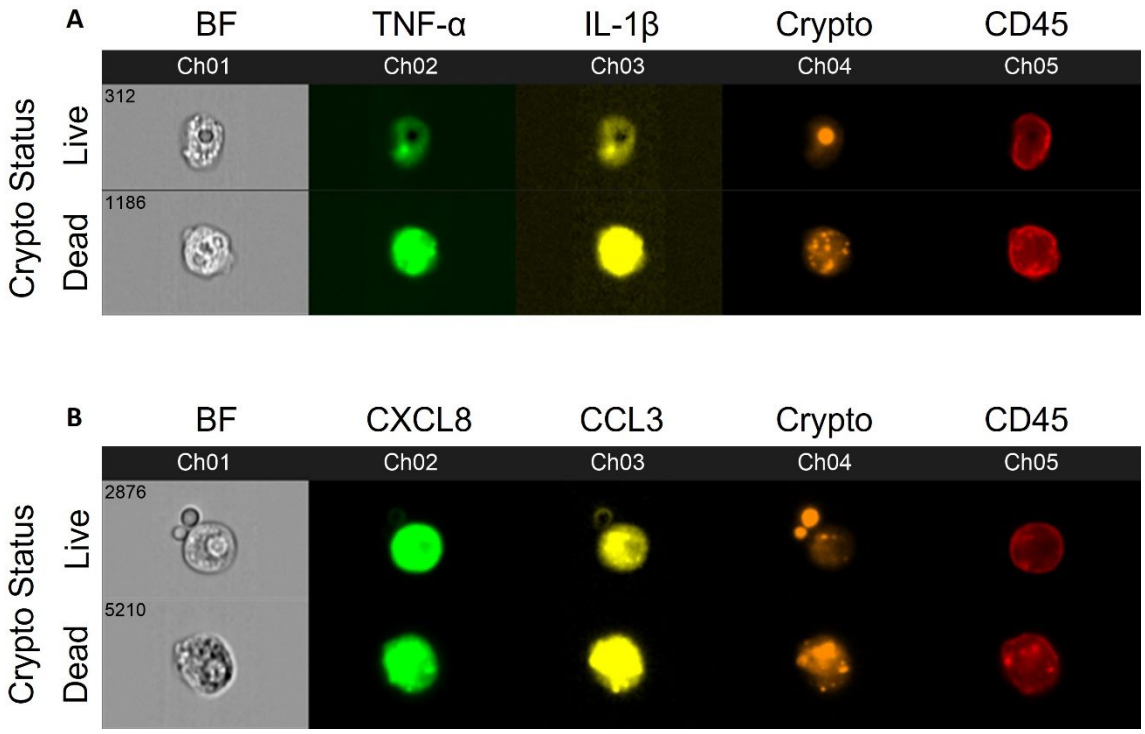

Figure S3.7. Representative Images of TNF-α Markers and Cryptococcal Morphology. Processed human BAL cells were enriched for phagocytic APCs and incubated with the fluorescent mCherry expressing *C. neoformans* strain JLCN920 for 2h and then stained with fluorescent antibodies for imaging flow cytometric analysis. Representative images of internalized *C. neoformans* to determine fate of the fungus. Budding and round fungal cells were considered as living while condensed and debris were deemed as dead cells. (A) Representative images for TNF-α and IL-1β. (B) Representative images for CXCL8 and CCL3. Combination of positive and negative gating was used to identify individual markers and cryptococcal interaction. Controls included single-color samples for color compensation.

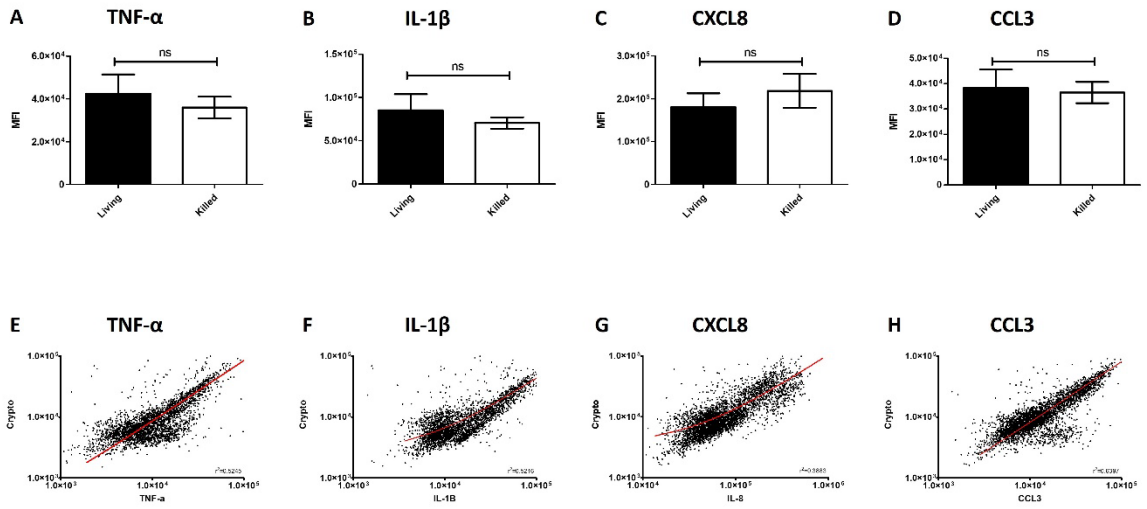

Figure S3.8. TNF-α Signaling Is Not an Indicator for Cryptococcal Fate. Processed human BAL cells were enriched for phagocytic APCs and incubated with fluorescent mCherry expressing *C. neoformans* strain JLCN920 for 2h and then stained with fluorescent antibodies for imaging flow cytometric analysis. Analysis revealed no significant differences between living and killed cryptococcal cells for cytokines TNF-α (A), IL-1β (B), CXCL8 (C), or CCL3 (D). Examination of fluorescent strengths for cryptococcal intensities (y-axis) against TNF-α (E), IL-1β (F), CXCL8 (G), or CCL3 (H) (x-axis) exhibited a strong positive correlation. Data shown for panels A-D are mean fluorescent intensities (MFI) of individual viable $CD45^{+}$ phagocytic APCs from three individual experiments (n=3). Panels (E-H) show pooled data from the 3 experiments in panels (A-D) of the same cells. Trend line is represented by the red line. Two-tailed *t*-tests were performed to compare pairs of MFIs with notation "ns" to represent no significance. Linear regression was performed to compare correlations of cryptococcal interaction with TNF- α markers. Slopes of all interactions were significantly non-zero ($p < 0.0001$).

CHAPTER IV

CONCLUSIONS

The focus of this research was to understand the capabilities of primary innate phagocytes against the fungal pathogen *C. neoformans,* and the investigations of our studies into these capabilities are presented in chapters II and III. Previous work into cryptococcal killing has focused on the oxidative mechanisms that immune cells use to kill the fungus, and considering that *C. neoformans* uses melanin to protect against this type of activity, we wanted to focus our research efforts into the nonoxidative (or enzymatic) means by which our phagocytes kill that pathogen [28]. The lysosome organelle is the compartment responsible for the destruction of many different types of pathogens and is host to many different compounds that enable it to achieve these means [157]. Many fungal pathogen survival strategies revolve around either the escape of this compartment or disabling/attenuating its functionality [283]. It is currently unclear if immune cells have any ability to destroy these pathogens enzymatically outside of the lysosome. The results of these studies are the focus of chapter II. Additionally, due to differences in the nature of antifungal activity by macrophages and dendritic cells, we also investigated differential antifungal activities of individual subsets of these phagocytes that reside in the human lung [75,98,214]. Since primary cryptococcosis first is established in the lungs, investigations into those resident immune cells, rather than cells circulating in the bloodstream, is a more applicable model to study differential interactions. To understand these differences, we used single-cell

RNA sequencing (scRNA-seq) to investigate differential gene expression and discovered changes that would potentiate the cell's ability to kill *C. neoformans*. These data are the focus of chapter III.

Investigating the anticryptococcal properties of the lysosomal contents of dendritic cells (DCs), we found that several different molecular weight fractions of the total lysosomal extract have killing characteristics. A mass spectrometry analysis was conducted on the total lysosomal extract, and we found it contained over 3000 different proteins. These findings were expected as the lysosomes are responsible for the breakdown of many different molecules including pathogens (bacterial, fungal, viral, etc.), biomolecules (proteins, lipids, carbohydrates, etc.), and other cellular debris [157]. Furthermore, out of the ten total individual lysosomal proteins tested in this study, five displayed anticryptococcal properties. Of these five, three (HNE, MMP25, and MPO) have shown antimicrobial properties directly acting as proteases against Gram negative bacteria [187,189,284] while the other two (coronin and NOSTRIN) are associated with antibacterial activity through indirect means [190,191]. Human neutrophil elastase (HNE) is a serine proteinase that cleaves protein through the catalytic triad of histidine, aspartate, and serine. This lysosomal protein is of particular importance in the defense of cryptococcosis, as it is often found in the anticryptococcal neutrophil extracellular traps (NETs), and previous work has shown that HNE can inhibit the growth of *C. neoformans* when the NETs themselves are not inhibited by the cryptococcal capsular component GXM [285]. MMP25 is a member of the matrix metalloproteinases that are endopeptidases [188]. While not much outside of this study is known about the anticryptococcal properties of these proteins, they are abundant during lung inflammation, which coincides with early cryptococcosis [286]. Myeloperoxidase (MPO) is an enzyme that catalyzes hypohalous acid from hydrogen peroxide and is abundant in lung neutrophils. The anticryptococcal properties demonstrated by human lysosomal extract is congruent with previous studies also showing its anticryptococcal properties in a murine model [287]. The first nonenzymatic anticryptococcal protein, coronin, has not been previously

investigated in the context of cryptococcosis, but it may assist in fungal killing as is an actin binding protein that facilitates phagocytosis in leukocytes [190]. The other nonenzymatic anticryptococcal protein was NOSTRIN (nitric oxide synthase trafficking) which also has not been evaluated against fungal infection. However, previous research showed that it does induce the release of nitric oxide which, in turn, is directly used to kill and inhibit the growth of *C. neoformans* [191,288]. Further, each of the proteins tested did not correspond to any one particular molecular weight fraction. In fact, many of these proteins were found in multiple different fractions, most notably coronin and MPO were found in eight and four individual fractions, respectively (Supplementary Table S2.1). The target for these proteins is currently unclear as their mechanism of action is unknown. However, it has been previously shown that they inhibit bacterial growth via disruption to the cell membrane or aiding the efficacy of ROS/RNS [187-192].

The five remaining proteins (calmodulin, calnexin, cystatin B, S100A6, and striatin) tested in this study all displayed little to no anticryptococcal properties despite their potential based on previous data and/or mechanisms [145,205,209,210,289]. Cystatin B is a molecule that inhibits cysteine proteases such as the anticryptococcal protein cathepsin B [290]. However, we chose to test this molecule due to the fact that other cysteine protease inhibitors (calpain and CA-074) had a synergistic anticryptococcal effect when used in conjunction with cathepsin B [145]. In our study, this protein did not retain its anticryptococcal properties that the other inhibitors had. Striatin also showed no inhibition of *C. neoformans,* despite having broad-spectrum antimicrobial activity [289]. The remaining three proteins from our study displayed significantly increased fungal growth when compared to the control. The S100 family of proteins are characterized by an EF-hand type conformation in the calcium binding site [207]. Family members S100A8 and S100A9 combine to form a heterodimer called calprotectin which can inhibit cryptococcal growth through zinc exclusion [205]. However, the related protein S100A6 did not retain these anticryptococcal properties, but rather increased the growth of the fungus.

Both calmodulin and calnexin are calcium binding signaling proteins that have been shown to increase antimicrobial activity against pathogens, including Gram negative bacteria like *Pseudomonas* [209,210]. This efficacy was not retained in our study as shown by the significantly enhanced fungal growth when incubated with these two proteins. As for the molecular weight fractions, these ineffective proteins were found in many different factions as well as some fractions that displayed anticryptococcal properties (Supplementary Table S2.1).

Due to differences in testing procedures between laboratories, the Clinical and Laboratory Standards Institute (CLSI) have published standardized protocols for antifungal testing [165,168]. Using these protocols, we tested the five anticryptococcal lysosomal proteins in order to establish their efficacy under these standards. CLSI guidelines stipulate testing to be done in RPMI-MOPS media (pH 7.0) rather than the phosphate buffer (pH 5.5) we used previously to mimic intralysosomal pH[145,154]. Therefore, we tested the proteins in both conditions to evaluate any changes in activity due to changes in media and/or pH. Under these conditions, HNE, MMP25, and NOSTRIN not only retained their anticryptococcal activity in the acidic phosphate buffer, but also showed some activity in the neutral RPMI-MOPS. Changes in pH can change the conformation of antimicrobial proteins, which may affect their activity [291]. Having proteins retain some activity under neutral pH is promising for the use of these proteins to treat cryptococcosis where pH is more neutral in the tissues. The two remaining proteins (coronin and MPO) had different MIC values in RPMI-MOPS than in our initial assays. These changes highlight the need for standardized protocols in laboratories, as differences in methodology, incubation conditions/time, and fungal concentrations can all affect the results of the study.

To further understand the properties of killing and inhibition of our lysosomal proteins, we conducted further investigations into cryptococcal killing involving combinatorial assays and time-kill kinetic assays. Amphotericin B (AmpB) is fungicidal against *C. neoformans* and is usually the drug of choice against infection [47]. However, at high doses it can become toxic to the host so investigations in reducing dosage while still maintaining efficacy are needed [292].

Therefore, we conducted checkboard assays to test for any synergistic effects between our lysosomal proteins and AmpB. Despite retaining their original effective concentrations, none of the test proteins showed any synergistic (or antagonistic) effects when used in combination with AmpB. These results are not too surprising due to the tested cryptococcal strain (H99), while fully virulent, is still susceptible to AmpB. Investigations using strains resistant to AmpB may yield different results. We also developed a time course assay to determine the rate of killing for the lysosomal proteins. We took 2X the MIC values established above and incubated the lysosomal proteins with *C. neoformans* over 48 hours and calculated CFUs at defined intervals. We found that while all five proteins reached inhibitory levels after 48 hours, the rate at which they inhibit differed. NOSTRIN, HNE, and MPO all reached >75% inhibition by two hours while coronin and MMP25 needed at least 24 (the time for our initial assay) hours to reach the same levels of inhibition. Time-kill kinetic assays are useful for understanding interactions between the protein and pathogen and can infer differences in mechanisms of killing or resistance [293]. Our findings imply that there is more than one mode of fungal killing among our proteins, and further elucidation into the mechanism(s) is needed.

Before testing these proteins as therapeutics within an animal model, cytotoxicity tests must be completed prior in order to establish mammalian cells tolerate the anticryptococcal dosages. Therefore, we used a commercially available kit to test cytotoxicity in murine J774A.1 macrophages. Cytotoxicity standards state that cytotoxicity less than 30% is considered non-toxic [176]. All of our tested proteins had values <30%, or non-toxic [218]. These proteins show initial promise as therapeutics. However, their bioavailability in the bloodstream after medication (depending on the route) and physiological relevance in a live model have not been tested. Those types of data are difficult to gather until the complex interactions within a live model are studied. Furthermore, there may be other complex protein-protein interactions that should be investigated as well. These types of *in vitro* tests assess the bioaccessibility or the potential amount of active compound available for absorption [294]. The data generated from these studies are a starting

point from which more invasive bioavailability testing in live models can occur as the later must measure the metabolic endpoints which cannot be evaluated by *in vitro* methods [295].

Further considerations must be had before human testing as these lysosomal proteins are relatively large compared to current antifungals used for treatment. Amphotericin B is about 924 daltons and is one of the largest antifungal drugs while the tested lysosomal proteins are in the 30-80 kDa range and puts them in the category of large molecule drugs or biologics [218,296]. Being distinct from small molecule drugs, due to their size and complexity biologics carry unique characteristics in absorption, distribution, metabolism, and elimination (ADME) [297]. The major route of absorption for these molecules is through lymphatic uptake which is relatively slow and can lead to a longer peak concentration (including possible toxicities) [298]. Additionally, the volume of distribution in tissues can be small as it requires active transport through endocytosis rather than passive diffusion [299]. Finally, once inside cells they are usually metabolized through proteolytic degradation and eliminated by renal excretion [300]. Both of these processes can be hampered by lysosomal diseases and kidney impairment [192,301]. Aside from ADME, biologics can also be immunogenic and cause a host response which can eliminate them before their intended action [302]. All of these properties must be accounted for before first-in-human (FIH) dosing can even be researched [303].

Before phagocytosis and killing in the lysosome can occur, the immune cells must first recognize and internalize a pathogen. There have been reports that macrophages can either be fungicidal and kill the fungus or allow for its intracellular replication [75,214]. To study this, we investigated the initial interaction between *C. neoformans* and human innate phagocytic antigen presenting cells (APCs), such as macrophages and dendritic cells (DCs) in the lung. Previous studies have found heterogeneity among the once established homogenous groups of these cells within bronchial alveolar lavage (BAL) fluid and also in lung tissue [95,304,305]. Isolation of cells from within the alveolar spaces is an important step in identification because many different cells exist in the interstitial tissue of the lung, and additional monocyte-derived cells that can

migrate into the lung in response to infection [232]. Together, different research groups have found up to 8 individual subsets of macrophages and DCs (four each) [95,304]. Through the use of flow cytometric analysis, our data show these different subsets within BAL fluid in similar proportions as before. Furthermore, each of the six different subsets (three macrophage and three DCs) that we examined were able to interact with and uptake the fungus in different capacities. These differences are in line with the previous reports of these subsets having different phagocytic indices for bacterial species at low MOIs [95]. Furthermore, the high association of cryptococcal cells with pulmonary phagocytes were similar to what we observed in the murine model [98].

The next step in determining whether each subset is fungicidal or permissive for intracellular growth was to study cryptococcal fate, and we used intracellular morphology as a proxy for this as previously shown for both *Cryptococcus* and *Aspergillus* [145,306]. Earlier studies showed that *C. neoformans* adopts a c-shape or degrades into condensed blebs when dying in the lysosome or following treatment with lysosomal enzymes [145,154]. To examine this morphology, we used imaging flow cytometry in conjunction with an mCherry expressing *C. neoformans* strain (JLCN920). In this study, we found that two of the macrophage subsets ($CD14^{+}CD1c^{-}$, $CD14^{-}CD1c^{-}$), while able to phagocytose *C. neoformans*, were completely unable to kill any of the internalized fungal cells. Comparing this to the mouse model of infection, we see only one subset that exhibited significantly increased killing ($Ly6c^{-}$ monocyte-like macrophage) and one that allowed significantly increased intracellular growth ($CD11b^{+}$ DC) [98]. One can also compare these results against *Mycobacterium tuberculosis* (Mtb), as that pathogen has a similar disease presentation and resolution to *C. neoformans.* They both can survive intracellularly in innate phagocytes such as macrophages, and they both promote Th2 responses in evading the immune system [261]. However, unlike our study, with Mtb, alveolar macrophages are permissive to intracellular growth, while the interstitial macrophages were antibacterial [241].

Now that we have established that subsets differ in their anticryptococcal properties, the question shifts to what makes these subsets different from one another? Why do some subsets confer anticryptococcal properties, while others do not? Single-cell RNA sequencing (scRNA-seq) was used on the innate phagocytic APCs following incubation/uptake of *C. neoformans* to understand the transcriptomic differences that would impart killing versus permissive growth. We were unable to utilize traditional bulk RNA-seq on the different subsets due to the time requirements that cells need to be kept alive. Some subsets only survive ~4h after thawing, so flow sorting and bulk sequencing were not viable options. Computational clustering of the infected cohort showed twice as many different clusters when compared to the naïve cohort. This outcome was expected as only a portion of the cells will interact with the fungus and change their profile, doubling the number of clusters [307]. To understand what cell type each of the clusters corresponded to in the computational algorithm, we compared each cluster to subset-specific transcriptional markers that have previously established [95]. However, none of these markers correlated with any of the clusters, or even aligned with the macrophage differentiating gene *APOC1* [308]. So despite being different subsets, the cellular processes that dominate the interactions between immune cells and fungus drive the differences to a greater extent than the subtle differences between subsets.

Since obvious patterns of computational clustering were not readily apparent, we used a trajectory analysis to determine dynamic patterns of differences between clusters to infer relationships and cellular processes [309]. Applying these analyses to the infected cohort revealed two major branching paths (trajectories) that the clusters follow: one showing anticryptococcal characteristics (with genes for fatty acid metabolism, antigen presentation, and scavenger receptors upregulated) and the other being permissive for allowing intracellular cryptococcal growth (mitochondrial genes upregulated). Two genes of note were upregulated in the anticryptococcal clusters: FABP4 and MARCO. FABP4 has been shown to integrate lipid metabolism with inflammation and, therefore, a protective response [310]. Additionally, MARCO

is a scavenger receptor that contributes to early defense against cryptococcal infection [263]. This receptor is mainly expressed on phagocytic APCs and can be upregulated during both fungal and bacterial infections to both directly facilitate in phagocytosis and modulation of cell recruitment and proinflammatory cytokines[311-313]. The fatty acid metabolism in the protective set also mirrors the opposite phenotype in Mtb in which the antibacterial responses come from glycolytic processes and the permissive cells utilize fatty acids [242]. However, our data in the human cells supported what we observed in the murine model, which shows similar expression of antigen presentation and mitochondrial genes [98].

Following the anticryptococcal clusters, we next sought to understand the processes and changes in transcriptional profiles involved in the killing *C. neoformans*. Due to trajectory analyses arranging clusters in a logical pseudotemporal order, we can see these differences in a single incubation period [262]. Clusters in the early stages of cryptococcal killing have increased expression of recognition genes (scavenger receptors MARCO and CXCL16) as well as lysosomal markers (LAMP1/2) and anticryptococcal proteins (PSAP and CTSB) [145,273]. These line up with the previously mentioned MARCO that orchestrates early cryptococcal defenses [263]. In the later stages, these genes give way to more signaling genes that include JUN and FOS (which form the transcription factor AP-1) and TNF-α response genes (including chemokines CCL3 and CXCL8) [278,280]. These signaling genes have been shown to lead to Th1 and Th17 type cytokine responses, which are applicable for protective responses against *C. neoformans* [75,268].

With the evidence that the anticryptococcal cells increase regulation of TNF-α response genes, we wanted to correlate whether these increased transcript levels coincide with the killing cryptococcal morphology displayed earlier. Analyzing the fluorescent intensities of TNF-α, IL-1β, CXCL8, and CCL3, we found there was no correlation between these markers and cryptococcal morphology. This is possibly due to the lag time in protein production during a transition state. As the cell transitions to the killing phenotype, it needs to make the mRNA first

before gearing up the machinery to manufacture the protein. Only during steady state where cells are undergoing long term processes such as proliferation can mRNA and protein levels be accurately correlated. Short term and dynamic processes (as in our study) can induce these differences leading to nearly 80% variance in abundance [282]. Instead, we saw differences in TNF-α (and downstream markers) protein levels in cells that have interacted with *C. neoformans* versus those that have not. This initial interaction happens prior to killing and, therefore, is likely to have more time to proceed to the later signaling stages before killing can occur.

Putting these scRNA-seq data together, a sequence of events occurs as subsets of phagocytic APCs kill the fungus (Figure 3.10). This starts with the recognition of oxidized low-density lipoproteins (oxLDL) by scavenger receptors (MARCO and CXCL16) with are abundant in FABP4^{Hi} cells. The source of oxLDL is currently unclear and may be derived from either endogenous (lung surfactant) or exogenous (fungal vesicles) sources [93,269]. Whatever the source, these will get taken up and increase the intracellular concentration of lipids which will signal FABP4. This intermediary between metabolism and inflammation can then signal the response genes that activate either through JNK-AP-1 or IKK-NF-κβ pathways [264]. These pathways can regulate anticryptococcal cytokines/chemokines such as TNF-α, CCL3, CXCL8, IL-12 and IL-23 [278-280]. Concomitant to these, the immune cell is also actively killing the fungus through both oxidative and non-oxidative mechanisms which can then lead to antigen presentation through either MHC-I or MHC-II [145,272,275,314]. Our studies found the anticryptococcal lysosomal proteins cathepsin B and saposin being upregulated in this scenario. There may be other genes within these data that may confirm our previous findings on anticryptococcal lysosomal proteins. However, the cells used to generate those data were from murine DCs while this study used human lung cells (a mix of macrophages and DCs) and, therefore, genes may not be the same across cell types and host. Additionally, in the model are feedback loops in the form of JUN/FOS directly feeding into FABP4 and TNF-α cross-feeding

into AP-1 [268,281]. As all these processes take place, there is a sizable downregulation of mitochondrial genes which can occur directly through FABP4 signaling [271].

These data suggests that the axis for cryptococcal defense seem to rotate around the modulation of FABP4. Going forward, we must first validate these findings empirically to better understand the role of FABP4, fatty acid metabolism, and their modulatory networks in host defense against fungal pathogens. There have been previous studies showing both the viability of knockout (KO) mice and the efficacy of pharmaceutical inhibition of FABP4. One such study was able to investigate KO mice up to 9 months in age which is longer than needed for murine models of cryptococcosis [113,252,315]. Further studies have found that the FABP4 inhibitor BMS309403 can influence the modulation inflammation and macrophage programming [316-318]. While not directly related to fungal pathogens, the aforementioned studies do show a link between fatty acid metabolism and host defense, and this link is shown to play a role in the resolution of sepsis in mice [319]. The other side to all of this is the host response as it correlates with an upregulation of FABP4. It is possible to supplement media to induce fatty acid metabolism (and the induction of FABP4), however, care must be taken as even low levels can impact models in the form of lipotoxicity [320,321]. Further studies can investigate the levels of FABP4 in naïve cells, but this type of assay can be limiting as tissue resident cells have a short lifespan and are not suitable for FACS or magnetic sorting in addition to standard sequencing preparation work.

Typically, Th1 type $CD4^+$ T cell responses are responsible for eliminating the pathogen, however, in cases where the patient has a compromised immune system (as with HIV/AIDS) this type of response is not always possible [47]. In treating someone with both cryptococcal meningitis and AIDS, care and a proper treatment regimen must be followed to ensure the highest possible survival rate. This includes the treatment of the fungal infection with antifungal drugs prior to treating HIV with antiretroviral therapies (ARTs), to prevent cryptococcal immune reconstitution inflammatory syndrome (C-IRIS) [322]. This presents as exaggerated and even

destructive inflammatory responses as the result of the rapid reversal of a weakened immune system to create a Th1 cytokine storm [323]. Due to these difficulties, we have explored other means by which to treat this disease. Both the who (anticryptococcal phagocytic APC) and the how (nonoxidative lysosomal proteins) were explored in these studies. Future work will need to explore these properties in detail to elucidate both the full pathways and the mechanisms by which cryptococcal killing occurs. Differences in metabolism between killing versus permissive cells may be paramount, as innate immune cells respond differently depending on the invading pathogen [98,242,324]. And by using and exploiting endogenous proteins and pathways to kill *C. neoformans*, we do not risk both C-IRIS and toxic antifungal compounds.

With over 225,000 yearly cases which carry an 80% mortality rate, cryptococcal meningitis is one of the leading causes of death in HIV/AIDS patients [31]. These numbers are unacceptably high and the need to find new ways to combat this pathogen is paramount. Due to lower overall funding for the development of novel compounds against *C. neoformans* and fungal diseases, in general, the importance of chapter II becomes apparent [51]. We found not only new compounds which inhibit the growth of the fungus, but there may be multiple modes of inhibition among the proteins. Furthermore, they are all well tolerated in mammalian cells which means further testing in an animal model of cryptococcosis is possible. Chapter III searches for differences among our immune cells and reveals a cryptococcal killing and permissive phenotype. Transcriptional variations between these two phenotypes will give us possible avenues with which to attack the pathogen. In addition, the metabolomic changes gives us clues about how cells are investing their energy as they become stressed by the fungus. Many of these differences are similar to our findings using mice. Therefore, we can now begin to validate some of these finding and study specific genes and pathways to elucidate the specific mechanisms of antifungal activity [98]. Considering that *C. neoformans* is distributed worldwide, these findings can go a long way in combating a disease which can affect many people.

REFERENCES

1 Kwon-Chung, K. J. *et al.* The Case for Adopting the "Species Complex" Nomenclature for the Etiologic Agents of Cryptococcosis. *mSphere* **2**, doi:10.1128/mSphere.00357-16 (2017).

2 Cogliati, M. Global Molecular Epidemiology of Cryptococcus neoformans and Cryptococcus gattii: An Atlas of the Molecular Types. *Scientifica (Cairo)* **2013**, 675213, doi:10.1155/2013/675213 (2013).

3 May, R. C., Stone, N. R., Wiesner, D. L., Bicanic, T. & Nielsen, K. Cryptococcus: from environmental saprophyte to global pathogen. *Nat Rev Microbiol* **14**, 106-117, doi:10.1038/nrmicro.2015.6 (2016).

4 Meyer, W., Mitchell, T. G., Freedman, E. Z. & Vilgalys, R. Hybridization probes for conventional DNA fingerprinting used as single primers in the polymerase chain reaction to distinguish strains of Cryptococcus neoformans. *J Clin Microbiol* **31**, 2274-2280, doi:10.1128/jcm.31.9.2274-2280.1993 (1993).

5 Boekhout, T. *et al.* Hybrid genotypes in the pathogenic yeast Cryptococcus neoformans. *Microbiology (Reading)* **147**, 891-907, doi:10.1099/00221287-147-4-891 (2001).

6 Litvintseva, A. P., Thakur, R., Vilgalys, R. & Mitchell, T. G. Multilocus sequence typing reveals three genetic subpopulations of Cryptococcus neoformans var. grubii (serotype A), including a unique population in Botswana. *Genetics* **172**, 2223-2238, doi:10.1534/genetics.105.046672 (2006).

7 Hagen, F. *et al.* Recognition of seven species in the *Cryptococcus gattii*/*Cryptococcus neoformans* species complex. *Fungal Genetics and Biology* **78**, 16-48, doi:10.1016/j.fgb.2015.02.009 (2015).

8 Chayakulkeeree, M. & Perfect, J. R. Cryptococcosis. *Infect Dis Clin North Am* **20**, 507-544, v-vi, doi:10.1016/j.idc.2006.07.001 (2006).

9 Abassi, M., Boulware, D. R. & Rhein, J. Cryptococcal Meningitis: Diagnosis and Management Update. *Curr Trop Med Rep* **2**, 90-99, doi:10.1007/s40475-015-0046-y (2015).

10 Fang, W., Fa, Z. & Liao, W. Epidemiology of Cryptococcus and cryptococcosis in China. *Fungal Genet Biol* **78**, 7-15, doi:10.1016/j.fgb.2014.10.017 (2015).

11 Springer, D. J. *et al.* Cryptococcus gattii VGIII isolates causing infections in HIV/AIDS patients in Southern California: identification of the local environmental source as arboreal. *PLoS Pathog* **10**, e1004285, doi:10.1371/journal.ppat.1004285 (2014).

12 Chowdhary, A., Rhandhawa, H. S., Prakash, A. & Meis, J. F. Environmental prevalence of Cryptococcus neoformans and Cryptococcus gattii in India: an update. *Crit Rev Microbiol* **38**, 1-16, doi:10.3109/1040841X.2011.606426 (2012).

13 Wickes, B. L., Mayorga, M. E., Edman, U. & Edman, J. C. Dimorphism and haploid fruiting in Cryptococcus neoformans: association with the alpha-mating type. *Proc Natl Acad Sci U S A* **93**, 7327-7331, doi:10.1073/pnas.93.14.7327 (1996).

14 Kozubowski, L. & Heitman, J. Profiling a killer, the development of Cryptococcus neoformans. *FEMS Microbiol Rev* **36**, 78-94, doi:10.1111/j.1574-6976.2011.00286.x (2012).
15 Almeida, F., Wolf, J. M. & Casadevall, A. Virulence-Associated Enzymes of Cryptococcus neoformans. *Eukaryot Cell* **14**, 1173-1185, doi:10.1128/EC.00103-15 (2015).
16 Vaishnav, V. V., Bacon, B. E., O'Neill, M. & Cherniak, R. Structural characterization of the galactoxylomannan of Cryptococcus neoformans Cap67. *Carbohydr Res* **306**, 315-330, doi:10.1016/s0008-6215(97)10058-1 (1998).
17 Bose, I., Reese, A. J., Ory, J. J., Janbon, G. & Doering, T. L. A yeast under cover: the capsule of Cryptococcus neoformans. *Eukaryot Cell* **2**, 655-663, doi:10.1128/EC.2.4.655-663.2003 (2003).
18 Heiss, C., Klutts, J. S., Wang, Z., Doering, T. L. & Azadi, P. The structure of Cryptococcus neoformans galactoxylomannan contains beta-D-glucuronic acid. *Carbohydr Res* **344**, 915-920, doi:10.1016/j.carres.2009.03.003 (2009).
19 De Jesus, M., Chow, S. K., Cordero, R. J., Frases, S. & Casadevall, A. Galactoxylomannans from Cryptococcus neoformans varieties neoformans and grubii are structurally and antigenically variable. *Eukaryot Cell* **9**, 1018-1028, doi:10.1128/EC.00268-09 (2010).
20 Steenbergen, J. N., Shuman, H. A. & Casadevall, A. Cryptococcus neoformans interactions with amoebae suggest an explanation for its virulence and intracellular pathogenic strategy in macrophages. *Proc Natl Acad Sci U S A* **98**, 15245-15250, doi:10.1073/pnas.261418798 (2001).
21 Fu, M. S. *et al.* Amoeba Predation of Cryptococcus neoformans Results in Pleiotropic Changes to Traits Associated with Virulence. *mBio* **12**, doi:10.1128/mBio.00567-21 (2021).
22 Kozel, T. R., Pfrommer, G. S., Guerlain, A. S., Highison, B. A. & Highison, G. J. Role of the capsule in phagocytosis of Cryptococcus neoformans. *Rev Infect Dis* **10 Suppl 2**, S436-439, doi:10.1093/cid/10.supplement_2.s436 (1988).
23 Yauch, L. E., Lam, J. S. & Levitz, S. M. Direct inhibition of T-cell responses by the *Cryptococcus* capsular polysaccharide glucuronoxylomannan. *PLoS Pathog* **2**, e120, doi:10.1371/journal.ppat.0020120 (2006).
24 Vecchiarelli, A. *et al.* The polysaccharide capsule of *Cryptococcus neoformans* interferes with human dendritic cell maturation and activation. *J Leukoc Biol* **74**, 370-378, doi:10.1189/jlb.1002476 (2003).
25 Syme, R. M., Bruno, T. F., Kozel, T. R. & Mody, C. H. The capsule of Cryptococcus neoformans reduces T-lymphocyte proliferation by reducing phagocytosis, which can be restored with anticapsular antibody. *Infect Immun* **67**, 4620-4627, doi:10.1128/IAI.67.9.4620-4627.1999 (1999).
26 Vecchiarelli, A. *et al.* Cryptococcus neoformans galactoxylomannan is a potent negative immunomodulator, inspiring new approaches in anti-inflammatory immunotherapy. *Immunotherapy* **3**, 997-1005, doi:10.2217/imt.11.86 (2011).
27 Wang, Y. & Casadevall, A. Susceptibility of melanized and nonmelanized Cryptococcus neoformans to nitrogen- and oxygen-derived oxidants. *Infect Immun* **62**, 3004-3007, doi:10.1128/iai.62.7.3004-3007.1994 (1994).
28 Ikeda, R., Sugita, T., Jacobson, E. S. & Shinoda, T. Effects of melanin upon susceptibility of Cryptococcus to antifungals. *Microbiol Immunol* **47**, 271-277, doi:10.1111/j.1348-0421.2003.tb03395.x (2003).
29 Perfect, J. R. Cryptococcus neoformans: the yeast that likes it hot. *FEMS Yeast Res* **6**, 463-468, doi:10.1111/j.1567-1364.2006.00051.x (2006).

30 Goldman, D. L. *et al.* Serologic evidence for Cryptococcus neoformans infection in early childhood. *Pediatrics* **107**, E66, doi:10.1542/peds.107.5.e66 (2001).
31 Rajasingham, R. *et al.* Global burden of disease of HIV-associated cryptococcal meningitis: an updated analysis. *The Lancet Infectious Diseases* **17**, 873-881, doi:10.1016/s1473-3099(17)30243-8 (2017).
32 Molloy, S. F. *et al.* Cryptococcal meningitis: A neglected NTD? *PLoS Negl Trop Dis* **11**, e0005575, doi:10.1371/journal.pntd.0005575 (2017).
33 Chen, L. C., Goldman, D. L., Doering, T. L., Pirofski, L. & Casadevall, A. Antibody response to Cryptococcus neoformans proteins in rodents and humans. *Infect Immun* **67**, 2218-2224, doi:10.1128/IAI.67.5.2218-2224.1999 (1999).
34 Setianingrum, F., Rautemaa-Richardson, R. & Denning, D. W. Pulmonary cryptococcosis: A review of pathobiology and clinical aspects. *Med Mycol* **57**, 133-150, doi:10.1093/mmy/myy086 (2019).
35 Zhang, Y. *et al.* Clinical analysis of 76 patients pathologically diagnosed with pulmonary cryptococcosis. *Eur Respir J* **40**, 1191-1200, doi:10.1183/09031936.00168011 (2012).
36 Qu, Y. *et al.* Primary pulmonary cryptococcosis: evaluation of CT characteristics in 26 immunocompetent Chinese patients. *Acta Radiol* **53**, 668-674, doi:10.1258/ar.2012.110612 (2012).
37 Spec, A., Raval, K. & Powderly, W. G. End-Stage Liver Disease Is a Strong Predictor of Early Mortality in Cryptococcosis. *Open Forum Infect Dis* **3**, ofv197, doi:10.1093/ofid/ofv197 (2016).
38 Tashiro, H. *et al.* Clinical impact of advanced chronic kidney disease in patients with non-HIV pulmonary cryptococcosis. *BMC Pulm Med* **20**, 116, doi:10.1186/s12890-020-1149-3 (2020).
39 Bicanic, T. & Harrison, T. S. Cryptococcal meningitis. *Br Med Bull* **72**, 99-118, doi:10.1093/bmb/ldh043 (2004).
40 Bechmann, I., Galea, I. & Perry, V. H. What is the blood-brain barrier (not)? *Trends Immunol* **28**, 5-11, doi:10.1016/j.it.2006.11.007 (2007).
41 Vu, K., Garcia, J. A. & Gelli, A. Cryptococcal Meningitis and Anti-virulence Therapeutic Strategies. *Front Microbiol* **10**, 353, doi:10.3389/fmicb.2019.00353 (2019).
42 Casadevall, A. Cryptococci at the brain gate: break and enter or use a Trojan horse? *J Clin Invest* **120**, 1389-1392, doi:10.1172/JCI42949 (2010).
43 Santiago-Tirado, F. H., Onken, M. D., Cooper, J. A., Klein, R. S. & Doering, T. L. Trojan Horse Transit Contributes to Blood-Brain Barrier Crossing of a Eukaryotic Pathogen. *MBio* **8**, doi:10.1128/mBio.02183-16 (2017).
44 Sorrell, T. C. *et al.* Cryptococcal transmigration across a model brain blood-barrier: evidence of the Trojan horse mechanism and differences between Cryptococcus neoformans var. grubii strain H99 and Cryptococcus gattii strain R265. *Microbes Infect* **18**, 57-67, doi:10.1016/j.micinf.2015.08.017 (2016).
45 Alvarez, M. & Casadevall, A. Phagosome extrusion and host-cell survival after *Cryptococcus neoformans* phagocytosis by macrophages. *Curr Biol* **16**, 2161-2165, doi:10.1016/j.cub.2006.09.061 (2006).
46 Johnston, S. A. & May, R. C. The human fungal pathogen *Cryptococcus neoformans* escapes macrophages by a phagosome emptying mechanism that is inhibited by Arp2/3 complex-mediated actin polymerisation. *PLoS Pathog* **6**, e1001041, doi:10.1371/journal.ppat.1001041 (2010).
47 Perfect, J. R. *et al.* Clinical practice guidelines for the management of cryptococcal disease: 2010 update by the infectious diseases society of america. *Clin Infect Dis* **50**, 291-322, doi:10.1086/649858 (2010).
48 Palacios, D. S., Dailey, I., Siebert, D. M., Wilcock, B. C. & Burke, M. D. Synthesis-enabled functional group deletions reveal key underpinnings of amphotericin B ion

channel and antifungal activities. *Proc Natl Acad Sci U S A* **108**, 6733-6738, doi:10.1073/pnas.1015023108 (2011).
49 Carolus, H., Pierson, S., Lagrou, K. & Van Dijck, P. Amphotericin B and Other Polyenes-Discovery, Clinical Use, Mode of Action and Drug Resistance. *J Fungi (Basel)* **6**, doi:10.3390/jof6040321 (2020).
50 Groll, A. H. *et al.* Comparative efficacy and distribution of lipid formulations of amphotericin B in experimental Candida albicans infection of the central nervous system. *J Infect Dis* **182**, 274-282, doi:10.1086/315643 (2000).
51 Perfect, J. R. The antifungal pipeline: a reality check. *Nature Reviews Drug Discovery* **16**, 603-616, doi:10.1038/nrd.2017.46 (2017).
52 Rodero, L. *et al.* In vitro susceptibility studies of Cryptococcus neoformans isolated from patients with no clinical response to amphotericin B therapy. *J Antimicrob Chemother* **45**, 239-242, doi:10.1093/jac/45.2.239 (2000).
53 Mesa-Arango, A. C., Scorzoni, L. & Zaragoza, O. It only takes one to do many jobs: Amphotericin B as antifungal and immunomodulatory drug. *Front Microbiol* **3**, 286, doi:10.3389/fmicb.2012.00286 (2012).
54 Vermes, A., Guchelaar, H. J. & Dankert, J. Flucytosine: a review of its pharmacology, clinical indications, pharmacokinetics, toxicity and drug interactions. *J Antimicrob Chemother* **46**, 171-179, doi:10.1093/jac/46.2.171 (2000).
55 Bennett, J. E. *et al.* A comparison of amphotericin B alone and combined with flucytosine in the treatment of cryptoccal meningitis. *N Engl J Med* **301**, 126-131, doi:10.1056/NEJM197907193010303 (1979).
56 Edlind, T. D. & Katiyar, S. K. Mutational analysis of flucytosine resistance in Candida glabrata. *Antimicrob Agents Chemother* **54**, 4733-4738, doi:10.1128/AAC.00605-10 (2010).
57 Pasko, M. T., Piscitelli, S. C. & Van Slooten, A. D. Fluconazole: a new triazole antifungal agent. *DICP* **24**, 860-867, doi:10.1177/106002809002400914 (1990).
58 Iyer, K. R., Revie, N. M., Fu, C., Robbins, N. & Cowen, L. E. Treatment strategies for cryptococcal infection: challenges, advances and future outlook. *Nat Rev Microbiol* **19**, 454-466, doi:10.1038/s41579-021-00511-0 (2021).
59 Birnbaum, J. E. Pharmacology of the allylamines. *J Am Acad Dermatol* **23**, 782-785, doi:10.1016/0190-9622(90)70288-s (1990).
60 Guerra, C. R., Ishida, K., Nucci, M. & Rozental, S. Terbinafine inhibits Cryptococcus neoformans growth and modulates fungal morphology. *Mem Inst Oswaldo Cruz* **107**, 582-590, doi:10.1590/s0074-02762012000500003 (2012).
61 Krysan, D. J. Toward improved anti-cryptococcal drugs: Novel molecules and repurposed drugs. *Fungal Genet Biol* **78**, 93-98, doi:10.1016/j.fgb.2014.12.001 (2015).
62 Campuzano, A. & Wormley, F. L. Innate Immunity against Cryptococcus, from Recognition to Elimination. *J Fungi (Basel)* **4**, doi:10.3390/jof4010033 (2018).
63 Nelson, B. N., Hawkins, A. N. & Wozniak, K. L. Pulmonary Macrophage and Dendritic Cell Responses to Cryptococcus neoformans. *Frontiers in Cellular and Infection Microbiology* **10**, doi:10.3389/fcimb.2020.00037 (2020).
64 Fonseca, F. L. *et al.* Immunomodulatory effects of serotype B glucuronoxylomannan from Cryptococcus gattii correlate with polysaccharide diameter. *Infect Immun* **78**, 3861-3870, doi:10.1128/IAI.00111-10 (2010).
65 Nakamura, Y. *et al.* Dectin-2 deficiency promotes Th2 response and mucin production in the lungs after pulmonary infection with Cryptococcus neoformans. *Infect Immun* **83**, 671-681, doi:10.1128/IAI.02835-14 (2015).
66 Hole, C. R. *et al.* Antifungal Activity of Plasmacytoid Dendritic Cells against *Cryptococcus neoformans In Vitro* Requires Expression of Dectin-3 (CLEC4D) and

Reactive Oxygen Species. *Infect Immun* **84**, 2493-2504, doi:10.1128/IAI.00103-16 (2016).
67 Drummond, R. A. & Lionakis, M. S. Mechanistic Insights into the Role of C-Type Lectin Receptor/CARD9 Signaling in Human Antifungal Immunity. *Front Cell Infect Microbiol* **6**, 39, doi:10.3389/fcimb.2016.00039 (2016).
68 Yamamoto, H. *et al.* Defect of CARD9 leads to impaired accumulation of gamma interferon-producing memory phenotype T cells in lungs and increased susceptibility to pulmonary infection with Cryptococcus neoformans. *Infect Immun* **82**, 1606-1615, doi:10.1128/IAI.01089-13 (2014).
69 Tucker, S. C. & Casadevall, A. Replication of Cryptococcus neoformans in macrophages is accompanied by phagosomal permeabilization and accumulation of vesicles containing polysaccharide in the cytoplasm. *Proc Natl Acad Sci U S A* **99**, 3165-3170, doi:10.1073/pnas.052702799 (2002).
70 Levitz, S. M. & Farrell, T. P. Growth inhibition of *Cryptococcus neoformans* by cultured human monocytes: role of the capsule, opsonins, the culture surface, and cytokines. *Infect Immun* **58**, 1201-1209 (1990).
71 Gaylord, E. A., Choy, H. L. & Doering, T. L. Dangerous Liaisons: Interactions of Cryptococcus neoformans with Host Phagocytes. *Pathogens* **9**, doi:10.3390/pathogens9110891 (2020).
72 Leopold Wager, C. M. & Wormley, F. L. Classical versus alternative macrophage activation: the Ying and the Yang in host defense against pulmonary fungal infections. *Mucosal Immunology* **7**, 1023-1035, doi:10.1038/mi.2014.65 (2014).
73 Leopold Wager, C. M., Hole, C. R., Wozniak, K. L., Olszewski, M. A. & Wormley, F. L., Jr. STAT1 signaling is essential for protection against Cryptococcus neoformans infection in mice. *J Immunol* **193**, 4060-4071, doi:10.4049/jimmunol.1400318 (2014).
74 Vecchiarelli, A. *et al.* Role of human alveolar macrophages as antigen-presenting cells in *Cryptococcus neoformans* infection. *Am J Respir Cell Mol Biol* **11**, 130-137, doi:10.1165/ajrcmb.11.2.8049074 (1994).
75 Mukaremera, L. & Nielsen, K. Adaptive Immunity to *Cryptococcus neoformans* Infections. *J Fungi (Basel)* **3**, doi:10.3390/jof3040064 (2017).
76 Wozniak, K. L., Vyas, J. M. & Levitz, S. M. In vivo role of dendritic cells in a murine model of pulmonary cryptococcosis. *Infect Immun* **74**, 3817-3824, doi:10.1128/IAI.00317-06 (2006).
77 Ardavin, C. *et al.* Origin and differentiation of dendritic cells. *Trends in Immunology* **22**, 691-700, doi:Doi 10.1016/S1471-4906(01)02059-2 (2001).
78 Steinman, R. M. Decisions about dendritic cells: past, present, and future. *Annu Rev Immunol* **30**, 1-22, doi:10.1146/annurev-immunol-100311-102839 (2012).
79 Sun, D. *et al.* Real-Time Imaging of Interactions of Neutrophils with Cryptococcus neoformans Demonstrates a Crucial Role of Complement C5a-C5aR Signaling. *Infect Immun* **84**, 216-229, doi:10.1128/IAI.01197-15 (2016).
80 Mednick, A. J., Feldmesser, M., Rivera, J. & Casadevall, A. Neutropenia alters lung cytokine production in mice and reduces their susceptibility to pulmonary cryptococcosis. *Eur J Immunol* **33**, 1744-1753, doi:10.1002/eji.200323626 (2003).
81 Wozniak, K. L., Kolls, J. K. & Wormley, F. L., Jr. Depletion of neutrophils in a protective model of pulmonary cryptococcosis results in increased IL-17A production by gammadelta T cells. *BMC Immunol* **13**, 65, doi:10.1186/1471-2172-13-65 (2012).
82 O'Meara, T. R. *et al.* Cryptococcus neoformans Rim101 Is Associated with Cell Wall Remodeling and Evasion of the Host Immune Responses. *mBio* **4**, doi:10.1128/mBio.00522-12 (2013).

83 Sawai, C. M. *et al.* Hematopoietic Stem Cells Are the Major Source of Multilineage Hematopoiesis in Adult Animals. *Immunity* **45**, 597-609, doi:10.1016/j.immuni.2016.08.007 (2016).
84 Cybulsky, M. I., Cheong, C. & Robbins, C. S. Macrophages and Dendritic Cells: Partners in Atherogenesis. *Circ Res* **118**, 637-652, doi:10.1161/CIRCRESAHA.115.306542 (2016).
85 Schulz, C. *et al.* A lineage of myeloid cells independent of Myb and hematopoietic stem cells. *Science* **336**, 86-90, doi:10.1126/science.1219179 (2012).
86 Hoeffel, G. *et al.* Adult Langerhans cells derive predominantly from embryonic fetal liver monocytes with a minor contribution of yolk sac-derived macrophages. *J Exp Med* **209**, 1167-1181, doi:10.1084/jem.20120340 (2012).
87 Davies, L. C., Jenkins, S. J., Allen, J. E. & Taylor, P. R. Tissue-resident macrophages. *Nat Immunol* **14**, 986-995, doi:10.1038/ni.2705 (2013).
88 Sun, D. *et al.* Fungal dissemination is limited by liver macrophage filtration of the blood. *Nat Commun* **10**, 4566, doi:10.1038/s41467-019-12381-5 (2019).
89 Koutsouras, G. W., Ramos, R. L. & Martinez, L. R. Role of microglia in fungal infections of the central nervous system. *Virulence* **8**, 705-718, doi:10.1080/21505594.2016.1261789 (2017).
90 Lohmann-Matthes, M. L., Steinmüller, C. & Franke-Ullmann, G. Pulmonary macrophages. *European Respiratory Journal* **7**, 1678-1689, doi:10.1183/09031936.94.07091678 (1994).
91 Morales-Nebreda, L., Misharin, A. V., Perlman, H. & Budinger, G. R. The heterogeneity of lung macrophages in the susceptibility to disease. *Eur Respir Rev* **24**, 505-509, doi:10.1183/16000617.0031-2015 (2015).
92 Nelson, B. N. *et al.* Protective interaction of human phagocytic APC subsets with Cryptococcus neoformans induces genes associated with metabolism and antigen presentation. *Frontiers in Immunology* **13**, doi:10.3389/fimmu.2022.1054477 (2022).
93 Gross, N. T., Hultenby, K., Mengarelli, S., Camner, P. & Jarstrand, C. Lipid peroxidation by alveolar macrophages challenged with Cryptococcus neoformans, Candida albicans or Aspergillus fumigatus. *Med Mycol* **38**, 443-449, doi:10.1080/mmy.38.6.443.449 (2000).
94 Osterholzer, J. J. *et al.* Role of dendritic cells and alveolar macrophages in regulating early host defense against pulmonary infection with *Cryptococcus neoformans*. *Infect Immun* **77**, 3749-3758, doi:10.1128/IAI.00454-09 (2009).
95 Patel, V. I. *et al.* Transcriptional Classification and Functional Characterization of Human Airway Macrophage and Dendritic Cell Subsets. *J Immunol* **198**, 1183-1201, doi:10.4049/jimmunol.1600777 (2017).
96 Zaynagetdinov, R. *et al.* Identification of myeloid cell subsets in murine lungs using flow cytometry. *Am J Respir Cell Mol Biol* **49**, 180-189, doi:10.1165/rcmb.2012-0366MA (2013).
97 Misharin, A. V., Morales-Nebreda, L., Mutlu, G. M., Budinger, G. R. S. & Perlman, H. Flow Cytometric Analysis of Macrophages and Dendritic Cell Subsets in the Mouse Lung. *American Journal of Respiratory Cell and Molecular Biology* **49**, 503-510, doi:10.1165/rcmb.2013-0086MA (2013).
98 Hawkins, A. N., Determann, B. F., II, Nelson, B. N. & Wozniak, K. L. Transcriptional Changes in Pulmonary Phagocyte Subsets Dictate the Outcome Following Interaction With The Fungal Pathogen Cryptococcus neoformans. *Front Immunol* **12**, 722500, doi:10.3389/fimmu.2021.722500 (2021).
99 McQuiston, T. J. & Williamson, P. R. Paradoxical roles of alveolar macrophages in the host response to Cryptococcus neoformans. *J Infect Chemother* **18**, 1-9, doi:10.1007/s10156-011-0306-2 (2012).

100 Trombetta, E. S. & Mellman, I. Cell biology of antigen processing in vitro and in vivo. *Annu Rev Immunol* **23**, 975-1028, doi:10.1146/annurev.immunol.22.012703.104538 (2005).
101 Upham, J. W. The role of dendritic cells in immune regulation and allergic airway inflammation. *Respirology* **8**, 140-148, doi:10.1046/j.1440-1843.2003.00465.x (2003).
102 Kaiko, G. E., Horvat, J. C., Beagley, K. W. & Hansbro, P. M. Immunological decision-making: how does the immune system decide to mount a helper T-cell response? *Immunology* **123**, 326-338, doi:10.1111/j.1365-2567.2007.02719.x (2008).
103 Hoag, K. A., Lipscomb, M. F., Izzo, A. A. & Street, N. E. IL-12 and IFN-gamma are required for initiating the protective Th1 response to pulmonary cryptococcosis in resistant C.B-17 mice. *Am J Respir Cell Mol Biol* **17**, 733-739, doi:10.1165/ajrcmb.17.6.2879 (1997).
104 Ranger, A. M., Das, M. P., Kuchroo, V. K. & Glimcher, L. H. B7-2 (CD86) is essential for the development of IL-4-producing T cells. *Int Immunol* **8**, 1549-1560, doi:10.1093/intimm/8.10.1549 (1996).
105 Ohshima, Y. *et al.* OX40 Costimulation Enhances Interleukin-4 (IL-4) Expression at Priming and Promotes the Differentiation of Naive Human CD4+ T Cells Into High IL-4–Producing Effectors. *Blood* **92**, 3338-3345, doi:10.1182/blood.V92.9.3338 (1998).
106 Wiesner, D. L. *et al.* Chitin recognition via chitotriosidase promotes pathologic type-2 helper T cell responses to cryptococcal infection. *PLoS Pathog* **11**, e1004701, doi:10.1371/journal.ppat.1004701 (2015).
107 Park, H. *et al.* A distinct lineage of CD4 T cells regulates tissue inflammation by producing interleukin 17. *Nat Immunol* **6**, 1133-1141, doi:10.1038/ni1261 (2005).
108 Zhang, Y. *et al.* Robust Th1 and Th17 immunity supports pulmonary clearance but cannot prevent systemic dissemination of highly virulent *Cryptococcus neoformans* H99. *Am J Pathol* **175**, 2489-2500, doi:10.2353/ajpath.2009.090530 (2009).
109 Guo, X. *et al.* Cryptococcus neoformans Infection Induces IL-17 Production by Promoting STAT3 Phosphorylation in CD4(+) T Cells. *Front Immunol* **13**, 872286, doi:10.3389/fimmu.2022.872286 (2022).
110 Mills, K. H. Induction, function and regulation of IL-17-producing T cells. *Eur J Immunol* **38**, 2636-2649, doi:10.1002/eji.200838535 (2008).
111 Wozniak, K. L., Hardison, S. E., Kolls, J. K. & Wormley, F. L. Role of IL-17A on resolution of pulmonary C. neoformans infection. *PLoS One* **6**, e17204, doi:10.1371/journal.pone.0017204 (2011).
112 Mathur, A. N. *et al.* Stat3 and Stat4 direct development of IL-17-secreting Th cells. *J Immunol* **178**, 4901-4907, doi:10.4049/jimmunol.178.8.4901 (2007).
113 Leopold Wager, C. M. *et al.* IFN-gamma immune priming of macrophages in vivo induces prolonged STAT1 binding and protection against Cryptococcus neoformans. *PLoS Pathog* **14**, e1007358, doi:10.1371/journal.ppat.1007358 (2018).
114 Hole, C. R. *et al.* Induction of memory-like dendritic cell responses in vivo. *Nat Commun* **10**, 2955, doi:10.1038/s41467-019-10486-5 (2019).
115 Netea, M. G., Quintin, J. & van der Meer, J. W. Trained immunity: a memory for innate host defense. *Cell Host Microbe* **9**, 355-361, doi:10.1016/j.chom.2011.04.006 (2011).
116 Caballero Van Dyke, M. C. & Wormley, F. L., Jr. A Call to Arms: Quest for a Cryptococcal Vaccine. *Trends Microbiol* **26**, 436-446, doi:10.1016/j.tim.2017.10.002 (2018).
117 Antachopoulos, C. & Walsh, T. J. Immunotherapy of Cryptococcus infections. *Clin Microbiol Infect* **18**, 126-133, doi:10.1111/j.1469-0691.2011.03741.x (2012).
118 Lindell, D. M., Moore, T. A., McDonald, R. A., Toews, G. B. & Huffnagle, G. B. Generation of Antifungal Effector CD8+ T Cells in the Absence of CD4+ T Cells during

Cryptococcus neoformans Infection. *The Journal of Immunology* **174**, 7920-7928, doi:10.4049/jimmunol.174.12.7920 (2005).
119 Zaragoza, O. *et al.* *Advances in Applied Microbiology* 133-216 (2009).
120 Perfect, J. R., Granger, D. L. & Durack, D. T. Effects of antifungal agents and gamma interferon on macrophage cytotoxicity for fungi and tumor cells. *J Infect Dis* **156**, 316-323, doi:10.1093/infdis/156.2.316 (1987).
121 Joly, V., Saint-Julien, L., Carbon, C. & Yeni, P. In vivo activity of interferon-gamma in combination with amphotericin B in the treatment of experimental cryptococcosis. *J Infect Dis* **170**, 1331-1334, doi:10.1093/infdis/170.5.1331 (1994).
122 Pappas, P. G. *et al.* Recombinant interferon- gamma 1b as adjunctive therapy for AIDS-related acute cryptococcal meningitis. *J Infect Dis* **189**, 2185-2191, doi:10.1086/420829 (2004).
123 Siddiqui, A. A. *et al.* IFN-gamma at the site of infection determines rate of clearance of infection in cryptococcal meningitis. *J Immunol* **174**, 1746-1750, doi:10.4049/jimmunol.174.3.1746 (2005).
124 Jarvis, J. N. *et al.* Adjunctive interferon-gamma immunotherapy for the treatment of HIV-associated cryptococcal meningitis: a randomized controlled trial. *AIDS* **26**, 1105-1113, doi:10.1097/QAD.0b013e3283536a93 (2012).
125 Neal, L. M. *et al.* CD4(+) T Cells Orchestrate Lethal Immune Pathology despite Fungal Clearance during *Cryptococcus neoformans* Meningoencephalitis. *MBio* **8**, doi:10.1128/mBio.01415-17 (2017).
126 Wozniak, K. L., Olszewski, M. A. & Wormley, F. L., Jr. Molecules at the interface of *Cryptococcus* and the host that determine disease susceptibility. *Fungal Genet Biol* **78**, 87-92, doi:10.1016/j.fgb.2014.10.013 (2015).
127 Levitz, S. M. The Ecology of *Cryptococcus neoformans* and the Epidemiology of Cryptococcosis. *Rev Infect Dis* **13**, 1163-1169 (1991).
128 Gibson, J. F. & Johnston, S. A. Immunity to *Cryptococcus neoformans* and *C. gattii* during cryptococcosis. *Fungal Genet Biol* **78**, 76-86, doi:10.1016/j.fgb.2014.11.006 (2015).
129 Pappas, P. G. *et al.* Invasive fungal infections among organ transplant recipients: results of the Transplant-Associated Infection Surveillance Network (TRANSNET). *Clin Infect Dis* **50**, 1101-1111, doi:10.1086/651262 (2010).
130 Nyazika, T. K. *et al.* Epidemiology and aetiologies of cryptococcal meningitis in Africa, 1950-2017: protocol for a systematic review. *BMJ Open* **8**, e020654, doi:10.1136/bmjopen-2017-020654 (2018).
131 Warkentien, T. & Crum-Cianflone, N. F. An update on Cryptococcosis among HIV-infected patients. *Int J STD AIDS* **21**, 679-684, doi:10.1258/ijsa.2010.010182 (2010).
132 Armstrong-James, D., Meintjes, G. & Brown, G. D. A neglected epidemic: fungal infections in HIV/AIDS. *Trends Microbiol* **22**, 120-127, doi:10.1016/j.tim.2014.01.001 (2014).
133 Denning, D. W. & Hope, W. W. Therapy for fungal diseases: opportunities and priorities. *Trends Microbiol* **18**, 195-204, doi:10.1016/j.tim.2010.02.004 (2010).
134 Molloy, S. F. *et al.* Antifungal Combinations for Treatment of Cryptococcal Meningitis in Africa. *N Engl J Med* **378**, 1004-1017, doi:10.1056/NEJMoa1710922 (2018).
135 Bicanic, T. *et al.* Toxicity of Amphotericin B Deoxycholate-Based Induction Therapy in Patients with HIV-Associated Cryptococcal Meningitis. *Antimicrob Agents Chemother* **59**, 7224-7231, doi:10.1128/AAC.01698-15 (2015).
136 Sudan, A. *et al.* Pharmacokinetics and pharmacodynamics of fluconazole for cryptococcal meningoencephalitis: implications for antifungal therapy and *in vitro* susceptibility breakpoints. *Antimicrob Agents Chemother* **57**, 2793-2800, doi:10.1128/AAC.00216-13 (2013).

137 Bicanic, T., Harrison, T., Niepieklo, A., Dyakopu, N. & Meintjes, G. Symptomatic relapse of HIV-associated cryptococcal meningitis after initial fluconazole monotherapy: the role of fluconazole resistance and immune reconstitution. *Clin Infect Dis* **43**, 1069-1073, doi:10.1086/507895 (2006).
138 Wozniak, K. L. Interactions of *Cryptococcus* with Dendritic Cells. *J Fungi (Basel)* **4**, doi:10.3390/jof4010036 (2018).
139 Holt, P. G., Schonhegrad, M. A. & Oliver, J. Mhc Class-Ii Antigen-Bearing Dendritic Cells in Pulmonary Tissues of the Rat - Regulation of Antigen Presentation Activity by Endogenous Macrophage Populations. *Journal of Experimental Medicine* **167**, 262-274, doi:DOI 10.1084/jem.167.2.262 (1988).
140 Schonhegrad, M. A., Oliver, J., Mcmenamin, P. G. & Holt, P. G. Studies on the Density, Distribution, and Surface Phenotype of Intraepithelial Class-Ii Major Histocompatability Complex Antigen (Ia)-Bearing Dendritic Cells (Dc) in the Conducting Airways. *Journal of Experimental Medicine* **173**, 1345-1356, doi:DOI 10.1084/jem.173.6.1345 (1991).
141 Wozniak, K. L. *et al.* Insights into the mechanisms of protective immunity against *Cryptococcus neoformans* infection using a mouse model of pulmonary cryptococcosis. *PLoS One* **4**, e6854, doi:10.1371/journal.pone.0006854 (2009).
142 Bright, N. A., Gratian, M. J. & Luzio, J. P. Endocytic delivery to lysosomes mediated by concurrent fusion and kissing events in living cells. *Curr Biol* **15**, 360-365, doi:10.1016/j.cub.2005.01.049 (2005).
143 de Duve, C. The lysosome turns fifty. *Nat Cell Biol* **7**, 847-849, doi:10.1038/ncb0905-847 (2005).
144 Luzio, J. P. *et al.* Lysosome-endosome fusion and lysosome biogenesis. *J Cell Sci* **113**, 1515-1524 (2000).
145 Hole, C. R., Bui, H., Wormley, F. L., Jr. & Wozniak, K. L. Mechanisms of dendritic cell lysosomal killing of *Cryptococcus*. *Sci Rep* **2**, 739, doi:10.1038/srep00739 (2012).
146 Lennon-Dumenil, A. M. *et al.* Analysis of protease activity in live antigen-presenting cells shows regulation of the phagosomal proteolytic contents during dendritic cell activation. *J Exp Med* **196**, 529-540, doi:10.1084/jem.20020327 (2002).
147 Guermonprez, P., Valladeau, J., Zitvogel, L., Thery, C. & Amigorena, S. Antigen presentation and T cell stimulation by dendritic cells. *Annu Rev Immunol* **20**, 621-667, doi:10.1146/annurev.immunol.20.100301.064828 (2002).
148 Wozniak, K. L. Dendritic Cells at the Interface of Fungal Immunity. *Current Fungal Infection Reports* **1**, 89-95 (2007).
149 de Medeiros, L. N. *et al.* Backbone dynamics of the antifungal Psd1 pea defensin and its correlation with membrane interaction by NMR spectroscopy. *Biochim Biophys Acta* **1798**, 105-113, doi:10.1016/j.bbamem.2009.07.013 (2010).
150 Silva, P. M., Goncalves, S. & Santos, N. C. Defensins: antifungal lessons from eukaryotes. *Front Microbiol* **5**, 97, doi:10.3389/fmicb.2014.00097 (2014).
151 Thevissen, K. *et al.* Defensins from insects and plants interact with fungal glucosylceramides. *J Biol Chem* **279**, 3900-3905, doi:10.1074/jbc.M311165200 (2004).
152 Honey, K. & Rudensky, A. Y. Lysosomal cysteine proteases regulate antigen presentation. *Nat Rev Immunol* **3**, 472-482, doi:10.1038/nri1110 (2003).
153 Kelly, R. M., Chen, J., Yauch, L. E. & Levitz, S. M. Opsonic requirements for dendritic cell-mediated responses to *Cryptococcus neoformans*. *Infect Immun* **73**, 592-598, doi:10.1128/IAI.73.1.592-598.2005 (2005).
154 Wozniak, K. L. & Levitz, S. M. *Cryptococcus neoformans* enters the endolysosomal pathway of dendritic cells and is killed by lysosomal components. *Infect Immun* **76**, 4764-4771, doi:10.1128/IAI.00660-08 (2008).

155 Davis, M. J. *et al. Cryptococcus neoformans*-induced macrophage lysosome damage crucially contributes to fungal virulence. *J Immunol* **194**, 2219-2231, doi:10.4049/jimmunol.1402376 (2015).
156 Diamond, R. D. & Bennett, J. E. Growth of *Cryptococcus neoformans* within human macrophages *in vitro*. *Infect Immun* **7**, 231-236 (1973).
157 Luzio, J. P., Pryor, P. R. & Bright, N. A. Lysosomes: fusion and function. *Nat Rev Mol Cell Biol* **8**, 622-632, doi:10.1038/nrm2217 (2007).
158 Savina, A. & Amigorena, S. Phagocytosis and antigen presentation in dendritic cells. *Immunol Rev* **219**, 143-156, doi:DOI 10.1111/j.1600-065X.2007.00552.x (2007).
159 Chaturvedi, A. K., Weintraub, S. T., Lopez-Ribot, J. L. & Wormley, F. L., Jr. Identification and characterization of *Cryptococcus neoformans* protein fractions that induce protective immune responses. *Proteomics* **13**, 3429-3441, doi:10.1002/pmic.201300213 (2013).
160 Steinbach, W. J., Reedy, J. L., Cramer, R. A., Jr., Perfect, J. R. & Heitman, J. Harnessing calcineurin as a novel anti-infective agent against invasive fungal infections. *Nat Rev Microbiol* **5**, 418-430, doi:10.1038/nrmicro1680 (2007).
161 de Jong, N. W. M. *et al.* Immune evasion by a staphylococcal inhibitor of myeloperoxidase. *Proc Natl Acad Sci U S A* **114**, 9439-9444, doi:10.1073/pnas.1707032114 (2017).
162 Liachko, N. F. *et al.* The phosphatase calcineurin regulates pathological TDP-43 phosphorylation. *Acta Neuropathol* **132**, 545-561, doi:10.1007/s00401-016-1600-y (2016).
163 Walkup, W. G. *et al.* A model for regulation by SynGAP-alpha1 of binding of synaptic proteins to PDZ-domain 'Slots' in the postsynaptic density. *Elife* **5**, doi:10.7554/eLife.16813 (2016).
164 Rahayu, P., Marcelline, F., Sulistyaningrum, E., Suhartono, M. T. & Tjandrawinata, R. R. Potential effect of striatin (DLBS0333), a bioactive protein fraction isolated from *Channa striata* for wound treatment. *Asian Pacific Journal of Tropical Biomedicine* **6**, 1001-1007, doi:10.1016/j.apjtb.2016.10.008 (2016).
165 CLSI. *Reference Method for Broth Dilution Antifungal Susceptibility Testing of Yeasts*. 4th edn, Vol. CLSI standard M27 (Clinical and Laborartory Standards Institutue, Wayne, PA, 2017).
166 Cordeiro, R. A. *et al.* Minimum inhibitory concentrations of amphotericin B, azoles and caspofungin against Candida species are reduced by farnesol. *Med Mycol* **51**, 53-59, doi:10.3109/13693786.2012.692489 (2013).
167 Singh-Babak, S. D. *et al.* Global analysis of the evolution and mechanism of echinocandin resistance in Candida glabrata. *PLoS Pathog* **8**, e1002718, doi:10.1371/journal.ppat.1002718 (2012).
168 Xie, J. L., Singh-Babak, S. D. & Cowen, L. E. Minimum Inhibitory Concentration (MIC) Assay for Antifungal Drugs. *Bio-protocol* **2**, e252, doi:10.21769/BioProtoc.252 (2012).
169 Bonifacio, B. V. *et al.* Antifungal Activity of a Hydroethanolic Extract From Astronium urundeuva Leaves Against Candida albicans and Candida glabrata. *Front Microbiol* **10**, 2642, doi:10.3389/fmicb.2019.02642 (2019).
170 Klepser, M. E., Ernst, E. J., Lewis, R. E., Ernst, M. E. & Pfaller, M. A. Influence of test conditions on antifungal time-kill curve results: proposal for standardized methods. *Antimicrob Agents Chemother* **42**, 1207-1212, doi:10.1128/AAC.42.5.1207 (1998).
171 Zhang, L. J. & Gallo, R. L. Antimicrobial peptides. *Curr Biol* **26**, R14-19, doi:10.1016/j.cub.2015.11.017 (2016).
172 Bahar, A. A. & Ren, D. Antimicrobial peptides. *Pharmaceuticals (Basel)* **6**, 1543-1575, doi:10.3390/ph6121543 (2013).

173 Verma, S., Dixit, R. & Pandey, K. C. Cysteine Proteases: Modes of Activation and Future Prospects as Pharmacological Targets. *Front Pharmacol* **7**, 107, doi:10.3389/fphar.2016.00107 (2016).
174 Houst, J., Spizek, J. & Havlicek, V. Antifungal Drugs. *Metabolites* **10**, doi:10.3390/metabo10030106 (2020).
175 Bidaud, A. L., Schwarz, P., Herbreteau, G. & Dannaoui, E. Techniques for the Assessment of In Vitro and In Vivo Antifungal Combinations. *J Fungi (Basel)* **7**, doi:10.3390/jof7020113 (2021).
176 ISO. *Tests for in vitro cytotoxicity*. 3rd edn, Vol. Biological evaluation of medical devices (International Organization for Standardization, Switzerland, 2009).
177 Thakur, A., Mikkelsen, H. & Jungersen, G. Intracellular Pathogens: Host Immunity and Microbial Persistence Strategies. *J Immunol Res* **2019**, 1356540, doi:10.1155/2019/1356540 (2019).
178 Embgenbroich, M. & Burgdorf, S. Current Concepts of Antigen Cross-Presentation. *Front Immunol* **9**, 1643, doi:10.3389/fimmu.2018.01643 (2018).
179 Newman, S. L. & Holly, A. *Candida albicans* is phagocytosed, killed, and processed for antigen presentation by human dendritic cells. *Infect Immun* **69**, 6813-6822, doi:10.1128/IAI.69.11.6813-6822.2001 (2001).
180 Gildea, L. A., Ciraolo, G. M., Morris, R. E. & Newman, S. L. Human dendritic cell activity against *Histoplasma capsulatum* is mediated via phagolysosomal fusion. *Infect Immun* **73**, 6803-6811, doi:10.1128/IAI.73.10.6803-6811.2005 (2005).
181 Clemens, D. L., Lee, B. Y. & Horwitz, M. A. Virulent and avirulent strains of *Francisella tularensis* prevent acidification and maturation of their phagosomes and escape into the cytoplasm in human macrophages. *Infect Immun* **72**, 3204-3217, doi:10.1128/IAI.72.6.3204-3217.2004 (2004).
182 Wong, C. O. *et al.* Lysosomal Degradation Is Required for Sustained Phagocytosis of Bacteria by Macrophages. *Cell Host Microbe* **21**, 719-730 e716, doi:10.1016/j.chom.2017.05.002 (2017).
183 Lin, Y. *et al.* Hepatitis B virus is degraded by autophagosome-lysosome fusion mediated by Rab7 and related components. *Protein Cell* **10**, 60-66, doi:10.1007/s13238-018-0555-2 (2019).
184 Wall, G., Herrera, N. & Lopez-Ribot, J. L. Repositionable Compounds with Antifungal Activity against Multidrug Resistant *Candida auris* Identified in the Medicines for Malaria Venture's Pathogen Box. *J Fungi (Basel)* **5**, doi:10.3390/jof5040092 (2019).
185 Van Dijck, P. *et al.* Methodologies for *in vitro* and *in vivo* evaluation of efficacy of antifungal and antibiofilm agents and surface coatings against fungal biofilms. *Microb Cell* **5**, 300-326, doi:10.15698/mic2018.07.638 (2018).
186 Castro-Lopez, N. & Hung, C. Y. Immune Response to Coccidioidomycosis and the Development of a Vaccine. *Microorganisms* **5**, doi:10.3390/microorganisms5010013 (2017).
187 Belaaouaj, A., Kim, K. S. & Shapiro, S. D. Degradation of outer membrane protein A in *Escherichia coli* killing by neutrophil elastase. *Science* **289**, 1185-1188, doi:10.1126/science.289.5482.1185 (2000).
188 Pei, D. Leukolysin/MMP25/MT6-MMP: a novel matrix metalloproteinase specifically expressed in the leukocyte lineage. *Cell Res* **9**, 291-303, doi:10.1038/sj.cr.7290028 (1999).
189 Klebanoff, S. J. Myeloperoxidase: friend and foe. *J Leukoc Biol* **77**, 598-625, doi:10.1189/jlb.1204697 (2005).
190 Pieters, J. in *The Coronin Family of Proteins* Vol. 48 *Subcellular Biochemistry* (eds C. S. Clemen, V. Rybakin, & L. Eichinger) Ch. 10, 116-123 (Landes Bioscience, 2008).

191 Zimmermann, K. *et al.* NOSTRIN: a protein modulating nitric oxide release and subcellular distribution of endothelial nitric oxide synthase. *Proc Natl Acad Sci U S A* **99**, 17167-17172, doi:10.1073/pnas.252345399 (2002).
192 Bonam, S. R., Wang, F. & Muller, S. Lysosomes as a therapeutic target. *Nat Rev Drug Discov* **18**, 923-948, doi:10.1038/s41573-019-0036-1 (2019).
193 Cui, J., Ren, B., Tong, Y., Dai, H. & Zhang, L. Synergistic combinations of antifungals and anti-virulence agents to fight against Candida albicans. *Virulence* **6**, 362-371, doi:10.1080/21505594.2015.1039885 (2015).
194 Fajardo, M. *et al.* Calnexin, calreticulin and cytoskeleton-associated proteins modulate uptake and growth of Legionella pneumophila in Dictyostelium discoideum. *Microbiology (Reading)* **150**, 2825-2835, doi:10.1099/mic.0.27111-0 (2004).
195 Richter, C., Helaly, S. E., Thongbai, B., Hyde, K. D. & Stadler, M. Pyristriatins A and B: Pyridino-Cyathane Antibiotics from the *Basidiomycete Cyathus* cf. *striatus*. *J Nat Prod* **79**, 1684-1688, doi:10.1021/acs.jnatprod.6b00194 (2016).
196 Yano, J. *et al.* The acute neutrophil response mediated by S100 alarmins during vaginal *Candida* infections is independent of the Th17-pathway. *PLoS One* **7**, e46311, doi:10.1371/journal.pone.0046311 (2012).
197 Xiao, P. P., Hu, Y. H. & Sun, L. Scophthalmus maximus cystatin B enhances head kidney macrophage-mediated bacterial killing. *Dev Comp Immunol* **34**, 1237-1241, doi:10.1016/j.dci.2010.07.008 (2010).
198 Donato, R., Sorci, G. & Giambanco, I. S100A6 protein: functional roles. *Cell Mol Life Sci* **74**, 2749-2760, doi:10.1007/s00018-017-2526-9 (2017).
199 Pol, E. & Bjork, I. Role of the single cysteine residue, Cys 3, of human and bovine cystatin B (stefin B) in the inhibition of cysteine proteinases. *Protein Sci* **10**, 1729-1738, doi:10.1110/ps.11901 (2001).
200 Castets, F. *et al.* A novel calmodulin-binding protein, belonging to the WD-repeat family, is localized in dendrites of a subset of CNS neurons. *J Cell Biol* **134**, 1051-1062, doi:10.1083/jcb.134.4.1051 (1996).
201 Benoist, M., Gaillard, S. & Castets, F. The striatin family: a new signaling platform in dendritic spines. *J Physiol Paris* **99**, 146-153, doi:10.1016/j.jphysparis.2005.12.006 (2006).
202 Poggeler, S. & Kuck, U. A WD40 repeat protein regulates fungal cell differentiation and can be replaced functionally by the mammalian homologue striatin. *Eukaryot Cell* **3**, 232-240, doi:10.1128/ec.3.1.232-240.2004 (2004).
203 Cole, A. M. *et al.* Calcitermin, a novel antimicrobial peptide isolated from human airway secretions. *FEBS Lett* **504**, 5-10, doi:10.1016/s0014-5793(01)02731-4 (2001).
204 Yano, J., Noverr, M. C. & Fidel, P. L., Jr. Cytokines in the host response to *Candida vaginitis*: Identifying a role for non-classical immune mediators, S100 alarmins. *Cytokine* **58**, 118-128, doi:10.1016/j.cyto.2011.11.021 (2012).
205 Mambula, S. S., Simons, E. R., Hastey, R., Selsted, M. E. & Levitz, S. M. Human neutrophil-mediated nonoxidative antifungal activity against *Cryptococcus neoformans*. *Infection and Immunity* **68**, 6257-6264, doi:Doi 10.1128/Iai.68.11.6257-6264.2000 (2000).
206 Wozniak, K. L., Hole, C. R., Yano, J., Fidel, P. L., Jr. & Wormley, F. L., Jr. Characterization of IL-22 and antimicrobial peptide production in mice protected against pulmonary *Cryptococcus neoformans* infection. *Microbiology* **160**, 1440-1452, doi:10.1099/mic.0.073445-0 (2014).
207 Donato, R. *et al.* Functions of S100 proteins. *Curr Mol Med* **13**, 24-57 (2013).
208 Deloulme, J. C. *et al.* S100A6 and S100A11 are specific targets of the calcium- and zinc-binding S100B protein *in vivo*. *J Biol Chem* **275**, 35302-35310, doi:10.1074/jbc.M003943200 (2000).

209 Chiasson, D., Ekengren, S. K., Martin, G. B., Dobney, S. L. & Snedden, W. A. Calmodulin-like proteins from Arabidopsis and tomato are involved in host defense against Pseudomonas syringae pv. tomato. *Plant Mol Biol* **58**, 887-897, doi:10.1007/s11103-005-8395-x (2005).
210 Fregno, I. *et al.* ER-to-lysosome-associated degradation of proteasome-resistant ATZ polymers occurs via receptor-mediated vesicular transport. *Embo J* **37**, doi:10.15252/embj.201899259 (2018).
211 Wang, B., Han, S., Lien, L. & Chang, L. J. Lentiviral calnexin-modified dendritic cells promote expansion of high-avidity effector T cells with central memory phenotype. *Immunology* **128**, 43-57, doi:10.1111/j.1365-2567.2009.03067.x (2009).
212 Murphy, J. W. Protective cell-mediated immunity against Cryptococcus neoformans. *Res Immunol* **149**, 373-386; discussion 519-322, doi:10.1016/s0923-2494(98)80761-x (1998).
213 Chang, Y. C. *et al.* Cryptococcal yeast cells invade the central nervous system via transcellular penetration of the blood-brain barrier. *Infect Immun* **72**, 4985-4995, doi:10.1128/IAI.72.9.4985-4995.2004 (2004).
214 Johnston, S. A. & May, R. C. *Cryptococcus* interactions with macrophages: evasion and manipulation of the phagosome by a fungal pathogen. *Cell Microbiol* **15**, 403-411, doi:10.1111/cmi.12067 (2013).
215 Mansour, M. K., Reedy, J. L., Tam, J. M. & Vyas, J. M. Macrophage Cryptococcus interactions: an update. *Curr Fungal Infect Rep* **8**, 109-115, doi:10.1007/s12281-013-0165-7 (2014).
216 Ristow, L. C. & Davis, J. M. The granuloma in cryptococcal disease. *PLoS Pathog* **17**, e1009342, doi:10.1371/journal.ppat.1009342 (2021).
217 Coelho, C., Bocca, A. L. & Casadevall, A. The intracellular life of *Cryptococcus neoformans*. *Annu Rev Pathol* **9**, 219-238, doi:10.1146/annurev-pathol-012513-104653 (2014).
218 Nelson, B. N. *et al.* Antifungal activity of dendritic cell lysosomal proteins against Cryptococcus neoformans. *Sci Rep* **11**, 13619, doi:10.1038/s41598-021-92991-6 (2021).
219 Levitz, S. M. *et al. Cryptococcus neoformans* resides in an acidic phagolysosome of human macrophages. *Infect Immun* **67**, 885-890 (1999).
220 Scherer, A. K., Hopke, A., Sykes, D. B., Irimia, D. & Mansour, M. K. Host defense against fungal pathogens: Adaptable neutrophil responses and the promise of therapeutic opportunities? *PLoS Pathog* **17**, e1009691, doi:10.1371/journal.ppat.1009691 (2021).
221 Decken, K. *et al.* Interleukin-12 is essential for a protective Th1 response in mice infected with Cryptococcus neoformans. *Infect Immun* **66**, 4994-5000, doi:10.1128/IAI.66.10.4994-5000.1998 (1998).
222 Szymczak, W. A., Sellers, R. S. & Pirofski, L. A. IL-23 dampens the allergic response to Cryptococcus neoformans through IL-17-independent and -dependent mechanisms. *Am J Pathol* **180**, 1547-1559, doi:10.1016/j.ajpath.2011.12.038 (2012).
223 Flaczyk, A. *et al.* IL-33 signaling regulates innate and adaptive immunity to Cryptococcus neoformans. *J Immunol* **191**, 2503-2513, doi:10.4049/jimmunol.1300426 (2013).
224 Leopold Wager, C. M., Hole, C. R., Wozniak, K. L. & Wormley, F. L., Jr. *Cryptococcus* and Phagocytes: Complex Interactions that Influence Disease Outcome. *Front Microbiol* **7**, 105, doi:10.3389/fmicb.2016.00105 (2016).
225 Casadevall, A., Coelho, C. & Alanio, A. Mechanisms of Cryptococcus neoformans-Mediated Host Damage. *Front Immunol* **9**, 855, doi:10.3389/fimmu.2018.00855 (2018).
226 Rothe, C. *et al.* A prospective longitudinal study of the clinical outcomes from cryptococcal meningitis following treatment induction with 800 mg oral fluconazole in Blantyre, Malawi. *PLoS One* **8**, e67311, doi:10.1371/journal.pone.0067311 (2013).

227 Fisher, M. C. *et al.* Tackling the emerging threat of antifungal resistance to human health. *Nat Rev Microbiol*, doi:10.1038/s41579-022-00720-1 (2022).
228 McCarty, T. P. & Pappas, P. G. Antifungal Pipeline. *Front Cell Infect Microbiol* **11**, 732223, doi:10.3389/fcimb.2021.732223 (2021).
229 Hole, C. R. & Wormley, F. L., Jr. Vaccine and immunotherapeutic approaches for the prevention of cryptococcosis: lessons learned from animal models. *Front Microbiol* **3**, 291, doi:10.3389/fmicb.2012.00291 (2012).
230 Zhou, Q. & Murphy, W. J. Immune response and immunotherapy to Cryptococcus infections. *Immunol Res* **35**, 191-208, doi:10.1385/IR:35:3:191 (2006).
231 Guilliams, M. *et al.* Alveolar macrophages develop from fetal monocytes that differentiate into long-lived cells in the first week of life via GM-CSF. *J Exp Med* **210**, 1977-1992, doi:10.1084/jem.20131199 (2013).
232 Hou, F., Xiao, K., Tang, L. & Xie, L. Diversity of Macrophages in Lung Homeostasis and Diseases. *Front Immunol* **12**, 753940, doi:10.3389/fimmu.2021.753940 (2021).
233 Dewhurst, J. A. *et al.* Characterisation of lung macrophage subpopulations in COPD patients and controls. *Sci Rep* **7**, 7143, doi:10.1038/s41598-017-07101-2 (2017).
234 Demedts, I. K., Bracke, K. R., Maes, T., Joos, G. F. & Brusselle, G. G. Different roles for human lung dendritic cell subsets in pulmonary immune defense mechanisms. *Am J Respir Cell Mol Biol* **35**, 387-393, doi:10.1165/rcmb.2005-0382OC (2006).
235 Steinbach, K., Vincenti, I. & Merkler, D. Resident-Memory T Cells in Tissue-Restricted Immune Responses: For Better or Worse? *Front Immunol* **9**, 2827, doi:10.3389/fimmu.2018.02827 (2018).
236 Nguyen, Q. P., Deng, T. Z., Witherden, D. A. & Goldrath, A. W. Origins of CD4(+) circulating and tissue-resident memory T-cells. *Immunology* **157**, 3-12, doi:10.1111/imm.13059 (2019).
237 Rahimi, R. A., Nepal, K., Cetinbas, M., Sadreyev, R. I. & Luster, A. D. Distinct functions of tissue-resident and circulating memory Th2 cells in allergic airway disease. *J Exp Med* **217**, doi:10.1084/jem.20190865 (2020).
238 Xu, S. & Shinohara, M. L. Tissue-Resident Macrophages in Fungal Infections. *Front Immunol* **8**, 1798, doi:10.3389/fimmu.2017.01798 (2017).
239 Willcocks, S. & Wren, B. W. Shared characteristics between Mycobacterium tuberculosis and fungi contribute to virulence. *Future Microbiol* **9**, 657-668, doi:10.2217/fmb.14.29 (2014).
240 Marino, S. *et al.* Macrophage polarization drives granuloma outcome during Mycobacterium tuberculosis infection. *Infect Immun* **83**, 324-338, doi:10.1128/IAI.02494-14 (2015).
241 Huang, L., Nazarova, E. V., Tan, S., Liu, Y. & Russell, D. G. Growth of Mycobacterium tuberculosis in vivo segregates with host macrophage metabolism and ontogeny. *J Exp Med* **215**, 1135-1152, doi:10.1084/jem.20172020 (2018).
242 Pisu, D., Huang, L., Grenier, J. K. & Russell, D. G. Dual RNA-Seq of Mtb-Infected Macrophages In Vivo Reveals Ontologically Distinct Host-Pathogen Interactions. *Cell Rep* **30**, 335-350 e334, doi:10.1016/j.celrep.2019.12.033 (2020).
243 Patel, V. I., Booth, J. L., Dozmorov, M., Brown, B. R. & Metcalf, J. P. Anthrax Edema and Lethal Toxins Differentially Target Human Lung and Blood Phagocytes. *Toxins (Basel)* **12**, doi:10.3390/toxins12070464 (2020).
244 Lewalle, P., Rouas, R., Lehmann, F. & Martiat, P. Freezing of dendritic cells, generated from cryopreserved leukaphereses, does not influence their ability to induce antigen-specific immune responses or functionally react to maturation stimuli. *J Immunol Methods* **240**, 69-78, doi:10.1016/s0022-1759(00)00173-3 (2000).

245 Butler, A., Hoffman, P., Smibert, P., Papalexi, E. & Satija, R. Integrating single-cell transcriptomic data across different conditions, technologies, and species. *Nat Biotechnol* **36**, 411-420, doi:10.1038/nbt.4096 (2018).
246 Qiu, X. *et al.* Reversed graph embedding resolves complex single-cell trajectories. *Nat Methods* **14**, 979-982, doi:10.1038/nmeth.4402 (2017).
247 Heung, L. J. Innate Immune Responses to *Cryptococcus*. *J Fungi (Basel)* **3**, doi:10.3390/jof3030035 (2017).
248 Travaglini, K. J. *et al.* A molecular cell atlas of the human lung from single-cell RNA sequencing. *Nature* **587**, 619-625, doi:10.1038/s41586-020-2922-4 (2020).
249 Wang, L. *et al.* Single-cell transcriptomic analysis reveals the immune landscape of lung in steroid-resistant asthma exacerbation. *Proc Natl Acad Sci U S A* **118**, doi:10.1073/pnas.2005590118 (2021).
250 Lauer, S. J. *et al.* Two copies of the human apolipoprotein C-I gene are linked closely to the apolipoprotein E gene. *Journal of Biological Chemistry* **263**, 7277-7286, doi:10.1016/s0021-9258(18)68638-7 (1988).
251 de la Cruz Lopez, K. G., Toledo Guzman, M. E., Sanchez, E. O. & Garcia Carranca, A. mTORC1 as a Regulator of Mitochondrial Functions and a Therapeutic Target in Cancer. *Front Oncol* **9**, 1373, doi:10.3389/fonc.2019.01373 (2019).
252 Fa, Z. *et al.* TNF-alpha-Producing Cryptococcus neoformans Exerts Protective Effects on Host Defenses in Murine Pulmonary Cryptococcosis. *Front Immunol* **10**, 1725, doi:10.3389/fimmu.2019.01725 (2019).
253 Kawakami, K., Qifeng, X., Tohyama, M., Qureshi, M. H. & Saito, A. Contribution of tumour necrosis factor-alpha (TNF-alpha) in host defence mechanism against Cryptococcus neoformans. *Clin Exp Immunol* **106**, 468-474, doi:10.1046/j.1365-2249.1996.d01-870.x (1996).
254 Yang, Y. *et al.* Regulation of SIRT1 and Its Roles in Inflammation. *Front Immunol* **13**, 831168, doi:10.3389/fimmu.2022.831168 (2022).
255 Palmieri, M. *et al.* Characterization of the CLEAR network reveals an integrated control of cellular clearance pathways. *Hum Mol Genet* **20**, 3852-3866, doi:10.1093/hmg/ddr306 (2011).
256 Xu, J. *et al.* Disruption of Early Tumor Necrosis Factor Alpha Signaling Prevents Classical Activation of Dendritic Cells in Lung-Associated Lymph Nodes and Development of Protective Immunity against Cryptococcal Infection. *mBio* **7**, doi:10.1128/mBio.00510-16 (2016).
257 Shourian, M., Ralph, B., Angers, I., Sheppard, D. C. & Qureshi, S. T. Contribution of IL-1RI Signaling to Protection against Cryptococcus neoformans 52D in a Mouse Model of Infection. *Front Immunol* **8**, 1987, doi:10.3389/fimmu.2017.01987 (2017).
258 Guillot, L., Carroll, S. F., Badawy, M. & Qureshi, S. T. *Cryptococcus neoformans* induces IL-8 secretion and CXCL1 expression by human bronchial epithelial cells. *Respir Res* **9**, 9, doi:10.1186/1465-9921-9-9 (2008).
259 Olszewski, M. A. *et al.* The role of macrophage inflammatory protein-1 alpha/CCL3 in regulation of T cell-mediated immunity to Cryptococcus neoformans infection. *J Immunol* **165**, 6429-6436, doi:10.4049/jimmunol.165.11.6429 (2000).
260 Yauch, L. E. & Levitz, S. M. in *Molecular Principles of Fungal Pathogenesis* (ed Joseph Heitman) Ch. 36, 537-554 (ASM Press, 2003).
261 Suresh, C. S., Ninan, M. M., Zachariah, A. & Michael, J. S. Cryptococcosis with Tuberculosis: Overlooked Coinfections. *J Glob Infect Dis* **13**, 139-141, doi:10.4103/jgid.jgid_330_20 (2021).
262 Van den Berge, K. *et al.* Trajectory-based differential expression analysis for single-cell sequencing data. *Nat Commun* **11**, 1201, doi:10.1038/s41467-020-14766-3 (2020).

263 Xu, J. *et al.* Scavenger Receptor MARCO Orchestrates Early Defenses and Contributes to Fungal Containment during Cryptococcal Infection. *J Immunol* **198**, 3548-3557, doi:10.4049/jimmunol.1700057 (2017).
264 Furuhashi, M., Saitoh, S., Shimamoto, K. & Miura, T. Fatty Acid-Binding Protein 4 (FABP4): Pathophysiological Insights and Potent Clinical Biomarker of Metabolic and Cardiovascular Diseases. *Clin Med Insights Cardiol* **8**, 23-33, doi:10.4137/CMC.S17067 (2014).
265 Taban, Q., Mumtaz, P. T., Masoodi, K. Z., Haq, E. & Ahmad, S. M. Scavenger receptors in host defense: from functional aspects to mode of action. *Cell Commun Signal* **20**, 2, doi:10.1186/s12964-021-00812-0 (2022).
266 Gui, Y., Zheng, H. & Cao, R. Y. Foam Cells in Atherosclerosis: Novel Insights Into Its Origins, Consequences, and Molecular Mechanisms. *Front Cardiovasc Med* **9**, 845942, doi:10.3389/fcvm.2022.845942 (2022).
267 Makowski, L., Brittingham, K. C., Reynolds, J. M., Suttles, J. & Hotamisligil, G. S. The fatty acid-binding protein, aP2, coordinates macrophage cholesterol trafficking and inflammatory activity. Macrophage expression of aP2 impacts peroxisome proliferator-activated receptor gamma and IkappaB kinase activities. *J Biol Chem* **280**, 12888-12895, doi:10.1074/jbc.M413788200 (2005).
268 Hui, X. *et al.* Adipocyte fatty acid-binding protein modulates inflammatory responses in macrophages through a positive feedback loop involving c-Jun NH2-terminal kinases and activator protein-1. *J Biol Chem* **285**, 10273-10280, doi:10.1074/jbc.M109.097907 (2010).
269 Rizzo, J. *et al.* Cryptococcus extracellular vesicles properties and their use as vaccine platforms. *J Extracell Vesicles* **10**, e12129, doi:10.1002/jev2.12129 (2021).
270 Hall, C. J., Bouhafs, L., Dizcfalusy, U. & Sandstedt, K. Cryptococcus neoformans causes lipid peroxidation; therefore it is a potential inducer of atherogenesis. *Mycologia* **102**, 546-551, doi:10.3852/08-110 (2010).
271 Moreno-Vedia, J., Girona, J., Ibarretxe, D., Masana, L. & Rodriguez-Calvo, R. Unveiling the Role of the Fatty Acid Binding Protein 4 in the Metabolic-Associated Fatty Liver Disease. *Biomedicines* **10**, doi:10.3390/biomedicines10010197 (2022).
272 Warris, A. & Ballou, E. R. Oxidative responses and fungal infection biology. *Semin Cell Dev Biol* **89**, 34-46, doi:10.1016/j.semcdb.2018.03.004 (2019).
273 Rollin-Pinheiro, R., Singh, A., Barreto-Bergter, E. & Del Poeta, M. Sphingolipids as targets for treatment of fungal infections. *Future Med Chem* **8**, 1469-1484, doi:10.4155/fmc-2016-0053 (2016).
274 Kishimoto, Y., Hiraiwa, M. & O'Brien, J. S. Saposins: structure, function, distribution, and molecular genetics. *Journal of Lipid Research* **33**, 1255-1267, doi:10.1016/s0022-2275(20)40540-1 (1992).
275 Muntjewerff, E. M., Meesters, L. D. & van den Bogaart, G. Antigen Cross-Presentation by Macrophages. *Front Immunol* **11**, 1276, doi:10.3389/fimmu.2020.01276 (2020).
276 Gupta, M., Gupta, S. K., Hoffman, B. & Liebermann, D. A. Gadd45a and Gadd45b protect hematopoietic cells from UV-induced apoptosis via distinct signaling pathways, including p38 activation and JNK inhibition. *J Biol Chem* **281**, 17552-17558, doi:10.1074/jbc.M600950200 (2006).
277 You, W. *et al.* GADD45alpha drives brown adipose tissue formation through upregulating PPARgamma in mice. *Cell Death Dis* **11**, 585, doi:10.1038/s41419-020-02802-5 (2020).
278 Liu, W. *et al.* AP-1 activated by toll-like receptors regulates expression of IL-23 p19. *J Biol Chem* **284**, 24006-24016, doi:10.1074/jbc.M109.025528 (2009).

279 Liu, J. *et al.* Interleukin-12: an update on its immunological activities, signaling and regulation of gene expression. *Curr Immunol Rev* **1**, 119-137, doi:10.2174/1573395054065115 (2005).
280 Wang, J. *et al.* Tumor necrosis factor alpha- and interleukin-1beta-dependent induction of CCL3 expression by nucleus pulposus cells promotes macrophage migration through CCR1. *Arthritis Rheum* **65**, 832-842, doi:10.1002/art.37819 (2013).
281 Kyriakis, J. M. Activation of the AP-1 transcription factor by inflammatory cytokines of the TNF family. *Gene Expr* **7**, 217-231 (1999).
282 Liu, Y., Beyer, A. & Aebersold, R. On the Dependency of Cellular Protein Levels on mRNA Abundance. *Cell* **165**, 535-550, doi:10.1016/j.cell.2016.03.014 (2016).
283 Gilbert, A. S., Wheeler, R. T. & May, R. C. Fungal Pathogens: Survival and Replication within Macrophages. *Cold Spring Harb Perspect Med* **5**, a019661, doi:10.1101/cshperspect.a019661 (2014).
284 Vanlaere, I. & Libert, C. Matrix metalloproteinases as drug targets in infections caused by gram-negative bacteria and in septic shock. *Clin Microbiol Rev* **22**, 224-239, Table of Contents, doi:10.1128/CMR.00047-08 (2009).
285 Rocha, J. D. *et al.* Capsular polysaccharides from Cryptococcus neoformans modulate production of neutrophil extracellular traps (NETs) by human neutrophils. *Sci Rep* **5**, 8008, doi:10.1038/srep08008 (2015).
286 Greenlee, K. J., Werb, Z. & Kheradmand, F. Matrix metalloproteinases in lung: multiple, multifarious, and multifaceted. *Physiol Rev* **87**, 69-98, doi:10.1152/physrev.00022.2006 (2007).
287 Aratani, Y. *et al.* Contribution of the myeloperoxidase-dependent oxidative system to host defence against Cryptococcus neoformans. *J Med Microbiol* **55**, 1291-1299, doi:10.1099/jmm.0.46620-0 (2006).
288 Chaturvedi, V., Wong, B. & Newman, S. L. Oxidative killing of *Cryptococcus neoformans* by human neutrophils - Evidence that fungal mannitol protects by scavenging reactive oxygen intermediates. *Journal of Immunology* **156**, 3836-3840 (1996).
289 Anke, T. & Oberwinkler, F. The striatins--new antibiotics from the basidiomycete Cyathus striatus (Huds. ex Pers.) Willd. *J Antibiot (Tokyo)* **30**, 221-225, doi:10.7164/antibiotics.30.221 (1977).
290 Conus, S. & Simon, H. U. Cathepsins: key modulators of cell death and inflammatory responses. *Biochem Pharmacol* **76**, 1374-1382, doi:10.1016/j.bcp.2008.07.041 (2008).
291 Malik, E., Dennison, S. R., Harris, F. & Phoenix, D. A. pH Dependent Antimicrobial Peptides and Proteins, Their Mechanisms of Action and Potential as Therapeutic Agents. *Pharmaceuticals (Basel)* **9**, doi:10.3390/ph9040067 (2016).
292 Laniado-Laborin, R. & Cabrales-Vargas, M. N. Amphotericin B: side effects and toxicity. *Rev Iberoam Micol* **26**, 223-227, doi:10.1016/j.riam.2009.06.003 (2009).
293 Adusei, E. B. A., Adosraku, R. K., Oppong-Kyekyeku, J., Amengor, C. D. K. & Jibira, Y. Resistance Modulation Action, Time-Kill Kinetics Assay, and Inhibition of Biofilm Formation Effects of Plumbagin from Plumbago zeylanica Linn. *J Trop Med* **2019**, 1250645, doi:10.1155/2019/1250645 (2019).
294 Fernandez-Garcia, E., Carvajal-Lerida, I. & Perez-Galvez, A. In vitro bioaccessibility assessment as a prediction tool of nutritional efficiency. *Nutr Res* **29**, 751-760, doi:10.1016/j.nutres.2009.09.016 (2009).
295 Etcheverry, P., Grusak, M. A. & Fleige, L. E. Application of in vitro bioaccessibility and bioavailability methods for calcium, carotenoids, folate, iron, magnesium, polyphenols, zinc, and vitamins B(6), B(12), D, and E. *Front Physiol* **3**, 317, doi:10.3389/fphys.2012.00317 (2012).

296 Zhao, L., Ren, T. H. & Wang, D. D. Clinical pharmacology considerations in biologics development. *Acta Pharmacol Sin* **33**, 1339-1347, doi:10.1038/aps.2012.51 (2012).
297 Prueksaritanont, T. & Tang, C. ADME of biologics-what have we learned from small molecules? *AAPS J* **14**, 410-419, doi:10.1208/s12248-012-9353-6 (2012).
298 Wright, D. F., Winter, H. R. & Duffull, S. B. Understanding the time course of pharmacological effect: a PKPD approach. *Br J Clin Pharmacol* **71**, 815-823, doi:10.1111/j.1365-2125.2011.03925.x (2011).
299 Wang, W., Wang, E. Q. & Balthasar, J. P. Monoclonal antibody pharmacokinetics and pharmacodynamics. *Clin Pharmacol Ther* **84**, 548-558, doi:10.1038/clpt.2008.170 (2008).
300 Anselmo, A. C., Gokarn, Y. & Mitragotri, S. Non-invasive delivery strategies for biologics. *Nat Rev Drug Discov* **18**, 19-40, doi:10.1038/nrd.2018.183 (2019).
301 Meibohm, B. & Zhou, H. Characterizing the impact of renal impairment on the clinical pharmacology of biologics. *J Clin Pharmacol* **52**, 54S-62S, doi:10.1177/0091270011413894 (2012).
302 Sethu, S. *et al.* Immunogenicity to biologics: mechanisms, prediction and reduction. *Arch Immunol Ther Exp (Warsz)* **60**, 331-344, doi:10.1007/s00005-012-0189-7 (2012).
303 Shen, J. *et al.* Design and Conduct Considerations for First-in-Human Trials. *Clin Transl Sci* **12**, 6-19, doi:10.1111/cts.12582 (2019).
304 Tsoumakidou, M., Tzanakis, N., Papadaki, H. A., Koutala, H. & Siafakas, N. M. Isolation of myeloid and plasmacytoid dendritic cells from human bronchoalveolar lavage fluid. *Immunol Cell Biol* **84**, 267-273, doi:10.1111/j.1440-1711.2006.01428.x (2006).
305 Cuccarese, M. F. *et al.* Heterogeneity of macrophage infiltration and therapeutic response in lung carcinoma revealed by 3D organ imaging. *Nat Commun* **8**, 14293, doi:10.1038/ncomms14293 (2017).
306 Ibrahim-Granet, O. *et al.* Phagocytosis and intracellular fate of Aspergillus fumigatus conidia in alveolar macrophages. *Infect Immun* **71**, 891-903, doi:10.1128/IAI.71.2.891-903.2003 (2003).
307 Bossel Ben-Moshe, N. *et al.* Predicting bacterial infection outcomes using single cell RNA-sequencing analysis of human immune cells. *Nat Commun* **10**, 3266, doi:10.1038/s41467-019-11257-y (2019).
308 Dong, C. *et al.* RNA sequencing and transcriptomal analysis of human monocyte to macrophage differentiation. *Gene* **519**, 279-287, doi:10.1016/j.gene.2013.02.015 (2013).
309 Papalexi, E. & Satija, R. Single-cell RNA sequencing to explore immune cell heterogeneity. *Nat Rev Immunol* **18**, 35-45, doi:10.1038/nri.2017.76 (2018).
310 Steen, K. A., Xu, H. & Bernlohr, D. A. FABP4/aP2 Regulates Macrophage Redox Signaling and Inflammasome Activation via Control of UCP2. *Mol Cell Biol* **37**, doi:10.1128/MCB.00282-16 (2017).
311 Bowdish, D. M. *et al.* MARCO, TLR2, and CD14 are required for macrophage cytokine responses to mycobacterial trehalose dimycolate and Mycobacterium tuberculosis. *PLoS Pathog* **5**, e1000474, doi:10.1371/journal.ppat.1000474 (2009).
312 Gren, S. T. *et al.* A Single-Cell Gene-Expression Profile Reveals Inter-Cellular Heterogeneity within Human Monocyte Subsets. *PLoS One* **10**, e0144351, doi:10.1371/journal.pone.0144351 (2015).
313 Jozefowski, S., Yang, Z., Marcinkiewicz, J. & Kobzik, L. Scavenger receptors and beta-glucan receptors participate in the recognition of yeasts by murine macrophages. *Inflamm Res* **61**, 113-126, doi:10.1007/s00011-011-0395-5 (2012).
314 Sallusto, F. & Lanzavecchia, A. Efficient Presentation of Soluble-Antigen by Cultured Human Dendritic Cells Is Maintained by Granulocyte-Macrophage Colony-Stimulating Factor Plus Interleukin-4 and down-Regulated by Tumor-Necrosis-Factor-Alpha. *Journal of Experimental Medicine* **179**, 1109-1118, doi:DOI 10.1084/jem.179.4.1109 (1994).

315 Zhang, C. *et al.* Knocking out or pharmaceutical inhibition of fatty acid binding protein 4 (FABP4) alleviates osteoarthritis induced by high-fat diet in mice. *Osteoarthritis Cartilage* **26**, 824-833, doi:10.1016/j.joca.2018.03.002 (2018).
316 Bosquet, A. *et al.* FABP4 inhibitor BMS309403 decreases saturated-fatty-acid-induced endoplasmic reticulum stress-associated inflammation in skeletal muscle by reducing p38 MAPK activation. *Biochim Biophys Acta Mol Cell Biol Lipids* **1863**, 604-613, doi:10.1016/j.bbalip.2018.03.004 (2018).
317 Li, H. *et al.* Adipocyte Fatty Acid-Binding Protein Promotes Palmitate-Induced Mitochondrial Dysfunction and Apoptosis in Macrophages. *Front Immunol* **9**, 81, doi:10.3389/fimmu.2018.00081 (2018).
318 Batista-Gonzalez, A., Vidal, R., Criollo, A. & Carreno, L. J. New Insights on the Role of Lipid Metabolism in the Metabolic Reprogramming of Macrophages. *Front Immunol* **10**, 2993, doi:10.3389/fimmu.2019.02993 (2019).
319 Hu, B. *et al.* Hepatic Induction of Fatty Acid Binding Protein 4 Plays a Pathogenic Role in Sepsis in Mice. *Am J Pathol* **187**, 1059-1067, doi:10.1016/j.ajpath.2017.01.002 (2017).
320 Alsabeeh, N., Chausse, B., Kakimoto, P. A., Kowaltowski, A. J. & Shirihai, O. Cell culture models of fatty acid overload: Problems and solutions. *Biochim Biophys Acta Mol Cell Biol Lipids* **1863**, 143-151, doi:10.1016/j.bbalip.2017.11.006 (2018).
321 Romer, A., Rawat, D., Linn, T. & Petry, S. F. Preparation of fatty acid solutions exerts significant impact on experimental outcomes in cell culture models of lipotoxicity. *Biol Methods Protoc* **7**, bpab023, doi:10.1093/biomethods/bpab023 (2022).
322 Haddow, L. J. *et al.* Cryptococcal immune reconstitution inflammatory syndrome in HIV-1-infected individuals: proposed clinical case definitions. *The Lancet Infectious Diseases* **10**, 791-802, doi:10.1016/s1473-3099(10)70170-5 (2010).
323 Ruhwald, M. & Ravn, P. Immune reconstitution syndrome in tuberculosis and HIV-co-infected patients: Th1 explosion or cytokine storm? *AIDS* **21**, 882-884, doi:10.1097/QAD.0b013e3280b079c8 (2007).
324 Viola, A., Munari, F., Sanchez-Rodriguez, R., Scolaro, T. & Castegna, A. The Metabolic Signature of Macrophage Responses. *Front Immunol* **10**, 1462, doi:10.3389/fimmu.2019.01462 (2019).

VITA

Benjamin Norman Nelson

Candidate for the Degree of

Doctor of Philosophy

Dissertation: INSIGHTS INTO MECHANISMS OF ANTIFUNGAL ACTIVITY BY INNATE IMMUNE CELLS

Major Field: Microbiology, Cell and Molecular Biology

Biographical:

Education:

Completed the requirements for the Doctor of Philosophy in Microbiology, Cell and Molecular Biology at Oklahoma State University, Stillwater, Oklahoma in May, 2023.

Completed the requirements for the Bachelor of Science in Multidisciplinary Studies at the University of Oklahoma, Norman, Oklahoma in 2015.

Experience:

Research Assistant in the Laboratory of Karen L. Wozniak, Microbiology and Molecular Genetics Department, Oklahoma State University, 2017-2023

Peer Reviewed Publications:

Nelson, B. N., Hawkins, A. N. & Wozniak, K. L. Pulmonary Macrophage and Dendritic Cell Responses to Cryptococcus neoformans. *Frontiers in Cellular and Infection Microbiology* **10**, doi:10.3389/fcimb.2020.00037 (2020).

Nelson, B. N. *et al.* Antifungal activity of dendritic cell lysosomal proteins against Cryptococcus neoformans. *Sci Rep* **11**, 13619, doi:10.1038/s41598-021-92991-6 (2021).

Nelson, B. N. *et al.* Protective interaction of human phagocytic APC subsets with Cryptococcus neoformans induces genes associated with metabolism and antigen presentation. *Frontiers in Immunology* **13**, doi:10.3389/fimmu.2022.1054477 (2022).